

OPTOGALVANIC SPECTROSCOPY AND
CATAPHORETIC LASER ISOTOPE SEPARATION

Thesis by
Andrew Keith Gabriel

In Partial Fulfillment of the Requirements
for the Degree of
Doctor of Philosophy

California Institute of Technology
Pasadena, California

1981

(Submitted April 21, 1981)

ACKNOWLEDGMENTS

The topics in this thesis were originally suggested by Dr. William B. Bridges. The work was supported by the U. S. Department of Energy.

I wish to acknowledge the support of my wife, Holly, and her family.

I wish to thank Professor Thomas C. McGill and Professor James J. Morgan for their assistance.

Finally, the support, charity, and kindness of Dr. Charles Elachi was deeply appreciated.

TABLE OF CONTENTS

<u>Ch.I</u>	General Introduction	1
	References	11
<u>Ch.II</u>	Review of Cataphoresis and the Optogalvanic Effect	12
	A. Introduction	13
	B. Theory: Cataphoresis	14
	C. Experiments: Cataphoresis	18
	D. Introduction: OGE	21
	E. Experiments: OGE	22
	F. Theory: OGE	25
	References	38
<u>Ch.III</u>	Theory of the Positive Column Discharge	43
	A. Introduction	44
	B. Overview	44
	C. Choice of Discharge Media	52
	D. Rate Equations	55
	E. Macroscopic Parameters	83
	F. Calculated Results	91
	References	104
<u>Ch.IV</u>	Effect of Resonant Illumination	106
	A. Effect of Illumination-Steady State	107
	B. Results for Steady State PCD with Illumination	112
<u>Ch.V</u>	Transient OGE	137
	A. Introduction	138
	B. Numerical Integration	138
	C. Perturbation Theory	142
	References	158
<u>Ch.VI</u>	Electron Temperature	159
	A. Introduction	160
	B. Probe Techniques	160
	C. Effect of Illumination on T_e	169
	D. Experimental Results	172
	References	176
<u>Ch.VII</u>	Optogalvanic Effect Experimental Apparatus	177
	A. Introduction	178
	B. Experimental Setup and Procedures	178
	C. Striations in the H Discharge	184
	D. Experimental Problems	190
	E. Early Experiment with H Resonance Lamp	191
	References	196

Table of Contents - ctd.

<u>Ch.VIII</u>	Optically Assisted Cataphoretic Isotope Separation	197
	A. Introduction	198
	B. Cataphoresis-Theory of Shair and Remer	199
	C. Optical Assist	203
	D. Comparison with Experiment and Conclusion	208
	References	211
<u>Ch.IX</u>	Future Possibilities	212
	A. Introduction	213
	B. Extension of Theory and Simulation	213
C	C. Future Experiments	215
	References	224
<u>Appendix I</u>	Hydrogen Excitation Cross Sections	225
	References	231
<u>Appendix II</u>	Computer Programs	233
	Program #1	237
	Program #2	244
	Program #3	250
<u>Appendix III</u>	Positive Column Simulation with Fixed Diffusion Coefficient	256
	A. Introduction	257
	B. Computational Strategy	257
	C. Recombination	258
	D. Computational Results	260
	E. Discussion	267
	References	268
<u>Appendix IV</u>	Lineshapes and Absorption	269
	A. Introduction	270
	B. General Statement of the Problem	270
	C. Application to the OGE	283
	References	306

ABSTRACT

A microscopic theory for the positive column discharge (PCD) is developed using rate equations and power balance equations to model the microscopic discharge processes. Macroscopic variables are calculated from the microscopic parameters. The model is used to characterize a hydrogen-helium PCD.

The equations in the model are modified to account for the presence of resonant (H-alpha) radiation from an external source. The model is then used to predict the voltage change in a hydrogen PCD (the optogalvanic effect) as a function of current, illumination intensity, and gas pressure. The results compare very favorably with experiments conducted to measure the OGE.

Transient voltage changes induced by resonant illumination in a PCD are calculated by numerical integration of the model equations. Perturbation theory is applied to the equations to obtain more physical insight into the physics of the transient OGE.

The experimental apparatus used to measure the OGE and that used to measure the electron temperature (double probes) are described. A discussion of experimental problems covers some of the difficulties encountered.

The PCD model and OGE model are used to evaluate the practicality of separating hydrogen and deuterium by optically assisted cataphoresis in the PCD.

The possibility that recombination is a dominant process in the discharge is discussed in detail and rejected.

A careful description of the interaction of the illuminating radiation and the PCD plasma is given, with special attention to homogeneous and inhomogeneous broadening processes, saturation of absorption and saturation of the OGE, and the relative bandwidths of the illuminating radiation and discharge gas.

Some suggestions are made for future work.

Chapter I
GENERAL INTRODUCTION

I. GENERAL INTRODUCTION

The idea that originally motivated the work described in this thesis was to exploit the well-known phenomenon of binary gas separation in an electric discharge (cataphoresis) as a means of separating isotopes (Bridges, 1976, unpublished). Cataphoresis occurs in a binary discharge when the two constituent gases have different ionization potentials. The gas with the lower potential is generally more easily ionized by the discharge, and hence spends a larger fraction of its time in the ionic state than the gas with the higher potential. Since the electric field in the discharge pulls positive ions toward the cathode, the more readily ionized gas accumulates there. The resulting steady state distribution is then a tradeoff between the preferential drag the easily ionized gas receives and its tendency to diffuse against the concentration gradient that is established. Figures I-1 and accompanying text show the results of a demonstration of this effect.

Since isotopes of the same gas do not, in general, have ionization potentials that are very different, spontaneous cataphoretic isotope separation seems unlikely. However, if a laser or some other source of illumination is used to excite atoms of one isotope to a higher excited state, preferential ionization of that isotope may occur, resulting in separation. Thus the gas at the anode would be enriched in one isotope and the gas at the cathode enriched in the other. As a practical matter, the gases could then be exhausted through valves at either end of the discharge and piped to two new discharges where further enrichment could be performed, similar to the cascades used in gaseous diffusion

Fig. I-1A. Demonstration (Matveeva, 1959) of the separation of helium and argon in a gas discharge. The initial concentration was 9% argon in 1.6 torr helium. The discharge was run at 50 mA and was 150 cm long. Curve I shows the amount of Ar at the anode from the time when the discharge was initiated; Curve II shows the Ar at the anode when the discharge was turned off.

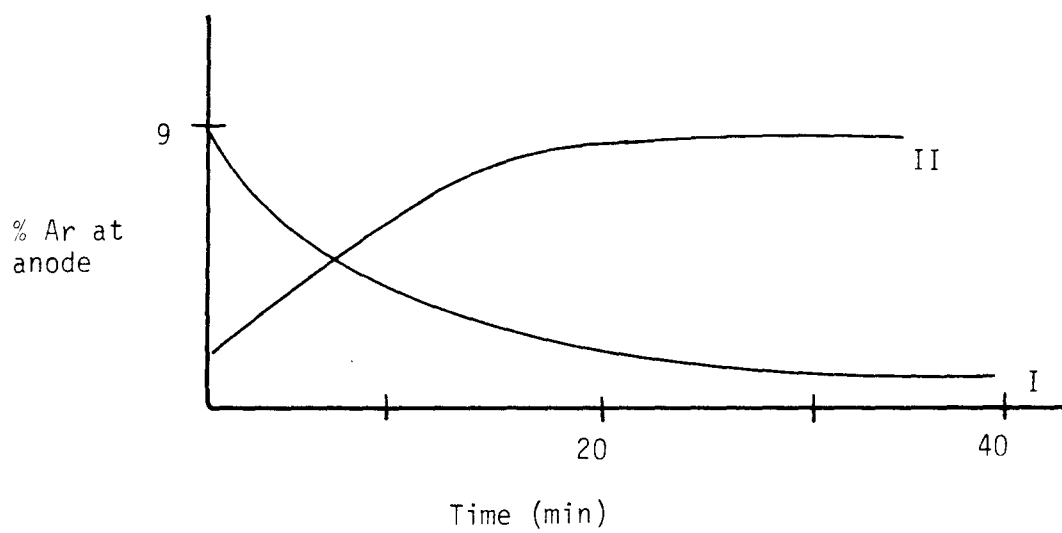
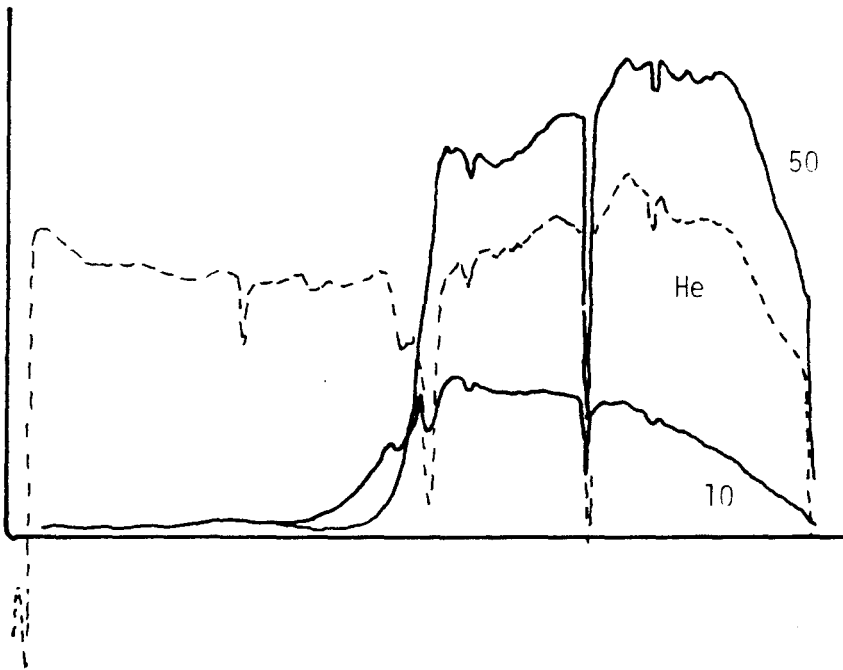
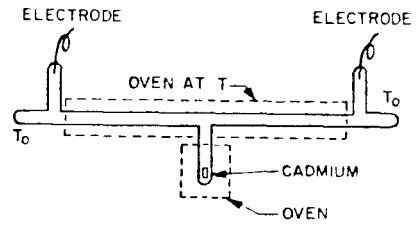


Fig. I-1B. Spatial distribution of cadmium in a He-Cd discharge (Sosnowski, 1969). A helium discharge (inset) was operated inside an oven. Cadmium was supplied from a separately heated sidearm. The relative intensity of the cadmium 4799\AA line as a function of distance along the discharge tube shows the cathoretic pumping of cadmium toward the anode. The helium 4921\AA line shows no large concentration gradient, indicating the helium buffer was not strongly pumped by the discharge. The sharp dips in the curve are caused by tube supports which blocked the light.



(Villani, 1976).

When a gas discharge is illuminated with intense radiation resonant with an absorption line of one of the constituent gases as in the above separation scheme, the gross characteristics of the discharge can be modified; for example, the voltage across the tube can change. This is the so-called optogalvanic effect, which has been known from the early days of gas discharges, where a typical experiment was to use one discharge to illuminate another containing the same gas (Meissner and Graffunder, 1927; Penning, 1928; Pike, 1936; Kenty, 1950; Meissner and Miller, 1953). More recently, tunable lasers have been used for illumination (Feldmann, 1979; Katayama et al., 1979; Ausschnitt and Bjorklund, 1979; Ausschnitt et al., 1978; Bridges, 1978), and optogalvanic spectroscopy is becoming more and more widely used (Keller, Engleman, Zalewski, King Travis, Schenck, Smyth, Luther, Green, Turk, Bentz, Crim, 1976-1979). Figure I-2 shows a simple example of the optogalvanic effect.

The goal of the research described in this thesis was to develop a detailed microscopic model of the interaction of resonant illumination with a discharge plasma, and to tie that model to the resulting macroscopic effects of both isotopically selective cataphoresis and discharge impedance or voltage changes.

The OGE is found to result from the fact that when power from external illumination is supplied to a discharge, the power required from the field sustaining the discharge is reduced. Thus, at constant current

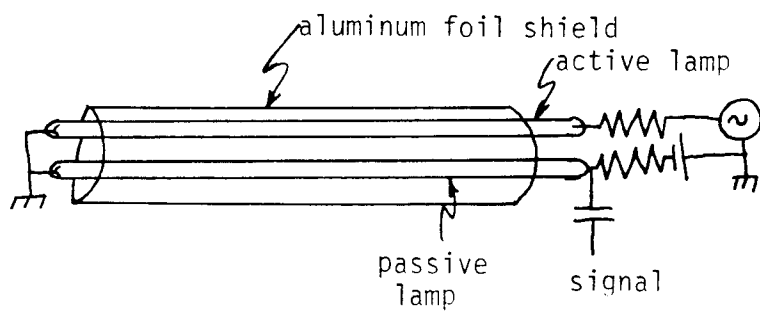
$$\frac{\text{Power from laser}}{\text{Power to discharge}} = \frac{\text{Change in discharge voltage}}{\text{Discharge voltage}}$$

If the illuminating laser beam has ≈ 20 mW within the absorption line and the discharge power is (50 mA)(200 volts) = 10W, the change in voltage is

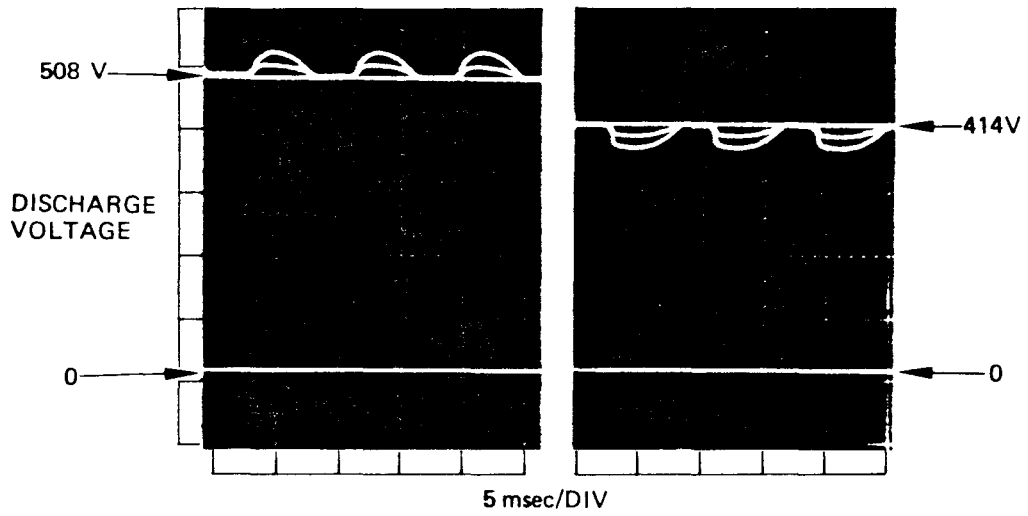
A. Apparatus. Two mercury germicidal lamps are side by side. The light from the active lamp is AC modulated and causes voltage changes in the passive DC lamp.

B. Oscilloscope trace of the voltage change in the passive lamp caused by ac illumination from the active lamp. The DC voltage is 414V.

Fig. I-2. A simple demonstration of the optogalvanic effect (from Bridges, 1978).



6084-10



(a) 5mA

(b) 20mA

$$\frac{20 \times 10^{-3} \text{ W}}{10 \text{ W}} \times 200 \text{ V} = 0.4 \text{ volts}$$

(NOTE: References for Chapter I are included in Chapter II references.)

Chapter II

REVIEW OF CATAPHORESIS AND THE OPTOGALVANIC EFFECT

II. REVIEW OF CATAPHORESIS AND THE OPTOGALVANIC EFFECT

A. INTRODUCTION

The phenomenon of separation of two gases in an electrical discharge has been known for a long time. Over the last 100 years there have been many papers on the subject, including three reviews (Lehmann, 1898; Loeb, 1958; Chanin, 1978). Some of the earliest experimental references are Baly (1893) and J. J. Thomson (1895). These papers and others (Lehmann, 1898; Skaupy, 1916; Skaupy and Bobek, 1925; Mierdel, 1929; Vygodski and Klarfeld, 1933; Penning, 1934) dealt with the spectroscopic observation of the separation of binary gas mixtures, typically two noble gases or one noble gas and one common molecular gas such as CO_2 . Later work in the 1950's centered on exploiting cataphoresis to purify gas mixtures.

Separation of hydrogen and deuterium was proposed and demonstrated by Groth and Harteck (1939), the first application of cataphoresis to isotope separation. However, their work hinged on the fact that hydrogen and deuterium have significantly different recombination coefficients. Recently Bridges (1978) proposed a laser-assisted cataphoretic separation scheme which is discussed in this investigation. A different scheme employing cataphoresis to separate isotopes, but depending on differential radiation trapping for isotopic selectivity was proposed by Silfvast (1977). In his scheme, two isotopes are in a discharge in their natural abundances. The pressure is adjusted until one isotope has its resonance radiation strongly trapped, while the other remains untrapped (the natural abundances cannot be equal). The trapped isotope is then preferentially ionized and

pumped to the cathode. In the late 1960's and early 1970's cataphoresis entered into the techniques of gas lasers, particularly the helium-cadmium laser (Goldsborough, 1969 ; Fendley et al., 1969; and Sosnowski, 1969). The same techniques are required in the less well known He-I⁺, He-Se⁺, He-Te⁺, and other charge-exchange ionization or Penning ionization lasers.

There are fewer publications of a theoretical nature in the literature; of these the most complete theories are in papers published in the last twenty years. All of the theories deal with the basic physics of cataphoresis: ions of the more easily ionized gas are "dragged" toward the cathode by the electric field; diffusion then opposes the concentration gradient that is created. A steady state concentration gradient results when these two forces are balanced.

B. THEORY: CATAPHORESIS

Druyvesteyn (1935) published the first theoretical analysis of cataphoresis in an attempt to explain the separation of a noble gas and magnesium vapor. Essentially, the theory consisted of equating the ion current to the cathode to the back diffusion current of neutral atoms. From this condition he found that the concentration of magnesium as a function of distance z along the discharge is given by

$$n_m(z) = n_m(0) - (\text{constant}) \frac{T_e^{1/2}}{T_g^2 R^2} p I z$$

where

T_e = electron temperature

T_g = neutral gas temperature

R = tube radius

n_m = magnesium concentration

p = neutral gas pressure

I = current

Two papers by Pekar that considered the theory of cataphoresis were published in 1967. In one paper, he calculated radial gas separation by equating the wall current induced by the ambipolar electric field to the radial back diffusion current. Some simplifying assumptions led to the conclusion that the radial separation decreased with an increase in pressure. In the second paper he generalized the analysis to cover longitudinal as well as radial separation, where electron temperature was calculated as a function of distance along the discharge. In the limit of a high density of the more easily ionized component, the longitudinal distribution of that component was given by the product of an exponential in z and a Mathieu function in z.

Sosnowski (1969) developed a simple theory for the longitudinal concentration of cadmium in the He-Cd laser. He made the assumptions that the fractional ionization of cadmium is a constant independent of concentration and that the electric field was constant in the discharge. Two radially averaged diffusion equations, one for Cd ions and one for Cd neutral atoms, were added to yield a general equation for steady state cataphoresis. The solution to that equation is

$$\frac{n}{n_0} = \frac{1 - \exp \beta(1 - \frac{z}{L})}{1 - \exp \beta}$$

where

n = concentration of Cd atoms and ions

n₀ = concentration of Cd atoms and ions at the Cd source

$$\beta = \frac{\alpha\mu EL}{D}$$

μ = cadmium ion mobility

E = positive column electric field

L = positive column length

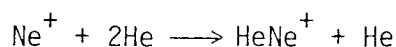
D = Cd diffusion coefficient

α = ionization fraction of Cd

The model was in excellent qualitative agreement with experimental observations, which are shown in Chapter I, Figure I-1.

Shaperev (1972) developed a theory similar to that of Druyvesteyn, based on equating the ion current flux to the reverse diffusion flux. He assumed that the less easily ionized ions were a constant fraction of the more easily ionized ions throughout the tube. By assuming a simple form for the ion production rates, and assuming a fixed electron temperature, he found that the more easily ionized gas had an exponential longitudinal profile, and reduced his result to that of Druyvesteyn in the limit of high density.

Cataphoresis in helium-neon mixtures was investigated theoretically by Gaur and Chanin (1969). Their intent was to include the effects of ion production and loss (as it occurs in the He-Ne laser) on the gas separation. By considering the kinetics of the important associative ionization process,



they calculated an exponential distribution of gas along the tube. A later paper by the same authors (Gaur and Chanin, 1970) extended the analysis to helium-argon mixtures.

Radial cataphoresis was also treated by Cayless (1963), who developed a numerical theory for fluorescent lamp discharges of mercury-noble gas mixtures. The theory included many excitation processes, the local distribution of ions, and a local electron temperature. He concluded that mercury is pumped from the center of the discharge to the walls, and the effect increases with current. A similar calculation was undertaken by von Tongeren (1974) for argon-cesium mixtures. Latush et al. (1976) performed an analysis of radial cataphoresis relevant to the helium-cadmium laser. They considered the radial diffusion of the He-Cd species and excitation processes of ground state atoms. Solving the radial diffusion equation with fixed electron temperature, they concluded that the cadmium density was a minimum at the center of the discharge.

Some investigators looked at the problem of the time dependence of longitudinal cataphoretic gas separation. The first theoretical analysis was that of Freudenthal (1967). In addition to a steady state model that was a straightforward extension of Druyvesteyn's theory, he calculated transient behavior from the diffusion equation. His principal conclusion was that the degree of gas separation as a function of time is a decaying exponential.

Shair and Remer (1968) developed the most complete theory of cataphoresis, accounting for transient and steady state effects as well as the presence of gas reservoirs ("endbulbs") in the discharge. They derived two radially averaged diffusion equations that described the motion of a more easily ionized gas in the presence of a buffer gas. Making the assumption that the charge fraction of the more easily ionized gas was a constant, they derived a general equation for time-dependent cataphoresis.

The main criticism of this theory is that it is not true that the charge fraction can be constant in the presence of a concentration gradient. Although the authors use the theory to calculate the separation of hydrogen and deuterium observed by Groth and Harteck (1939), it is not applicable unless, for some reason, one isotope is preferentially ionized and assumes the role of the more easily ionized gas.

C. EXPERIMENTS: CATAPHORESIS

A typical cataphoresis experiment consists of a gas-handling system for two or more gases, a discharge tube and associated electronics, and some means of evaluating the spatial concentration of the constituent gases in the discharge. The most popular technique is observation of the intensities of spectral lines in the sidelight of the discharge; the concentrations of the gas species are assumed to be proportional to the intensities of the lines originating from them. However, steep concentration gradients can cause changes in the local electron temperature and corresponding changes in the excitation probability gas particular line, so that the line intensities are not proportional to the neutral number density. An alternative technique is to take gas samples at opposite ends of the tube and analyze them in a mass spectrometer.

Noble gas mixtures have been studied extensively; Table II-1 contains some of the references. Other combinations of gases or metal vapor are listed in Table II-2.

There are three applications of cataphoresis: gas purification, improved excitation of metal-vapor lasers, and isotope separation.

Table II-1. Papers discussing cataphoretic separation of noble gases

Author	Year	Gases
Gaur et al.	1969	He-Ne
Reisz et al.	1954	Ar-Kr; Kr-Xe
Bhattacharya	1969	Kr-Xe
Hackam	1973	Ar-He
Remer and Shair	1971	Ar-He

Table II-2. Papers discussing cataphoretic separation of various gases

Author	Year	Gases
Tomers	1971	He-N ₂
Gaur et al.	1968	He-N ₂
Sanctorum	1975	N ₂ -Ne
Remer et al.	1971	He-Ne, He-O ₂ , He-CO, He-CO ₂
Druyvesteyn et al.	1934	Na-He, Na-Ne, Na-Ar, Na-Kr
Druyvesteyn	1935	Mg-Ne
Sosnowski	1969	He-Cd
Kenty	1958	Hg-He, Hg-Ne, Hg-Ar, He-Kr, Hg-Xe
Baly	1893	CO ₂ -CO, CO ₂ -SO ₂ , N ₂ -CO ₂ , H ₂ -Hg, He-I ₂ , H ₂ -CO, H ₂ -SO ₂ , H ₂ -CO ₂ , H ₂ -N ₂
Thomson	1895	H ₂ -Cl ₂
Beckey et al.	1953	H ₂ -D ₂
Springer et al.	1968	Cd-Noble Gas

The method of gas purification by cataphoresis is quite transparent; a mixture of gases is put in a discharge, and then exhausted from opposite ends of the tube. The exhaust from the cathode end will be enriched in the more easily ionized gas and the exhaust from the anode end enriched in the less easily ionized gas. Each of these two samples may be further purified by repeating the process. If high purity is desired, discharge contaminants and material sputtered from the cathode may become problems.

Cathaphoretic He-Cd lasers were developed by Sosnowski (1969), Goldsborough (1969), and Fendley et al. (1969). A heated source of cadmium metal was placed near the anode in the bore of a helium discharge. The Cd vapor, much more readily ionized than the helium, was rapidly pumped to the cathode. The discharge walls were heated to prevent the Cd from condensing, with the result that there was a substantial amount of Cd vapor throughout the discharge. The appropriate levels in Cd are excited by a Penning reaction with the $2s^3S$ metastables of He to obtain a population inversion.

It should be noted that this application of cataphoresis in gas lasers is in fact the prevention of cataphoresis through the use of a gas flow, either one-way or continuously via a return path connecting the anode to the cathode in which there is no discharge.

Using cataphoresis to enrich isotopes requires, as noted, some mechanism to distinguish one isotope from the other, such as preferential ionization of one isotope. Hydrogen-deuterium mixtures have been shown to separate spontaneously. According to Beckey et al. (1953), the mechanism is as follows: the mass ratio of H and D is 2, and as a consequence the hydrogen has a greater thermal velocity by $\sqrt{2}$. As a result, the hydrogen

atoms diffuse to the walls faster, and are there associated into molecules at a greater rate than deuterium atoms. Thus H is depleted compared to D, and H₂ is enriched relative to D₂. Thus, while both H and D atoms are ionized with equal probability per atom, there are more D atoms than H atoms, so that more D ions than H ions are dragged to the cathode by the electric field. Since the ionization potential of molecular H₂ exceeds that of atomic D by nearly 2 volts, few hydrogen ions are produced.

Another attempt to see spontaneous cataphoretic isotope separation was made by Freudenthal (1966). He failed to see any separation of ³⁶Ar and ⁴⁰Ar. Matsumura et al. (1980) observed slight enrichment of ²⁰Ne and ²²Ne in a discharge, which they attributed to the greater viscosity of the heavier isotope in the electron gas.

Cataphoretic isotope enrichment might be enhanced by selectively exciting one isotope with external illumination as proposed by Bridges (1978). This is discussed in detail in Chapter VIII.

D. INTRODUCTION: OGE

The recent flurry of work in the area of optogalvanic spectroscopy (Feldmann, Katayama, Auschnitt, Bridges, Keller, Engleman, Zalewski, King, Travis, Schenck, Smyth, Luther, Green, Turk, Bentz, Crim, 1976-1979) represents, as is often the case, the rediscovery and new application of an effect that was first reported many years ago. The oldest experiments consisted of measuring the voltage change in one discharge illuminated by an identical discharge as in Fig. I-2 (Meissner and Graffunder, 1927; Penning, 1928). Variations on this basic effect discussed below include illumination of a positive column with a tunable dye laser, illumination

of flames in an electric field with a laser, and illumination of hollow cathode lamps with a laser.

E. EXPERIMENTS: OGE

The earliest references found for the effect of resonant radiation on a discharge are Meissner et al. (1927) and Penning (1928). Meissner et al. demonstrated that the metastable atom populations in neon and argon discharges were affected by illumination from other discharges containing these same gases. Penning demonstrated that the starting voltage of a discharge containing 20 Torr neon and a small amount of argon (the so-called "Penning mixture") increased when illumination from another neon discharge was applied. Two subsequent papers by Pike (1936) confirmed the effect and used it to estimate the lifetimes of metastable neon atoms. Fourteen years later, Kenty (1950) measured the voltage change in externally illuminated mercury argon lamps (which is as large as 40%) as a function of current, and used it to comment on the role of mercury metastables in the discharge. In 1953, Meissner and Miller found that irradiation of a helium discharge positive column would change the I-V characteristic by as much as 15%, and tied the effect to the metastable concentration. Drouet and Novak (1971) measured the change in the electron distribution with neon illuminating neon.

The OGE was rediscovered several times with the advent of gas lasers in the 1960s. Several papers documented the effect of lasing on the populations of the laser discharge (Weaver and Frieberg, 1966; White and Rigden, 1963; Waksberg and Carswell, 1965; Parks and Javan, 1965). The decrease in current in He-Ne lasers was well documented (Garscadden

and Adams, 1966) shortly after the discovery of that laser.

Friberg and Weaver (1967) did an extensive investigation of the effect of 3.5μ lasing in a xenon discharge, and found that the current changed. Carswell and Wood (1967) found large current changes with the presence of 10.6μ lasing in CO_2 ; * Garscadden et al. (1969) measured the corresponding electron temperature changes; Skolnick (1970) used the OGE in the laser discharge itself to frequency stabilize a CO_2 laser, as did Nussmeier and Friedrich (1969, unpublished) and Smith and Moffatt (1979). Green et al. (1977) stabilized a dye laser to absorption lines in standard hollow cathode spectrometer lamps.

More recent work on optogalvanic spectroscopy has been conducted with dye lasers as the illumination source. In positive column discharges Feldmann (1979) used a dye laser to produce optogalvanic response of some molecules. Katayama et al. (1979) investigated optogalvanic response of excited states of neon to a dye laser. Ausschnitt and Bjorklund (1979) and Ausschnitt et al. (1978) investigated the transient behavior of a hydrogen positive column to pulsed H_2 illumination. Bridges (1978) found a large (30%) OGE when illuminating an excited state transition in cesium with a dye laser, and also reperformed Kenty's experiment by illuminating one mercury germicidal lamp with another.

Hollow cathode discharges have been particularly popular subjects for OGE experiments, since they are electrically quiet and exhibit OGE response from both the buffer gas (usually neon or argon) and the sputtered

* It is interesting to note that in their brief publication they said they would publish the theory in a more extensive paper to follow; it never did appear.

cathode material. Bridges (1978) demonstrated the OGE in an argon-uranium HCD, as well as in lithium and europium. A series of papers by Keller, Engleman, and Zalewski of the Los Alamos Scientific Laboratories and King, Travis, Schenck, Smyth, Luther, Green, Turk, Bentz and Crim at the National Bureau of Standards in 1976-1979 discussed various aspects of neon-uranium hollow cathode discharges.

An interesting technique for the optogalvanic detection of trace elements in flames has been developed by the NBS group. Green et al. (1976) detected sodium in a flame by optical excitation of the D line, and were able to detect the concentrations as low as 2 parts per billion. Similar work was performed by Schenck et al. (1978) and Turk et al. (1978). Travis et al. (1978) extended the work to cover many different metals. Schenck et al. (1978) investigated optogalvanic response of highly excited molecular states of metal oxides in flames.

The transient response of hollow cathodes to pulsed dye laser excitation was measured by Miron et al. (1979) and Erez et al. (1979). They also produced a simple theory for the lamp's response, which is discussed below.

The first demonstration of sub-Doppler optogalvanic response was given by Johnston (1978), who used a narrowband dye laser to excite a He-Ne discharge and found an "optogalvanic Lamb dip." Other sub-Doppler experiments were conducted by Goldsmith et al. (1979) who performed two-photon excitation experiments in Ne. A variation by Lawler et al. (1979) measured the two-photon response of He at an intermodulation frequency; a simple discussion of two-photon OGE was given by Vidal (1980).

Other variations on OGE experiments were investigated by Keller (1980), who postulated a simple model for noise limitations of OGE detection in hollow cathodes, and White et al. (1980), who investigated laser-induced dipole pair absorption.

F. THEORY: OGE

In contrast to the extensive experimental work on the optogalvanic effect, there are only five papers that present any theoretical calculations. The papers of Bridges (1978) and Lawler et al. (1979) deal with very simple rate equation models. The Pepper paper (1978) is a more detailed rate equation model, but contains errors as described below; the later Lawler paper (1981) is based on using Ohm's law to calculate impedance. A simple theory for the transient behavior of the optogalvanic effect is that of Erez et al. (1979).

The simplest theory for the steady state optogalvanic effect is that of Lawler et al. (1979). In the model considered by Lawler et al. n_u and n_l are, respectively, the upper and lower level populations on the lasing transition, and $\Delta n_{u,l}$ are the changes in levels induced by the laser; the total population change is $\Delta n_u - \Delta n_l$. If all electrons created by the radiation are collected with no collisional multiplication, the current increase due to the radiation (which will be called the OGE current for simplicity) is

$$i_s = e VR(\Delta n_u - \Delta n_l) \quad (\text{II.1})$$

where R is the difference in ionization rates of the two levels, V is the PCD volume.

The shortcomings of such a simple theory are manifold: First, it was assumed that the origin of the OGE signal was "extra" electrons generated in the body of the plasma; that is, the signal source was the electron current. In fact this is an oversimplification of what happens in a discharge. A perturbed electron density will affect the diffusion loss rates, the excitation rates R , and can also affect the electron temperature as well (which would, in turn, also affect R). Second, it is not required by equation (II.1) that energy be conserved. Third, no consideration is given to the presence of the external circuit driving the discharge, how it responds to the "extra" electrons, or how the response affects the discharge. Finally, the electron temperature itself was just assumed, and no depletion of the exciting beam by absorption was included. The theory was actually applied for a sub-Doppler experiment with two counterpropagating laser beams. The equation discussed above is the central assumption of that theory.

Slightly more complex is the theoretical model given by Bridges (1978). Even in its admitted simplicity, however, it does indicate problems that turn out to be important. Bridges' model considers a simple set of processes described by rate equations for three levels.

The processes included in this model are:

- a) Creation of (1) by electron collision rate $C_1 N_0$;
- b) Trapped spontaneous emission from 1 to 0, rate $\gamma A_{10} N_0$;
- c) Stimulated excitation of (2) from (1), rate $(W_{12} N_1 - W_{21} N_2)$;
- d) Spontaneous emission from (2), rate $A_{21} N_2 + A'_2 N_2$ where $A'_2 = \sum_{i=1} A_{2i}$ is the emission rate to all states but (1);

- e) Destruction of (2) by collisions, including those to higher levels and ionization; rate $D_2 N_2$.

Bridges then assumes that C and D are not altered by the presence of the radiation, and the OGE is directly proportional to N_2 (both, he notes, are doubtful assumptions); then

$$N_2 = K[S/(S+S_{3dB})] \quad \text{where } S \text{ is the laser flux density}$$

$$K = \frac{C_1 N_0}{(\gamma g_1 A_{10}/g_2 + A_2' + D_2)} \quad (II.2)$$

$$S_{3dB} = \frac{8\pi h\nu}{\lambda_{21}^2} \frac{1 + (A_2' + D_2)/A_{21}}{1 + (g_2 A_{21}/\gamma g_1 A_{10})[(A_2' + D_2)/A_{21}]}$$

where S_{3dB} is the laser flux necessary to reduce the OGE signal by a factor of two below a linear increase, and g_1, g_2 are the degeneracy factors.

While this model is considerably more detailed than the previous one it suffers from some of the same flaws. Electron temperature, necessary to calculate the electronic excitation rates, is assumed not to change. The assumption that OGE is simply proportional to N_2 is doubtful, and the generic destruction rates D_2 and A_2 are likely not well known. Finally, the results, as Bridges notes, are sensitive to the radiation trapping factor which is somewhat uncertain, as discussed in Chapter III. Nevertheless, his model gave qualitative agreement with the shape of the OGE saturation with laser, and came within an order of magnitude of predicting S_{3dB} observed experimentally in a cesium discharge.

A simple, admittedly phenomenological theory of the transient OGE is that of Erez et al. (1979). It is based on calculating how an electron

multiplication factor α depends on the discharge processes. α is defined as the number of electrons generated at the cathode by the emission of one electron by the cathode. If $\alpha > 1$, the current increases, and there is an increase in the voltage drop across the ballast resistor. At constant current,

$$d\alpha = \left(\frac{\partial\alpha}{\partial V}\right)_{n_i} \Delta V + \sum_i \left(\frac{\partial\alpha}{\partial n_i}\right)_{V, n_j} \Delta n_i = 0 \quad (\text{II.3})$$

where V is the tube voltage and n_i are the atomic level populations.

Rewriting,

$$\Delta V = -\beta \sum_i a_i \Delta n_i \quad (\text{II.4})$$

where
$$\beta = \left(\frac{\partial\alpha}{\partial V}\right)_{n_i}^{-1}, \quad a_i = \left(\frac{\partial\alpha}{\partial n_i}\right)_{n_j, V} \quad (\text{II.5})$$

The level rate equations are

$$\frac{d(\Delta n_i)}{dt} = \sum_j \gamma_{ji} \Delta n_j - \sum_j (n_i - n_j) \sigma_{ij} I_{ij} \quad (\text{II.6})$$

where γ_{ji} is the general rate out of j into i (no illumination), σ_{ij} is the optical cross-section of the i - j transition, and I_{ij} is the resonant light intensity. The two rate equations for the levels involved in the illuminated transition are then used explicitly with the assumption that all other levels relax with time T_i . That is,

$$\frac{d(\Delta n_1)}{dt} = \frac{\Delta n_1}{T_1} - (n_1 - n_2) \sigma_{12} I_{12} \quad (\text{II.7})$$

$$\frac{d(\Delta n_2)}{dt} = \frac{\Delta n_2}{T_2} - (n_2 - n_1) \sigma_{12} I_{12} \quad (\text{II.8})$$

In steady state the explicit solution for the voltage change is

$$\Delta V = -\beta\sigma_{12} I_{12}(a_2 T_2 - a_1 T_1)(n_1 - n_2) \quad (\text{II.9})$$

An expression for the transient optogalvanic response is obtained by assuming that

$$\frac{d\Delta n_1}{dt} = -\frac{d\Delta n_2}{dt} = (n_2 - n_1) \sigma_{12} I_{12} \quad (\text{laser on}) \quad (\text{II.10})$$

$$\frac{d(\Delta n_1)}{dt} = -\frac{\Delta n_1}{T_1} \quad ; \quad \frac{d(\Delta n_2)}{dt} = -\frac{\Delta n_2}{T_2} \quad (\text{II.11})$$

Integrating,

$$\Delta V = -\beta Q(n_1 - n_2)(a_2 e^{-t/T_2} - a_1 e^{-t/T_1}) \quad (\text{II.12})$$

and there is a decay characterized by two time constants. The quantity Q is the pulse energy of the laser, $Q \equiv \sigma_{12} \int I_{12}(t) dt$.

The strength of this theory as well as its principal weakness is its simplicity. It does account for the behavior of the OGE in an intuitive manner. However, it is in reality little more than a reduction to symbols of the assertion "each level decays exponentially with characteristic time constant, hence so does the OGE." In fact, the model presented in Section III finds this to be the case, but the conclusion is derived, not invoked by fiat. No analytical means is given for finding the rate constants T_1 and T_2 ; and no account is taken of the effect of illumination on electron temperature. Also, most of the variables in the theory, α , β , and Δn , cannot be calculated from the theory or measured directly in a discharge; they were simply fit to the experimental results.

The results, as might be expected, are in reasonable qualitative agreement with the experiments.

A second, more sophisticated theory by Lawler (1980) deals with the OGE resulting from illumination of a helium positive column with resonant (5876Å) illumination from a tunable dye laser. Lawler asserts that the dominant ion/electron production mechanism in He is associative ionization,



and that the OGE derives from change induced in the metastable population He^* by the external illumination. He finds the change in "efficiency of ionization per absorbed photon". By scaling with respect to this quantity, any direct calculation of ionization rates is avoided.

Lawler writes a generalized ion rate equation

$$G(n,E) = 0 = \frac{dN}{dt} \quad (\text{II.14})$$

where G is an ion production term minus an ion loss term and N is the ion density. Similarly the current may also be written

$$i = F(n,E) \quad (\text{II.15})$$

A perturbation applied to the plasma changes both equations:

$$\frac{\partial G}{\partial n} \Delta n + \frac{\partial G}{\partial E} \Delta E + E Q = 0 = \frac{dN}{dt} \quad (\text{II.16})$$

where E is the ionization efficiency per photon and Q is the photon flux.

Similarly,

$$\Delta i = \frac{\partial F}{\partial n} \Delta n + \frac{\partial F}{\partial E} \Delta E \quad (\text{II.17})$$

The OGE response is calculated from

$$Z \Delta i = - \ell \Delta E \quad (\text{II.18})$$

where Z is the resistance of the ballast plus power supply, ℓ is the column length, and

$$\Delta i = -E Q \left[\frac{\partial F}{\partial n} \frac{\partial G}{\partial n} \right] \frac{dV}{di} \left(\frac{dV}{di} + z \right) \quad (\text{II.19})$$

The explicit forms of F and G used to evaluate the above expression are

$$F(n, E) = e n \mu E \pi R^2 2 h_0 \quad (\text{II.20})$$

where e is the electronic charge, μ is electron mobility, and h_0 is a constant.

$$G(n, E) = g(E) n^2 - n (2kT_e/m_p)^{1/2} 2\pi R \ell S_0 h_0 \quad (\text{II.21})$$

where $g(E)$ is all the ion production rate proportional to n^2 , m_p is the ion mass, and S_0 is a constant of order 1. Accordingly,

$$\frac{\partial F}{\partial n} \frac{\partial G}{\partial n} = e R \mu E / [S_0 \ell (2kT_e/m_p)^{1/2}] \quad (\text{II.22})$$

Assuming some form for $g(E)$, the OGE may be calculated as a function of E/P, using the measured column resistance for dV/dI .

This model is clever in that it avoids explicit calculation of excitation rates by relying solely on the "ionization efficiency" E and the perturbations ΔR to evaluate the effect of the laser on the plasma. There

are numerous opportunities for technical improvements which the author acknowledges; particularly a better account of the role of metastables.

The objection to this work is that it expresses relationships between quasi-empirical variables, such as $\frac{dV}{dI}$ and E . It does not offer a quantitative treatment of the microscopic processes in the discharge, or how they cause changes in the macroscopic behavior of the plasma. Finally, the model is based on the associative ionization processes peculiar to He, and may not be easily adapted to other gases.

Lawler's theory is in fair agreement with his experimental observations.

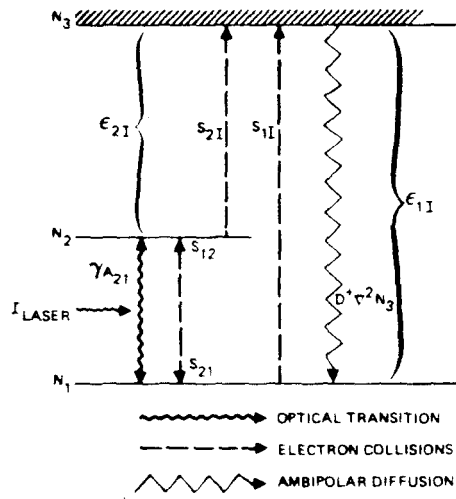
The model considered by Pepper (1978) is closest to the present work, and is the most detailed model of the optogalvanic effect that has been published. It also, unfortunately, contains a fatal error. Pepper solves simultaneously the rate equations, power balance equations, and an implicit expression for the electron temperature; the three states in his model are treated as a ternary system of gases. Figure II-2 shows the various processes treated. Pepper's rate equations are (see Section III for a discussion of the terms)

$$\begin{aligned} \frac{dN_1}{dt} = & B\left(\frac{g_1}{g_2} N_2 - N_1\right)I + N_2 A_{21} \gamma - N_1 n_1 (S_{12} + S_{13}) \\ & + N_2 n_e S_{21} - D^+ v^2 N_3 = 0 \end{aligned} \quad (\text{II.23})$$

$$\begin{aligned} \frac{dN_2}{dt} = & B\left(N_1 - \frac{g_1}{g_2} N_2\right)I + N_1 n_e S_{12} - N_2 n_e (S_{23} + S_{21}) \\ & - N_2 A_{21} \gamma = 0 \end{aligned} \quad (\text{II.24})$$

$$\frac{dN_3}{dt} = N_1 n_e S_{13} + N_2 n_e S_{23} + D^+ v^2 N_3 = 0 \quad (\text{II.25})$$

Fig. II-1. Processes in the model of Pepper (1978)



where

- A_{21} is the Einstein A coefficient;
- B_{12} is the Einstein B coefficient;
- g_i is the degeneracy of level i ;
- S_{ij} is the electron excitation rate from level i to level j ;
- γ is the Holstein radiation trapping factor for the $2 \rightarrow 1$ transition;
- D^+ is the ambipolar diffusion coefficient,

$$= (2.405/R)^{-2} \sum_j R_j S_{ji}$$

The electron temperature is computed from the expression of Dorgela, Alting, and Boers (1935):

$$\sum_{i=1}^3 f_i c_i^2 (qV_i/kT_e)^{-1/2} [1 + \frac{1}{2}(gV_i/kT_e)] e^{-qV_i/kT_e} = 1.72 \times 10^7 V^{1/2} \text{ s cm}^{-1} \quad (\text{II.26})$$

where

- $f_i = N_i/N_T =$ fractional population of level i
- $c_i = a_i V_i^{1/2} / b_i p$
- $a_i = d\sigma_i/d\varepsilon$ (slope of cross section)
- $b_i = 760 \mu_i/p$
- $\mu_i =$ mobility of i^{th} species
- $p =$ pressure.

Pepper solves these equations by iteration on a computer, varying the electron density R_e and electron temperature T_e until they are relaxed. Then, using the power relationship

$$EI = 7.85 n_e D^+ (\varepsilon_I + 5kT_e) \quad (\text{II.27})$$

where E is the electric field, I is the current, and ε_I is the atomic ionization potential, the electric field (and change in electric field with

illumination) are calculated.

While Pepper's analysis contains several good ideas (and was the starting point for the present work), it also contains inaccuracies and a serious error. First, his strategy was to iterate n_e until the "power in" was equal to the "power out," but there is no expression for the power in. In actuality, the set of equations is overdetermined; three rate equations, one electron temperature equation, and one power balance equation are given for only four variables, n_e , n_1 , n_2 , and T_e . The error is in Pepper's equation for n_3 ; the sign of the diffusion coefficient is wrong. Using the correct sign, the equation collapses immediately to $0 = 0$, and there are left four variables and four equations (including the power balance).

There are some limitations in Pepper's approach. First, no longitudinal attenuation by absorption of the external illumination is allowed. Considering that the illumination is applied to a resonance transition and is very strongly absorbed, this is a rather limiting approximation, particularly in light of the large ground state densities assumed in the calculation. Pepper uses sodium as an example, and the calculation is done in very high density regions ($N_0 \geq 10^{14} \text{ cm}^{-3}$) where the absorption depth is extremely short, meaning an experiment would necessarily involve exciting only a small part of the column or an extremely high illumination intensity. Second, no mention is made of the external circuit driving the discharge (constant current is implied but not stated explicitly). It is quite possible, as indicated in Chapter III, to calculate the field and current separately. Third, Pepper simultaneously

assumes that charge neutrality is obeyed, but that ions are in the spatial Schottky profile (see Chapter III) and electrons are uniformly distributed, a clear contradiction. All excited states are assumed uniformly distributed in radius, which is manifestly untrue (but may not be overly important). Fourth, no explicit consideration is given to the bandwidth of the illuminating source of dependence of the saturation intensity on that bandwidth.

REFERENCES - Chapter II

- Ausschnitt, C. P. and G. C. Bjorklund, *Optics Lett.* 4, 4-5 (1979).
- Ausschnitt, C. P., G. C. Bjorklund, and R. R. Freeman, *Appl. Phys. Lett.* 33, 851-853 (1978).
- Baly, E.C.C., *Phil. Mag.* 35, 200 (1893).
- Beckey, H. D., W. E. Groth, and K. H. Weige, *Naturf.* 8a, 556 (1953).
- Bentz, B. L., see K. C. Smyth (1979).
- Bhattacharya, A. K., *Appl. Phys. Lett.* 15, 362 (1969).
- Bridges, W. B., *J. Opt. Soc. Amer.* 68, 352-360 (1978).
- Carswell, A. I. and J. I. Wood, *J. Appl. Phys.* 38, 3028-3030 (1967).
- Cayless, M. A., *Brit. J. Appl. Phys.* 14, 863 (1963).
- Chanin, L. M., *Gaseous Electronics*, V.I (Academic Press, 1978).
- Crim, F. F., see K. C. Smyth (1978).
- Dorgela, H., B. Alting, and J. Boers, *Phys. Haag.* 2, 959-967 (1935).
- Drouet, M. G. and J. P. Novak, *Phys. Lett.* 34A, 199-200 (1971).
- Druyvesteyn, M. and N. Marmoltz, *Phil. Mag.* 7, 1 (1934).
- Druyvesteyn, M., *Physica* 2, 255 (1935).
- Engelman, R., see R. A. Keller (1979).
- Erez, G., S. Levi, and E. Miron, accepted for publication, 1980.
- Feldmann, D., *Optics Commun.* 29, 67-72 (1979).
- Fendley, J. R. Jr., I. Goroy, K. G. Hernquist, and C. Sun, *RCA Rev.* 30, 422 (1969).
- Frieberg, R. J. and L. A. Weaver, *J. Appl. Phys.* 38, 250-262 (1967).
- Freudenthal, J., Thesis, Utrecht (1966).
- Freudenthal, J., *J. Appl. Phys.* 38, 4818 (1967a); *Physica* 36, 354 (1967b).

- Garscadden, A. and S. L. Adams, Proc. IEEE 54, 427-428 (1966).
- Garscadden, A. and P. Bletzinger, Ninth Int'l. Conf. Phenom. Ion. Gases, Bucharest (1969), p. 251.
- Gaur, J. P. and L. M. Chanin, Rev. Sci. Instrum. 39, 1948 (1968); J. Appl. Phys. 40, 256 (1969); J. Appl. Phys. 41, 106 (1970).
- Goldsborough, J. P., Appl. Phys. Lett. 15, 159 (1969).
- Goldsmith, J., A. I. Ferguson, J. E. Lawler, and A. I. Schawlow, Optics Lett. 4, 230-232 (1979).
- Green, R. B., R. A. Keller, G. G. Luther, P. V. Schenck, J. C. Travis, G. G. Luther, Appl. Phys. Lett. 29, 727-729 (1976); J. Amer. Chem. Soc. 98, 517-518 (1976).
- Green, R. B., R. A. Keller, G. G. Luther, P. K. Schenck, J. C. Travis, IEEE J. Quant. Electron. 13, 63-64 (1977).
- Grolleau, B. and Y. Catherine, Phys. Lett. 45A, 225 (1973).
- Groth, W. and F. Harteck, Naturwissenschaften 27, 190 (1939).
- Hackam, R., J. Appl. Phys. 44, 3113 (1973)
- Johnston, T. F., Laser Focus, 58 (March 1978).
- Katayama, D. H., J. M. Cook, V. E. Bondybey, and T. A. Miller, Chem. Phys. Lett. 62, 542-546 (1979).
- Keller, R. A., R. Engelman, and E. F. Zalewski, J. Optl Soc. Amer. 69, 738-742 (1979); also, to be published (1981).
- Kenty, C., Phys. Rev. 80, 95-96 (1950).
- Kenty, C., Bull. Amer. Phys. Soc. 3, 82 (1958); J. Appl. Phys. 38, 4517 (1967).

- King, D. S., P. K. Schenck, K. C. Smyth, and J. C. Travis, *Appl. Opt.* 16, 2617-2619 (1977).
- Latush, E., G. N. Tolmachev, and V. Y. Khasilev, *Sov. J. Quant. Electron.* 6, 1027 (1976); Latush, E., V. Mikhalevskii, G. Tolmachev, and V. Khasilov, *Sov. J. Quant. Electron.* 6, 1251 (1976).
- Lawler, J. E., A. I. Ferguson, J.E.M. Goldsmith, D. J. Jackson, and A. L. Schawlow, *Phys. Rev. Lett.* 42, (1979).
- Lawler, J. E., *Phys. Rev. A*, Accepted for publication 1981.
- Lehmann, O., *Eick Lichterscheinungen*, 265 (1898).
- Loeb, L. B., *J. Appl. Phys.* 29, 1369 (1958)
- Luther, G. G., see R. B. Green (1977).
- Luther, G. G., see R. B. Green (1977).
- Matueeva, N. A., *Bull. Acad. Sci. USSR Phys. Ser. (English Ed.)* 23, 1009 (1959).
- Matsumura, Y. and T. Abe, *Jap. J. Appl. Phys.* 19, L457 (1980).
- Meissner, K. W. and W. Graffunder, *Ann. Physik* 84, 1009 (1927).
- Meissner, K. W. and W. F. Miller, *Phys. Rev.* 92, 896-898 (1953).
- Mierdel, G. , *Handbuch der Experimental Physik XIII* (Academische Verlagsgesellschaft, Leipzig, Germany, 1929).
- Miron, E., I. Smilanski, J. Liran, S. Lavi, G. Erez, *IEEE J. Quant. Elec.* 15, 194-196 (1979).
- Parks, J. H. and A. Javan, *Phys. Rev.* 139, A1351 (1965).
- Pekar, Yu A., *Sov. Phys.* 11, 1024 (1967a); *Sov. Phys.* 12, 800 (1967b).
- Penning, F. M., *Physica* 1, 763 (1934). (1934).
- Pepper, D. M., *IEEE J. Quant. Electron.* 14, 971-977 (1978).
- Pike, E. W., *Phys. Rev.* 49, 513-515 and 515-518 (1936).

- Remer, D. J. and Shair, F. H., Chem. Eng. Prog. Symp. Ser. 67,60, 112 (1971).
- Riesz, R. and G. Dieke, J. Appl. Phys. 25, 196 (1954).
- Sanctorum, C., 11th Int. Conf. on Phenomena in Ionized Gases, Eindhoven (1975), p. 70.
- Schenck, P. K., D. S. King, K. C. Smyth, J. C. Travis, and G. C. Turk, NBS Dimensions, 25-27 (April 1978)
- Schenck, P. K., W. Mallard, J. C. Travis, and K. Smith, J. Chem. Phys. 69, 5147-5150 (1978).
- Schenck, P. K. and K. C. Smyth, JOSA 68, 626 (1978).
- Shair, F. H. and Remer, D. S., J. Appl. Phys. 39, 5762 (1968).
- Shaperev, N., Sov. Phys. Tech. Phys. 18, 1111 (1972).
- Silfvast, W., Appl. Phys. Lett. 30, 179 (1977).
- Skaupy, F., Verh. Deut. Phys. Ges. 18, 230 (1916).
- Skaupy, F. and F. Bobek, Z. Tech. Phys. 6, 284 (1925).
- Skolnick, M. L., IEEE J. Quant. Electron. 4, 139-140 (1970).
- Smith, A.L.S. and S. Moffatt, Optics Commun. 30, 213-218 (1979).
- Smyth, K. C. et al., J. Amer. Chem. Soc. 101, 797 (1979); Chem. Phys. Lett. 55, 473 (1978); Smyth and Schenck, Chem. Phys. Lett., accepted for publication, 1980.
- Sosnowski, J. P., J. Appl. Phys. 40, 5138 (1969).
- Springer, R. H. and B. T. Barnes, J. Appl. Phys. 39, 3100 (1968).
- Thomson, J. J., Proc. Roy. Soc. (Lond.) 58, 244 (1895).
- Tombers, R. B., J. P. Gaur, and L. M. Chanin, J. Appl. Phys. 42, 4855 (1971).

- Travis, J. C. and G. C. Turk, in New Applications of Lasers to Chemistry, G. Hiefjate, ed., Am. Chem. Soc. Symposium Series 85, Washington, D.C. (1978).
- Turk, G. C., J. C. Travis, J. R. Devoe, and T. C. O'Haver, *Anal. Chem.* 50, 817-819 (1978).
- von Tongeren, H., *J. Appl. Phys.* 45, 89 (1974).
- Vidal, C. R., *Optics Lett.* 5, 158-159 (1980).
- Villani, S., Isotope Separation (American Nuclear Society, Hinsdale, Ill., 1976).
- Vygodskii, Ya S., and B. N. Klarfeld, *Zh. Tekh. Fiz.* 3, 610 (1933).
- Waksberg, A. L. and A. I. Carswell, *Appl. Phys. Lett.* 6, 137-138 (1965).
- Weaver, L. A. and R. J. Frieberg, *JAP* 37, 1528 (1966).
- White, A. D. and J. D. Rigden, *Appl. Phys. Lett.* 2, 211 (1963).
- White, J. C., R. R. Freeman, and P. F. Liao, *Optics Lett.* 5, 120-122 (1980).
- Zalewski, E. F., R. A. Keller, and R. Engelman, *J. Chem. Phys.* (accepted for publication, 1980).

Chapter III
THEORY OF POSITIVE COLUMN DISCHARGE

III. THEORY OF POSITIVE COLUMN DISCHARGE

A. INTRODUCTION

This chapter presents the details of an analytic model for the opto-galvanic effect in a positive column discharge (PCD). The first few pages present a general overview of a microscopic model, the strategy adopted to solve the equations, and the theory required to calculate macroscopic, measurable quantities from the model. The next sections describe in detail the application of the outlined model to a hydrogen discharge, and give computational and experimental results. The experiments are described in Chapter VII.

B. OVERVIEW

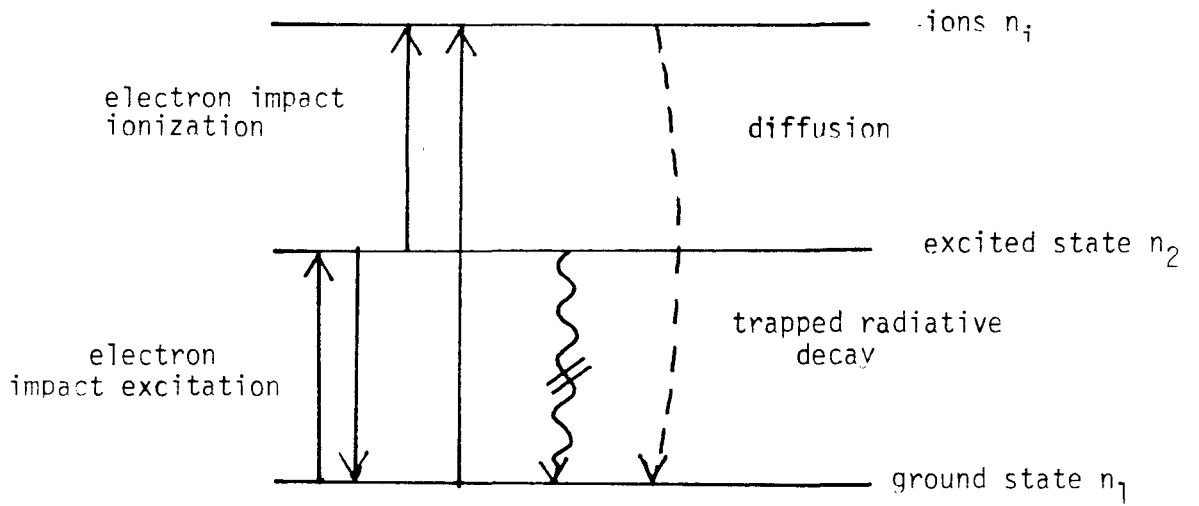
In an atomic positive column discharge, bound electrons are raised to excited states or stripped from atoms primarily by electron collisions. Electrons in excited states may decay to lower states through de-exciting collisions or by radiation. A simple atomic system and the excitation and de-excitation processes consisting of three levels are shown in Fig. III-1. Electrons and ions recombine when they diffuse to the walls.

The rate equations describing the levels in Fig. III-1 for a cylindrical PCD are:

Ionic State: n_c

$$\frac{dn_i}{dt} = n_1 n_e S_{1c} + n_2 n_e S_{2c} - D_a \nabla_r^2 n_c \quad (\text{III.1})$$

Fig. III.1 Simple Atomic System and Competing Rates



Excited State: n_2

$$\frac{dn_2}{dt} = n_1 n_e S_{12} - n_2 n_e S_{21} - n_2 n_e S_{2c} - A_{21} n_2 \quad (\text{III.2})$$

Ground State: n_1

$$\begin{aligned} \frac{dn_1}{dt} = D_a \nabla_r^2 n_c - n_1 n_e S_{12} - n_1 n_e S_{1c} \\ + n_2 n_e S_{21} + A_{21} n_2 \end{aligned} \quad (\text{III.3})$$

where n_e is the electron density

S_{ij} is the rate of transitions per incident electron per atom caused by electron collisions. The subscript "c" refers to the ionization continuum.

D_a is the ambipolar diffusion coefficient

A_{21} is the Einstein A coefficient for the radiative transition 2-1.

Charge balance (neutrality) is assumed to hold in the discharge

$$n_e = n_c$$

To eliminate the radial dependence from the equations, all electrons and ions are assumed to have the same radial distribution, for example, they can be assumed to be in the "fundamental diffusion mode" of the Schottky model discussed below. Thus,

$$D_a \nabla_r^2 n_i \approx D_a n_i / \Lambda^2$$

For steady state, free electrons and ions created in the PCD are assumed to be lost by recombination at the walls. From equation (III.1)

$$\frac{dn_i}{dt} = 0 \quad (\text{steady state}) \quad (\text{III.4})$$

which requires that $D_a = \Lambda^2(n_1 S_{1c} + n_2 S_{2c})$

The electric field in the discharge supplies power to free electrons which excite atoms; the power density supplied to atoms from these equations is

$$\begin{aligned} \text{Power density to atoms} = & n_1 n_e S_{1c} \epsilon_{1c} + n_2 n_e S_{2c} \epsilon_{2c} \\ & + n_1 n_e S_{12} \epsilon_{12} \end{aligned} \quad (\text{III.5})$$

where ϵ_{ij} is the transition energy from state i to state j . Additionally, power is supplied to maintain a "sheath" (a non-neutral layer of steep potential gradient) at the wall (discussed in detail below);

$$\text{Power density to sheath} = \frac{7.85 D_a n_e}{\pi R^2} (5 kT_e) \quad (\text{III.6})$$

The dominant mode of power loss from the discharge is the ϵ_{1c} liberated per recombination event at the wall after diffusion.

$$\text{Power density lost to diffusion} = \frac{7.85 D_a n_e}{\pi R^2} (\epsilon_{1c}) \quad (\text{III.7})$$

Additionally, there are small radiative losses:

$$\text{Power density lost to radiation} = n_2 A_{21} \epsilon_{21} \quad (\text{III.8})$$

Equating power supplied to power lost,

$$\text{Power to atoms} + \text{Power to sheath} = \text{Total Power} \equiv n_e \omega_e$$

$$= \text{Power to diffusion} + \text{Power to radiation} + \text{Power to sheath},$$

where $n_e \omega_e$ is the net power input to the atoms.

The power supplied to the atoms, sheath and diffusion is proportional to n_e ; the power radiated is not. Therefore, n_e may be found from the power balance:

$$\begin{aligned} n_e &= \frac{\text{Power to radiation}}{\frac{\text{Power to diffusion}}{n_e} + \frac{\text{Power to atoms}}{n_e}} \\ &= \frac{\text{Power to radiation}}{\omega_e - \frac{\text{Power to diffusion}}{n_e}} \end{aligned}$$

The macroscopic power P lost by radiation and wall heating must also be the ohmic power supplied from the electric field:

$$P = \underline{J} \cdot \underline{E} = n_e \omega_e \quad (\text{III.9})$$

where J is the current density and E is the electric field. Using Ohm's law, $\underline{J} = \sigma \underline{E}$,

$$\sigma E^2 = n_e \omega_e \quad (\text{III.10})$$

and the electric field is just

$$E = [n_e \omega_e / \sigma]^{1/2} \quad (\text{III.11})$$

The plasma conductivity σ may be calculated from microscopic variables. The standard expression for σ is

$$\sigma = \frac{n_e e^2}{m_e \nu_e} \quad (\text{III.12})$$

where e is the electronic charge, m_e is the electronic mass, and ν_e is the

inelastic collision rate. v_e may be calculated from the inelastic collision rates:

$$v_e = n_1 S_{12} + n_1 S_{1c} + n_2 S_{2c} \quad (\text{III.13})$$

Combining (III.11) and (III.12), E may be calculated solely from the microscopic variables

$$E = \frac{1}{e} \sqrt{m_e v_e \omega_e} \quad (\text{III.14})$$

The total discharge current $I = \pi R^2 J'$; using equations (III.10) and (III.11)

$$I = \pi R^2 n_e \sqrt{\frac{\omega_e}{m_e \omega_e}} \quad (\text{III.15})$$

which yields the current in terms of the macroscopic variables. The product EI is the net macroscopic power consumed.

$$EI = \pi R^2 n_e \omega_e \quad (\text{III.16})$$

The above equations (III.1), (III.2), (III.4), (III.13), (III.14), (III.15), and (III.16) constitute a simple, complete model for characterizing the microscopic and macroscopic properties of a PCD.

These seven equations may be solved in two ways. The first is to guess initial conditions $n_1(t=0)$ and $n_2(t=0)$ and integrate the equations in time numerically until stable populations result. Alternatively, to find just the steady state behavior, $dn_1/dt = 0$; from equation (III.1)

$$n_1 = \frac{D_a n_e / \Lambda^2 + n_2 m_e S_{21} + A_{21} n_2}{n_e S_{12} + n_e S_{1c}} \quad (\text{III.17})$$

Similarly, $dn_2/dt = 0$; from equation (III.2)

$$n_2 = \frac{n_1 n_e S_{12}}{n_e S_{21} + n_e S_{2c} + A_{21}} \quad (\text{III.18})$$

These two equations replace equations (III.1) and (III.2). Initial guesses for n_1 and n_2 can be made, and these nonlinear algebraic equations may then be solved numerically by iteration.

The addition of radiation resonant with the 2-1 transition from an external source changes three of these equations slightly. The rate equations become:

$$\begin{aligned} \frac{dn_1}{dt} &= (\text{previous equation}) - B_{12}n_1\bar{w} + B_{21}n_2\bar{w} \\ \frac{dn_2}{dt} &= (\text{previous equation}) + B_{12}n_1\bar{w} - B_{21}n_2\bar{w} \end{aligned}$$

where

B_{12}, B_{21} are the Einstein B coefficients

\bar{w} is the spectral power density of the external radiation

The power balance is altered by the addition of energy from the external illumination. EI is the ohmic power from the field and is augmented by the amount

$$(-B_{21}n_2\bar{w} + B_{12}n_1\bar{w}) \epsilon_{12} \quad (\text{III.19})$$

Therefore, if the PCD is run at constant current in the presence of external resonant illumination, the local change in field E may be calculated:

$$E = (\text{previous } E) - \frac{1}{I} (B_{21}n_2\bar{w} - B_{12}n_1\bar{w}) \epsilon_{12} \quad (\text{III.20})$$

This replaces equation (III.14). The remaining three equations, (III.4),

(III.13), and (III.15) are unchanged by the radiation. However, the numerical values computed from these equations will be different in the presence of radiation, since n_2 and n_1 also change with illumination present.

The above model allows evaluation of the local changes that occur in the presence of resonant radiation in a PCD. In practice, the PCD might be illuminated longitudinally with a laser, and some absorption of the laser radiation will occur, so the intensity of the illuminating radiation decreases from one end of the discharge to the other. The local change in E will decrease correspondingly. How much the laser light is absorbed depends on the absorption coefficient, which depends on the level populations in the discharge and the laser linewidth; this is treated in detail in Appendix IV.

The voltage change due to illumination measured at the terminals of a discharge is just the sum of the local field changes:

$$\Delta V = \int_0^L \Delta E(\text{local}) dz$$

where L is the length of the PCD.

C. CHOICE OF DISCHARGE MEDIA

The two types of experiments in gas discharges treated in this study, isotope separation and optogalvanic measurements, place some limitations on the choice of a discharge medium. If the application of the above theory is to be kept reasonably simple, there are additional restrictions. Finally, if the isotope separation work is to be

interesting in a practical sense, the isotope should be worth separating.

For either type of experiment (OGE or CLIS), the most important requirement is that it be fairly easy to make and operate a low pressure discharge with a positive column. This eliminates any materials that are hard to vaporize (have low vapor pressures). For the first experiments, it was desirable to choose a permanent gas so that the discharge did not have to be heated. Furthermore, the gas could not be so reactive that it would harm the discharge tube walls or electrodes.

In either type of experiment, the gas has to be excited by external illumination, either a laser or another discharge using the same material. In the latter case, the requirements are that the gas has at least one strong emission line that will not be absorbed by the glass tube that contains the discharge. In the case of laser illumination, the wavelength of the line should be within the tuning range of laser dyes that can be excited by the pump laser available in our laboratory. For an argon ion pump laser, this restricts the wavelengths that can be excited to the approximate range of $6700\text{\AA} - 5600\text{\AA}$.

In order to develop a quantitative understanding of the OGE, it is preferable to have an atom with a relatively simple energy level structure that does not form molecules. Furthermore, the excitation cross sections and the A coefficients should be well documented if any reasonable comparison with theory is to be made.

For CLIS experiments, the isotope shift of the line to be excited must exceed the line's Doppler width in a discharge. Otherwise, a more sophisticated, sub-Doppler approach must be adopted. The isotope shift

must also exceed the linewidth of the exciting source.

Hydrogen seemed like an excellent candidate in almost all respects. The red line of atomic hydrogen (H_{α} , $6563\overset{\circ}{\text{Å}}$) falls in the tuning range of an argon-pumped rhodamine 101 dye laser. Hydrogen A coefficients and electron impact cross sections are better documented than those of any other element. Although H_2 molecules may form in the discharge, they may be nearly eliminated with the addition of a helium buffer (Ausschnitt et al., 1978). The isotope shift is very large (4 cm^{-1} or 125 GHz), and may be resolved by even a relatively crude dye laser (Coherent Model 590) with a nominal bandwidth of 40 GHz.

There are also several drawbacks to using hydrogen. (1) Hydrogen, like many gases, tends to striate in a discharge. This means it tends to separate into small longitudinal regions of high excitation separated by regions of low excitation, giving the whole discharge a "striped" appearance. This is undesirable both because it is not well understood theoretically, and because the striations can be unstable and can produce electrical noise. The helium buffer, added to dissociate H_2 , also reduces the striations greatly. (2) The available red line is a transition between two excited states, so a simulation must include at least three atomic levels (an atom with excitation of a resonance line would only require two), but the hydrogen resonance line L_{α} is at $1215\overset{\circ}{\text{Å}}$, outside the tuning range of any single dye laser.

The next sections discuss the detailed application of the preceding theory to hydrogen.

D. RATE EQUATIONS

Returning to the detailed discussion of the microscopic processes (of which Section III-B presented an overview), rate equations describing the hydrogen atomic levels may be derived. On the microscopic level, the population of any atomic state in a hydrogen PCD is increased by processes that add electrons to that state and decreased by processes that deplete the state. The important processes in hydrogen that must be considered are:

- (i) electron collisional ionization from the ground state;
- (ii) electron collisional ionization from excited states;
- (iii) electron and ion collisional deactivation of excited states;
- (iv) spontaneous emission of radiation;
- (v) diffusion of all species.

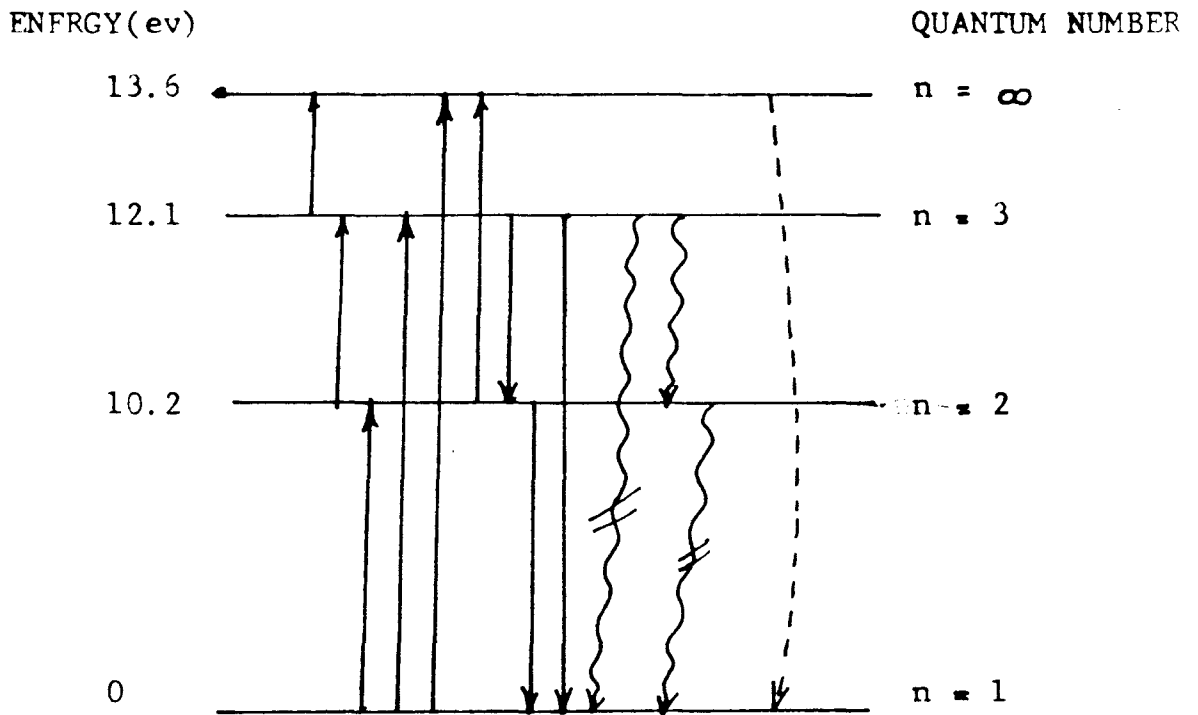
Clearly, this list is not complete, but it does include reactions for calculating the principal characteristics of a PCD.

A Grotrian diagram for hydrogen showing these processes is given in Fig. II-2. The four levels indicated are, with principal quantum number n :

- $n = 1$ the ground state
- $n = 2,3$ the first two excited states
- $n = \infty$ (continuum) free electrons

Each of the above processes depletes the population of the state at the "tail" of the arrow and augments the population of the state at the "tip."

Fig. III.2 Grotrian diagram for four levels of hydrogen. Black arrows represent electron collisional processes; wavy arrows indicate (net) spontaneous radiative transitions; black bars represent radiation trapping of resonance transitions discussed below; the dashed arrow represents ambipolar diffusion of electrons to the walls, followed by recombination.



The rate at which electron collision processes (i, ii, and iii) cause transitions between states i and j is

$$n_e n_i S_{ij} \quad \text{from } i \text{ to } j$$

$$n_e n_j S_{ji} \quad \text{from } j \text{ to } i$$

where n_c = ion density = n_e by charge neutrality
 n_e = electron density
 $n_{i,j}$ = population density of a,b
 S_{ij} = collision rate

The rate at which spontaneous emission (process iv) depletes state a or augments state b is

$$\gamma_{ij} A_{ij} n_i$$

where A_{ij} is the Einstein A coefficient
 γ_{ij} is the "trapping factor" that accounts for the reabsorption of emitted radiation

Electrons and ions in a PCD diffuse to the walls and recombine. This occurs at a rate

$$D_a \nabla_r^2 n_e$$

where D_a is the ambipolar diffusion coefficient
 ∇_r^2 is the radial Laplacian operator

Each of these processes and resulting rates is discussed in detail below.

The net rate of change of each level, dn/dt , is the sum of the rates putting electrons into that state decreased by the sum of rates removing electrons from that state. The net rate of change of the population of each level is given below.

Grand State (n_1)

$$\begin{aligned} \frac{dn_1}{dt} &= (0.269)(n_2 n_e S_{21} + n_3 n_e S_{31}) + D_a \nabla_r^2 n_e \\ &+ (0.432)(\gamma_{31} A_{31} n_3 + \gamma_{21} A_{21} n_2) \\ &= (0.432)(n_1 n_e)(S_{12} + S_{13} + S_{1c}) \end{aligned} \quad (\text{III.21a})$$

First Excited State (n_2)

$$\begin{aligned} \frac{dn_2}{dt} &= -(0.269)(n_2 n_e)(S_{21} + S_{23} + S_{2c}) \\ &+ (0.269) n_e n_e S_{32} + (0.432) n_e n_1 S_{12} \\ &+ (0.432) \gamma_{32} A_{32} n_3 \end{aligned} \quad (\text{III.21b})$$

Second Excited State (n_3)

$$\begin{aligned} \frac{dn_3}{dt} &= -(0.269) n_e n_3 (S_{31} + S_{32} + S_{3c}) \\ &+ (0.432) n_e n_1 S_{13} + (0.269) n_e n_2 S_{23} \\ &- (0.432)(\gamma_{32} A_{32} n_3) + \gamma_{31} A_{31} n_3 \end{aligned} \quad (\text{III.21c})$$

Continuum (free electrons or ions)

$$\begin{aligned} \frac{dn_e}{dt} &= (0.432) n_e n_1 S_{1c} + (0.269) n_e n_2 S_{2c} \\ &+ (0.269) n_e n_3 S_{3c} - D_a \nabla_r^2 n_e \end{aligned} \quad (\text{III.21d})$$

The numerical factors 0.432 and 0.269 appearing in the above equations account for the radial variations of the level populations as discussed in Section 3.f.

It is important to note that rate equations are not true on all time scales. For extremely short times, quantum uncertainty dictates that the system is not in a well defined state. However, these times are orders of magnitude shorter than those of interest in this work. Furthermore, ambipolar diffusion is not established instantaneously--it is established in the time that an electron of thermal velocity requires to travel one mean free path, here about 10^{-7} sec, and rate equations will not yield any valid information for times shorter than this.

1. Electron Impact Excitation and Ionization

a) Theory of impact excitation

The rate per incident electron per target atom at which the transition $i - j$ occurs, S_{ij} , is given by the standard energy integral (see for example, Hasted, 1973)

$$S_{ij} = \int_{\epsilon_j - \epsilon_i}^{\infty} F(\epsilon) \sigma_{ij}(\epsilon) \left[\frac{2\epsilon}{m_e} \right]^{1/2} d\epsilon \quad (\text{III.22})$$

where

ϵ_i, ϵ_j = energy of i, j levels

$\epsilon_{ij} = \epsilon_j - \epsilon_i$

$F(\epsilon)$ = electron distribution function

$\sigma_{ij}(\epsilon)$ = excitation cross section

m_e = electron mass

The total rate at which electrons cause the transition $i \rightarrow j$, Z_{ij} , is the product of the constituent species and S_{ij}

$$Z_{ij} = n_i n_e S_{ij} \quad (\text{III.23})$$

where n_i is the density of atoms in state i , and n_e is the electron density. The typical shape of a dipole allowed cross section is given in Fig. III-3. The product $f(\epsilon) \sigma(\epsilon) \sqrt{\epsilon}$ is also drawn in Fig. III-4 to show the region where impact excitation of the $i \rightarrow j$ transition occurs, in the high energy "tail" of the distribution function, but below the peak of the cross section. The cross section typically peaks at twice the threshold energy ϵ_{ij} , substantially above the peak of the Maxwellian, $kT_e/2$. If the electron distribution function is indeed Maxwellian and the cross section for a dipole-allowed transition is approximated by a linear rise above the threshold ϵ_{ij} , the excitation rate becomes

$$S_{ij} = \left(\frac{8}{\pi m_e}\right)^{1/2} \sigma_{ij \max} \phi(\epsilon_{ij}/kT_e) \exp(-\epsilon_{ij}/kT_e) \quad (\text{III.24})$$

where

$$\phi_{ij}(x) \equiv x^{3/2} \frac{(3+x)}{(1+x)^3} \quad (\text{III.25})$$

and

$$x \equiv \epsilon_{ij}/kT_e \quad (\text{III.26})$$

Since ϕ is a slowly varying function of x , the dominant energy dependence of S_{ij} arises from the exponential factor.

This formula is valid for \underline{i} either the ground state or an excited state, and \underline{j} either an excited state or the ionization continuum, provided

Fig. III-3 Ionization cross section and Maxwellian energy distribution. A Maxwellian (electron) distribution function is shown on the same graph,

$$f(\epsilon) = \left(\frac{m}{2\pi kT_e}\right) e^{-\epsilon/kT} \sqrt{\epsilon}$$

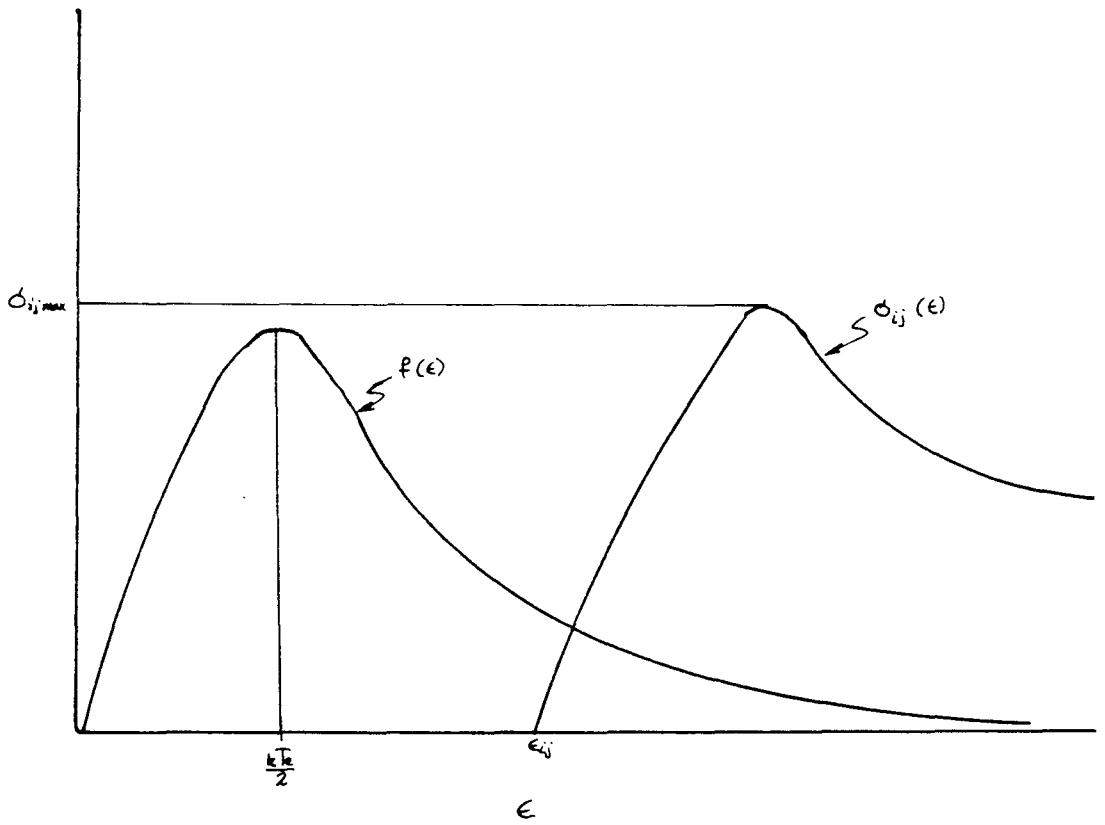
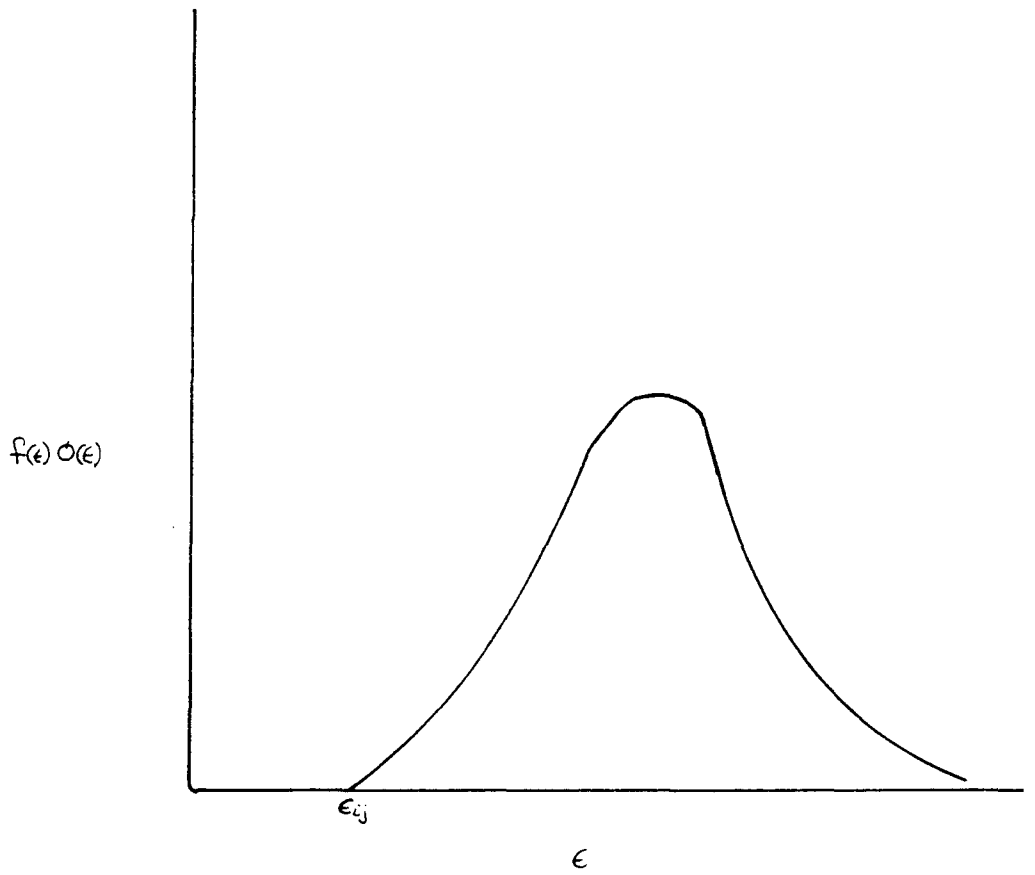


Fig. III-4 Product of a Maxwellian distribution and typical dipole allowed cross-section



the appropriate transition energy and peak cross section are used.

The assumption of a Maxwellian distribution for the electrons or any other distribution, for example a Druyvesteyn distribution (Acton and Swift, 1974), is always an approximation open to question. In particular, it might be expected that the high energy "tail" of the distribution would be depleted (as found in a He-Ne discharge by Heil and Wada (1965), for example. It is a questionable assumption that a low current discharge plasma can be characterized simply by one parameter, the electron temperature. At high electron densities, where electron collisions dominate all other processes, a Maxwellian distribution is usually a good assumption. In low-current discharges of the type under consideration, the high energy tail is usually depleted below that of a Maxwellian fit to the lower energy portion of the distribution because of the depletion in ionizing collisions. The justification for adopting the Maxwellian comes from a check made for a different type of error. The hydrogen peak cross sections, σ_{\max} involved in the calculation of the rates S_{ij} are not all well known (see Appendix I), and it was necessary to check the sensitivity of the model to variations in σ_{\max} (i.e., variations in S_{ij}). The result was that only the ground state ionization cross section had a strong effect on the model, and assuming a Maxwellian distribution for the corresponding excitation rate yielded results in good agreement with experiment. It is thus reasonable to assume a Maxwellian distribution throughout.

b) Theory of electron impact deactivation of excited states

The rate per incident electron per target atom at which the transition $j \rightarrow i$ occurs, S_{ji} , is given by

$$S_{ji}(kT_e) = \int_{\epsilon_j - \epsilon_i} F(\epsilon) \sigma_{ji}(\epsilon) (2\epsilon/m)^{1/2} d\epsilon \quad (\text{III.27})$$

where σ_{ji} is the cross section for the downward transition. The principle of detailed balance says that electron-atom collisions must exhibit time-reversal symmetry; from this, σ_{ji} can be related to σ_{ij} (Seaton, 1962) by

$$\sigma_{ji}(\epsilon) = \frac{\epsilon + \epsilon_{ij}}{\epsilon} \epsilon_{ij} (\epsilon + \epsilon_j) \frac{g_i}{g_j} \quad (\text{III.28})$$

where g_i, g_j are the level degeneracies. Equation (III.24) then yields

$$S_{ji} = g_i/g_j S_{ij} e^{\epsilon_{ij}/kT_e} \quad (\text{III.29})$$

from which the downward excitation rates may be computed.

c) Atomic hydrogen cross sections

There are extensive theoretical and experimental investigations of hydrogen cross sections in the literature. Most of the experimental work, however, is centered on transitions from the ground state, and excited state transitions must be taken from theory without substantial verification. A summary of the cross sections found in the literature is given in Appendix I. Table III.1 below gives the peak cross section values that are used in the model. Where there is uncertainty regarding a cross section, an average value is used; all cross sections represent total values summed over the magnetic sublevels.

The rates S_{ij} and S_{ji} for the transitions in the hydrogen PCD model are presented for several different electron temperatures in Table III.2 as calculated by equation (III.24) using $\sigma_{ij\max}$ from Table III.1 .

Table III-1 Peak cross sections used for computing excitation rates.
 a_0 is the Bohr radius.

Principal Quantum Numbers of Transition	Peak Cross Section, σ_{ij} πa_0^2
1-c	.75
2-c	18.0
3-c	95.9
1-2	.88
1-3	1.25×10^{-2}
2-3	50.0

Table III-2 . Excitation and de-excitation rates of hydrogen (S_{ij} and S_{ji}) as a function of electron temperature. Value in parentheses is the exponent of 10.

E_{ij}	Transition ↓ $i \rightarrow j$	Electron Temperature, T_e (eV)				
		1 eV	2 eV	3 eV	4 eV	5 eV
13.6	1-c	4.82 (-15)	5.93 (-12)	6.7 (-11)	2.3 (-10)	4.8 (-10)
3.4	2-c	2.4 (-9)	1.5 (-8)	2.6 (-8)	3.2 (-8)	3.4 (-8)
1.51	3-c	7.2 (-8)	1.3 (-7)	1.4 (-7)	1.3 (-7)	1.1 (-7)
10.2	1-2	1.7 (-13)	3.7 (-11)	2.3 (-10)	5.8 (-10)	1.0 (-9)
	2-1	1.1 (-9)	1.5 (-9)	1.7 (-9)	1.8 (-9)	1.9 (-9)
12.9	1-3	3.6 (-16)	2.1 (-13)	1.8 (-12)	5.4 (-12)	1.0 (-11)
	3-1	7.2 (-12)	9.8 (-12)	1.1 (-11)	1.2 (-11)	1.3 (-11)
1.89	2-3	3.4 (-8)	8.3 (-8)	9.7 (-8)	9.5 (-8)	8.9 (-8)
	3-2	5.1 (-7)	4.8 (-7)	4.1 (-7)	3.4 (-7)	2.9 (-7)

As before, where there is uncertainty in the value of a peak cross section, an average value is used. Note that S_{ij} , an integral of positive functions, is a monotonically increasing function of energy, and that $S_{ji} > S_{ij}$.

The excitation rates in Table III.2 are in fair agreement with values calculated from much more sophisticated LTE plasma models, the "collisional radiative" models. For a review of the extensive literature in this area, see Biberman et al. (1971); the best known work is that of Bates, Kingston, and McWhirter (1962); see Appendix III for a brief discussion.

2. Radiative Processes

The Einstein A coefficients for the three radiative transitions included in the model are known very accurately (Wiese, Smith, and Glennon, 1966). Their values are given in Table III-3

Table III-3 A-coefficients for the three lowest transitions of hydrogen

Transition (\AA)	A sec ⁻¹
n = 2 to n = 1 (1216)	4.699 x 10 ⁸
n = 3 to n = 1 (1026)	5.575 x 10 ⁷
n = 3 to n = 2 (6563)	4.41 x 10 ⁷

The A-coefficients given above are the values appropriate for a rarified gas; however, a photon emitted from a radiative transition terminating in a highly populated state may be reabsorbed or "trapped." The

result is that the net rates of some strongly allowed transitions are substantially lower than the A-values in Table III.3 . This effect is difficult to analyze theoretically for several reasons. First, the degree of trapping depends on two time scales, the time between emission and absorption by another atom, and the time between absorption and re-emission by the same atom. Second, how long a photon takes to get out of the discharge depends on the size of the plasma and local excitation conditions. Collisional-radiative LTE models are typically solved for infinite plasmas in the limiting excitation regimes of "optically thick" plasmas (highly trapped) and "optically thin" plasmas (no trapping). For small positive column discharges of the type under consideration, the classic analysis is that of Holstein (1947,1951). One of the results obtained by Holstein is that in a small cylindrical discharge the effective A-coefficient for the plasma as a whole is reduced by the factor γ , i.e., A is replaced by γA , where

$$\gamma = \frac{1.6}{(k_0 r (\pi \ln(k_0 r)))^{1/2}} \quad (\text{III.30})$$

and r = discharge tube radius; k_0 = absorption coefficient at Doppler line center. Accordingly, in the present model, the transitions terminating on the ground state are trapped, and trapping coefficients that range from 10^{-1} to 10^{-5} result from ground state densities ranging from 10^{15} to 10^{17} cm^{-3} (0.03 torr to 3 torr).

R. Bartman (1980) has explained to the author that the above application of equation (III.30) from Holstein's theory, while very widely used in the gas-laser literature, is in fact a gross oversimplification.

Holstein's analysis treated the decay of a radially uniform plasma with no pumping. The time constant γ_A is the dominant decay constant (lowest eigenvalue) of the fundamental spatial decay mode (eigenfunction), which is parabolic. The Schottky model of cylindrical discharges (developed in Section 3a) shows that the electron density and radiative excited states have a spatial profile given by the zeroth order Bessel function,

$$n(r) = n(0) J_0\left(\frac{2.4r}{R}\right) \quad (\text{III.31})$$

where R is the discharge column radius. Therefore evaluating radiation trapping in a cylindrical column involves many decay constants, since the projection of J_0 on the basis eigenstates of Holstein's equation involves many of those eigenstates. However, since $J_0\left(\frac{2.4r}{R}\right)$ is not too much different from a parabola for $r < R$, the dominant decay mode is principally the lowest-order one: The overlap integrals for higher-order modes are small. Pumping, such as impact excitation, however, is much harder to account for. Having said all this, equations (III.30) will still be used to account for trapping on the two transitions to the hydrogen ground state. The price of treating trapping to the next order of sophistication is much too high!

3. Diffusion

Plasma constituents can diffuse in several ways. Ions and electrons are subject to ambipolar diffusion; neutrals and excited atoms diffuse against any concentration gradient. In a cylindrical discharge with the anticipated small (10^{-6}) ionization fraction, it is eminently reasonable to assume that the ground state atoms have a uniform radial distribution,

and it is implicit throughout this work. Neglecting the small populations in the excited states, charged species are created predominantly by electron ionization of ground state atoms, and they are destroyed predominantly by radial ambipolar diffusion away from the center of the discharge and eventual recombination at the walls. (For a discussion of the alternative process, volume recombination, see Appendix III).

a) Schottky model

Assuming radial symmetry,

$$\begin{aligned} \text{Ion Production Rate} &= 2\pi r n_e n_1 S_{1c} \\ \text{Radial Diffusion Loss Rate} &= 2\pi r D_a \nabla_r^2 n_c \end{aligned}$$

Equating the production rate to the loss rate, and assuming charge neutrality, $n_e = n_i$,

$$\frac{\partial^2 n_e}{\partial r^2} + \frac{1}{r} \frac{\partial n_e}{\partial r} + \frac{n_1 S_{1c}}{D_a} n_e = 0 \quad (\text{III.32})$$

This is Bessel's equation, and has the solution

$$n_e(r) = n_e(0) J_0\left(\frac{2.4r}{R}\right) \quad (\text{III.33})$$

Requiring n_e to be zero at the walls, the additional constraint

$$\left[\frac{n_1 S_{1c}}{D_a} \right]^{1/2} = \frac{2.4}{R} \quad (\text{III.34})$$

obtains. This is the Schottky discharge model which, having no excited states or radiation, is the simplest positive column model. It is accurate only to the extent that direct ionization from the ground state dominates the discharge excitation processes. Furthermore, some value for the electron temperature must be assumed in order to calculate S_{1c} , when in

reality the electron temperature depends on the electric field and density of the discharge through the common discharge expression

$$E/p \sim T_e$$

This point also turns out to be important in the full model.

One frequently overlooked quirk of the Schottky model is that it does not yield the absolute value of the electron density of a discharge; it determines only the electron density relative to the density on axis. This occurs because the rates of the two processes in the model, collisional ionization and ambipolar diffusion, are both directly proportional to the electron density, which consequently vanishes from the equations. In reality, the electron density is determined principally by the current, which in turn is set by the power supply and ballast resistor of the external circuit. (Positive column discharges typically exhibit a negative incremental resistance and require an external means of limiting the current.)

b) Schottky model with radiation

Radiation from the spontaneous decay of an excited level to the ground state does not depend directly on the electron density. When such a process is added to the basic Schottky model, the electron density is no longer indeterminate, and can be calculated from the model. However, radiation is usually only a small perturbation on the excitation and diffusion in a discharge (i.e., the radiative energy loss is quite small). Thus the argument comes full circle; electron density is set principally by the external circuit, and radiative losses, being small, will adjust

to their "proper" value without grossly affecting the current. This point is belabored here because it turns out to be of the utmost importance in calculating and understanding the optogalvanic effect.

c) Discharge parameter

With this simplest Schottky model, it is possible to calculate some of the gross parameters of the discharge. It is instructive to cover them here, since the more complete model will include refinements on these same calculations.

First, the electrical conductivity of the plasma is given by (see, for example, Reif, 1965)

$$\sigma = n_e e^2 / m_e \nu_e$$

where ν_e is the electron collision frequency

$$\nu_e = n_1 S_{1c}$$

The net specific energy flow (per cm^3 , per electron) into the plasma ω_e is given by

$$\omega_e = n_1 S_{1c} \epsilon_{1c}$$

where ϵ_{1c} is the ionization potential. Finally, Ohm's law,

$$\underline{J} = \sigma \underline{E}$$

relates the current density to the electric field and conductivity.

d) Ambipolar diffusion

The ambipolar diffusion coefficient, D_a presents a special problem. In this simplest model, it has been assumed that all electrons are lost by recombination after diffusion to the walls. Equation (III.34) requires that D_a is pinned at a value that just balances the ion production rate. But an expression for D_a can also be derived by equating net electron and ion flux (Krall and Trivelpiece, 1973)

$$D_a = \frac{(T_e + T_i) D_i D_e}{T_i D_e + T_e D_i} \quad (\text{III.35})$$

where

$$D_i = \frac{kT_i}{m\nu_i} \quad (\text{III.36})$$

is the ion diffusion coefficient, ν_i is the ion-neutral collision frequency, and

$$D_e = \frac{kT_e}{m\nu_e} \quad (\text{III.37})$$

is the electron diffusion coefficient, with T_e, T_i , the electron and ion temperatures, respectively. The two expressions for D_a are related, and they yield similar results for hydrogen; for an electron temperature of 5 eV, $D_a \approx 5 \times 10^4 \text{ cm}^2/\text{sec}$. Unfortunately, this value is at odds with the value $700 \pm 50 \text{ cm}^2/\text{sec}$, measured by Persson and Brown (1955) in a pulsed afterglow experiment. However, Persson and Brown do not state the electron temperature, and their value is simply too low to be credible for a hydrogen positive column; were D_a really that small, the dominant process destroying charged species in the plasma would have to be volume

recombination. This possibility is discussed in detail in Appendix III. But in the OGE model being developed, a diffusion-loss-dominated (or "wall-dominated") plasma is assumed, and any external perturbation (such as radiation) may alter the production rate of ions and electrons. Requiring all ions and electrons to be lost by ambipolar diffusion means that D_a must be large enough to dispose of the ions created by impact ionization of excited states. Thus the proper value for D_a including the two upper states is

$$D_a = \Lambda^2 (n_1 S_{1c} + n_2 S_{2c} + n_3 S_{3c}) \quad (\text{III.38})$$

where

$$\Lambda^2 = (2.405/R)^2 \quad (\text{III.39})$$

In practice, the rate of excitation from the higher states is much less (10^{-3}) than the rate of ionization from the ground state. The essential point remains: D_a is set by the excitation conditions in the discharge, and volume recombination is disregarded.

But now, having set D_a from the rate equations, it is no longer possible to compute the electron density from equation (III.21d). In fact, this equation collapses completely when the above value of D_a is inserted. It is on this point that the analysis by Pepper (1978) went astray. The problem needs additional constraints to yield a unique solution. Specifically, it must be determined what physical processes set the electron density. As in the simplest Schottky model, the answer is radiation and the external circuit. The generalization of the equations describing the power flow, ω_e , to include excited states, will complete the model. This

is the subject of Section E.

For a fixed value of D_a , it is relatively straightforward to integrate the above equations numerically. The results of doing so (with the invocation of volume recombination) are presented in Appendix III, and the computer program is presented in Appendix II. Unfortunately, for the reasons discussed in detail in Appendix III, the results of this approach are not credible. Specifically, for almost any value of D_a , the plasma must be assumed recombination-dominated, which is very much at odds with the putative view of positive columns. Additionally, the three rate equations above do not specify that the power transferred to the plasma from the electric field is equal to the power dissipated by recombination, radiation, and gas heating. Finally, even if D_a is chosen very carefully so that realistic populations result, small perturbations (for example, illumination) cause the system to become unstable.

e) Higher order ambipolar diffusion modes and diffusion of the species

In the simple Schottky model above, there is only one possible spatial diffusion mode, $J_0(\frac{2.4r}{R})$. In a more elaborate model, including more processes (radiation, excited state ionization), it is possible that higher diffusion modes will play a role. Accounting for these would involve solving the radial diffusion equation with more complex excitation. In order to keep the problem tenable, it is therefore assumed that the fundamental diffusion mode dominates, i.e., $\nabla_r^2 D_a \approx D_a/\Lambda^2$, where

$$\Lambda = R/2.405$$

is the characteristic mode length.

There remains the possibility that excited neutral species will diffuse to the walls and be deactivated. However, when this was included in the model, it did not make any substantial difference. Excited state populations were reduced only a few percent below the values they assumed with no diffusion, and it was not deemed necessary to include this process.

f) Spatial approximations

The foregoing discussion of spatial diffusion modes does indicate a problem, however. What is the radial dependence of excited neutral states, and how may it be incorporated in the model? In hydrogen, it is probably a good assumption that excited states also have a $J_0\left(\frac{2.4r}{R}\right)$ electron profile since they are populated by electron collisions, and electrons collide principally with the heavily populated ground state (which is radially uniform). However, calculations for processes involving electrons and an excited state then must account for the "overlap" of two species, both with radial dependence of $J_0\left(\frac{2.4r}{R}\right)$. The problem can be treated simply by calculating two overlap integrals in advance and then using the appropriate numerical value in the rate equation. This scheme was first used by Kenty (1958).

In the first case the spatial overlap (normalized to πR^2) is given by

$$\frac{\int_0^R J_0\left(\frac{2.4r}{R}\right) 2\pi r dr}{\pi R^2} = 0.432$$

In the second case the normalized overlap is

$$\frac{\int_0^R J_0^2\left(\frac{2.4r}{R}\right) 2\pi r dr}{R^2} = 0.269$$

Hence the weighting factors in the rate equations are explained.

4. Other Reactions

Some of the reactions that have been omitted are:

- i) ground-state atom collisions
- ii) collisions between ground state atoms and excited atoms
- iii) ion-atom collisions
- iv) electron attachment
- v) volume recombination
- vi) molecular processes

i) Ground state atom-atom collisions are ignored since the gas temperature in the discharge, even at high currents, does not exceed several hundred degrees K. At these energies (0.01 - 0.1 eV) excitation of the first atomic transition (10.2 eV) is miniscule.

ii) Collisions between a ground state atom and an excited atom, and collisions involving two excited atoms are disregarded, since the density of excited atoms in a typical PCD is very low; at 1 Torr of hydrogen and 100 mA current, the density of the first excited state is $\sim 10^{-3}$ the density of the ground state. Accordingly, excitation resulting from such collisions is negligible because the energy of the constituent atoms is too small, and de-excitation is negligible because of the low densities involved.

iii) Collisions involving excitation of atoms by ions do not affect the positive column significantly. This is because the ion temperature and drift velocity are generally much lower than the corresponding quantities for electrons, in both cases because of the mass difference. The ions, therefore, have a temperature that is not too much different from the neutral temperature (ion-atom elastic collisions in fact tend to equalize the temperatures), and thus lack sufficient energy to excite neutrals. Excited atoms may be de-excited by ions. This is because ions, having a net charge, can interact with the dipole moment of an excited atom. However, the collision frequency of excited atoms and ions is small, since both are heavy and move slowly, and this process will not affect the discharge significantly. Even though the excited state densities and electron density are small, electronic deactivation cannot be ignored, and has been already included in the model. Electron excited atom collisions occur at a very high rate because electrons are light and have high velocities. Deactivation of excited atoms by neutrals or other excited atoms is unimportant since the interaction is at its strongest, dipole-dipole and at its weakest, neutral-neutral; the corresponding de-excitation rate is negligible.

iv) Electron attachment to atoms (resulting in negative ions) has a small effect under normal conditions because any such association (resulting in charged species) has a small binding energy and will be destroyed quickly by collisions with another species, with little macroscopic effect on the discharge. In fact, unusual conditions, such as a shock front are necessary to produce significant quantities of negative hydrogen ions (McDaniel, 1964).

v) The various types of electron-ion volume recombination (radiative and three-body) present special problems, as they are difficult both to measure and to calculate. Estimates of the values for the recombination coefficient for hydrogen vary over many orders of magnitude, from 10^{-4} to 10^{-10} (see McDaniel, 1964; Brown, 1965) and the models used to estimate them are very sophisticated (Bates et al., 1962). In the present work, it was found that a very large recombination coefficient ($10^{-4} - 10^{-5} \text{ cm}^{-3} \text{ sec}^{-1}$) was required before any substantial effect was seen on the positive column plasma. This is discussed at length in Appendix III.

vi) In almost any discharge (except noble gases), the formation of molecules is an essential part of the microscopic kinetic processes, and hydrogen is, unfortunately, no exception. The dominant mode of H_2 production in a low pressure discharge is by association of ground state neutrals at the discharge walls. At high pressures, three-body collisions result in molecular formation also, but at the pressures used in typical PCD's this process is truly negligible. In the body of the discharge, molecules can be dissociated principally by collisions with electrons. For hydrogen the dissociation energy is 4.5 eV, compared to 10.2 eV for excitation of the first excited state.) It might therefore be expected that hydrogen molecules would be present in the body of the discharge; in fact, they can be observed in some discharges. However, molecular association at the walls is critically dependent on surface conditions. Previous investigators looked at various factors affecting molecular dissociation and atomic association. Wood (1921) found that association was enhanced by the presence of water vapor above the inherent recombination rate for H on pyrex or SiO_2 , measured at $\sim 10^{-3}$. Goodyear and von Engel (1961) examined

molecular processes in RF electrodeless discharges. Corrigan and von Engel (1958) deduced a cross section for electron dissociation of H_2 ; Coffin (1959) concluded among other things that dissociation increased with discharge current. Shaw (1959) found that coating the walls of a hydrogen discharge with plastic reduced association. The addition of helium as a buffer gas in the hydrogen discharge will effectively dissociate the hydrogen molecules and act to suppress striations (Ausschnitt et al., 1978). Therefore, the present model does not include any molecular processes, and the experiments were performed with a helium buffer present (typically 5 Torr helium and 1 Torr hydrogen. The possible effects of the buffer on the discharge parameters are discussed in Appendix III.

The final assumption in the composition of this discharge model is that only a few excited states need be considered; specifically, only the ground state, first two excited states, and continuum (ionic) states are included (i.e., principal quantum numbers $n=1,2,3,\infty$). In a low pressure discharge (1 Torr) with low currents (≤ 100 mA), the ground state is by far the most populous. The ionization fraction is quite low, of the order of 10^{-6} . Therefore, the dominant processes are those associated with the ground state; in fact, in the simplest (Schottky) model of a discharge, no excited states were included at all. The excited states have low populations because they are energetically distant from the ground state (> 10 eV) in a plasma with an electron temperature of the order of 5 eV (Ausschnitt et al., 1978; see Chapter VI). Also, the higher the level, the more paths there are for radiative decay (only the 2s level could be termed metastable), and the less likely the radiation will be trapped. That is,

between the effects of the Boltzmann factor and radiative decay, the excited state population of the higher-lying levels becomes progressively smaller. This assumption is confirmed by the results of calculations using the model. Typically $n=3$, the highest level considered, has a population 10^{-6} of the ground state. Experimentally, some H_{β} radiation ($n=4$ to $n=2$) was observed, but little H_{γ} ($n=5$ to $n=2$) was observed, supporting the conclusion that the higher levels are sparsely populated. This simplification also finds some support in the literature; Grolleau, et al. (1973) report that in an excited hydrogen discharge, excited states contribute only a tiny fraction to the net production of hydrogen ions.

E. MACROSCOPIC PARAMETERS

Introduction

The preceding section covered the microscopic processes in a hydrogen PCD. This section discusses the macroscopic properties of the discharge and how they are related through the power balance to the microscopic processes, expanding the treatment begun in the overview to this chapter. The power balance is also used to derive the electron density.

1. Modes of Power Consumption

a) Sheath layer

Electrons are much lighter than ions and their mobility is greater by a factor of $(m_e/m_{ion})^{-1}$. Thus the flux of electrons toward the walls of a discharge greatly exceeds the ion flux, and the walls must acquire a net negative charge to repel most of the slower electrons. In steady state, the net flux of ions and electrons is equal, and the wall acquires this

"floating potential," given by

$$V_{\text{float}} = \frac{kT_e}{e} \ln(V_e/V_c)$$

where V_e, V_c are the electron and ion mean thermal velocities. Of course this means that ions are accelerated toward the walls in this gap, called the sheath. They acquire an energy of about $5 kT_e$ in passing through the sheath, and this energy (which is distinct from the excitation energy) must also be supplied to the plasma from the electric field.

b) Microscopic power distribution

The power input (per cm^3) from electric field that results in the excitation and ionization of atoms is, instead of equation (III.5),

$$\begin{aligned} P_{\text{in}} &= n_1 n_e (S_{1c} \epsilon_{1c} + S_{13} \epsilon_{13} + S_{12} \epsilon_{12}) \quad (0.432) \\ \text{atom} & \\ &+ n_2 n_e (S_{23} \epsilon_{23} + S_{2c} \epsilon_{2c}) \quad (0.269) \\ &+ n_3 n_e S_{3c} \quad (0.269) \end{aligned} \quad (\text{III.40})$$

An electron deactivating an excited state inherits the energy lost by the atom, so the net flow of energy from the field (per cm^3) into the atoms is

$$\begin{aligned} P_{\text{net}} &= P_{\text{in}} - 0.269 n_e n_2 S_{21} \epsilon_{12} \\ \text{atom} & \quad \text{atom} \\ & - 0.269 n_e n_3 (S_{32} \epsilon_{23} + S_{31} \epsilon_{13}) \end{aligned} \quad (\text{III.41})$$

When an ion diffuses to the wall and recombines, it transports energy from the plasma to the external world in the form of wall heating; this process is the dominant loss mechanism. The ion will liberate the energy ϵ_{1c}

(13.6 eV) that was required for its creation from a ground state atom. It will also lose whatever energy it has acquired in traversing the wall sheath and perhaps some of its thermal energy as well; if the wall is at some equilibrium temperature, the neutral atoms leaving it will have the thermal energy appropriate to the wall temperature. The total power (per cm³) delivered to the plasma from the field is then

$$P_{\text{total}} = P_{\text{net atom}} + \frac{7.85}{\pi R^2} D_a n_e(0)(5 kT_e) \equiv n_e \omega_e, \quad (\text{III.42})$$

since the wall flux Γ of ions in the assumed Schottky $J_0 \left(\frac{2.4r}{R} \right)$ profile is

$$\Gamma_{\text{ions}} = D_a \nabla_r n_e \Big|_{r=R} = 7.85 D_a n_e(r=0) \quad (\text{III.43})$$

and $5 kT_e$ is the energy acquired from acceleration through the sheath.

The total power per cm³ lost from a positive column is straightforward to calculate. Losses occur from radiation, recombination at the walls, and the aforementioned wall sheath.

The energy (per cm³) lost due to radiative decay is approximately (since the simple trapping factor γ may not be an accurate expression of this process as previously described)

$$P_{\text{radiative}} \approx (\gamma_{21} A_{21} \epsilon_{12} + \gamma_{31} A_{31} \epsilon_{13} + A_{32} \epsilon_{32}) (0.432) \quad (\text{III.44})$$

The energy lost (per cm³) through diffusion to the wall is

$$P_{\text{diffusion}} = \frac{7.85 D_a n_e}{\pi R^2} (\epsilon_{1c} + 5 kT_e) \quad (\text{III.45})$$

and thus

$$P_{\text{total}} = P_{\text{diffusion}} + P_{\text{radiation}} \quad (\text{III.46})$$

where gas heating or thermal loss from the discharge has been assumed small. The above equation may be solved for n_e :

$$n_e = \frac{P_{\text{radiation}}}{w_e - \frac{P_{\text{diffusion}}}{n_e}} \quad (\text{III.47})$$

This is the required additional constraint equation for electrons and the excited level populations are determinate, although not soluble analytically.

c) Gross parameters

The above model given n_1 (actually gas pressure p) and T_e as inputs, yields n_2, n_3 and the power flow in the discharge; it may be used to calculate gross PCD parameters as well.

The electron inelastic collision frequency, ν_e , in the presence of excited states is

$$\begin{aligned} \nu_e = & (0.432)n_1 (S_{1c} + S_{13} + S_{12}) \\ & + (0.269)n_2 (S_{23} + S_{2c}) \\ & + (0.269)n_3 (S_{3c}) \end{aligned} \quad (\text{III.48})$$

and thus the ohmic conductivity of the plasma column is known; as before, $\sigma = n_e e^2 / m_e \nu_e$, and Ohm's law, $J = \sigma E$ holds as in Section B.

Macroscopically, the power delivered to the plasma is $P = \underline{J} \cdot \underline{E} = \sigma E^2$. But P is known from the microscopic model; eliminating it from equation (III.42)

$$E = \frac{1}{\sqrt{.432}} \sqrt{m_e \nu_e \omega} \quad (\text{III.49})$$

The current $I = (0.432) \cdot \underline{J} \cdot \pi R^2$, and from Ohm's law,

$$I = \pi R^2 \sqrt{.432} e n_e \sqrt{w_e / m_e v_e}$$

Thus the model yields the plasma conductivity, electric field, and current for a given pressure and electron temperature. Due caution must be exercised in applying this model to data taken "at the terminals" of a discharge, since electrode processes, particularly the cathode fall, are not included.

d) Computational strategy

Initial computation with these equations yielded numerical results, but it was also obvious that the equations are somewhat difficult to work with, and need to be recast in a better form for numerical computation. There are two subtle problems. The first is that the electron density depends directly on the radiation loss, which is hard to calculate accurately because of trapping and represents, as noted previously, only a small perturbation on the plasma. Determining n_e directly from the radiation is like having a tiger by the tail; a small disturbance can have dramatic consequences.

Additionally, the rate equations are quite "stiff," meaning they involve multiple time scales. Terms which are large at $t=0$ and dominate the initial transient behavior ("fast" terms) can "fade" at longer times when other "slow" terms have a dominant effect. While sophisticated numerical integration routines can deal with this problem, much computer time is involved and results can be quite expensive to obtain.

Experimentally, as noted, the electron density is determined primarily by the external circuit and the small radiative loss adjusts to

some "proper" value. Heuristically, this suggests that fixing the current (i.e., making it an input) and then, with the fixed-current condition, making a first estimate of n_e , might be a good way to proceed. This estimate could then be used with the rate equations to yield the excited state populations, electric field, and power dissipated into diffusion and radiation. There is the added benefit that constant current (even with resonant external illumination) is relatively easy to achieve experimentally. Thus, if I is fixed as an input, n_e is given by

$$n_e = \frac{I}{\pi R^2 e \sqrt{.432}} \sqrt{\frac{\nu_e m_e}{\omega_e}}$$

where ν_e and ω_e actually depend, of course, on the level populations.

At low currents, the ionization fraction n_e/n_1 is small (10^{-6}), and the perturbation of the ground state may be assumed negligible;

$$\frac{dn_1}{dt} \approx 0$$

and n_1 is determined by the pressure only. In fact, all of the numerical results for the PCD described in the next section were computed twice, with and without this assumption, and no significant differences were noted.

The model now consists of the following set of equations:

Rate equations

$$\begin{aligned} \frac{dn_2}{dt} = & -(0.269)(n_2 n_e) S_{21} + S_{23} + S_{2c} \\ & + (0.269) n_e n_3 S_{32} + (0.432) n_e n_1 S_{12} \\ & + (0.432) \gamma_{32} A_{32} n_3 \end{aligned} \tag{III.50}$$

$$\begin{aligned} \frac{dn_3}{dt} = & -(0.269) n_e n_3 (S_{31} + S_{32} + S_{3c}) \\ & + (0.432) n_e n_1 S_{13} + (0.269)(n_e n_2 S_{23}) \\ & - (0.432)(\gamma_{32} A_{32} n_3 + \gamma_{31} A_{31} n_3) \end{aligned} \quad (\text{III.51})$$

Electron density

$$n_e = \frac{1}{\pi R^2} \frac{I}{\sqrt{.432}} \sqrt{\frac{\nu_e m_e}{\omega_e}} \quad (\text{III.52})$$

where ν_e , the collision frequency and ω_e , the power input are given by equations (III.48) and (III.42), respectively, and the electric field may be calculated from

$$E = \frac{1}{\sqrt{.432}} \sqrt{m_e \nu_e \omega_e} \quad (\text{III.53})$$

This model requires the pressure n_1 , the current I , and the electron temperature T_e as inputs. These three variables are not independent, and hence may not be specified arbitrarily.

Extending the model to include the interdependence of these parameters is possible, but not desirable. The dependence of T_e on n_1 , for example, may be calculated by the method of Dorgela, Alting, and Boers (1935), but their accuracy is suspect, especially when the method is extended to include excited states.

Since n_1 , I , and T_e may be measured, the alternative approach of specifying them consistently from experimental results is adopted. Figure VI-5 of Chapter VI contains the necessary data. An approximate linear fit to the T_e vs. I curves, useful for characterizing the PCD (results are

in the next section) is

$$I = (T_e - 2.5) / (.105 \times 10^{-3})$$

thus a range of T_e from 2.5 to 7 eV corresponds to a current range of 0 to 43 mA, independent of pressure within experimental error. (The later work on OGE uses measured values for T_e and I , removing the approximation inherent in this equation.

e) Steady state strategy

To find the steady state behavior of the model, equations (III.50) through (III.53), first the three parameters n_1 , T_e , and I are specified. Since in steady state

$$\frac{dn_2}{dt} = \frac{dn_3}{dt} = 0, \quad (III.54)$$

equation (III.50) for n_2 may be recast:

$$n_2 = \frac{0.432 n_e n_1 S_{13} + 0.269 n_e n_3 S_{32} + 0.432 n_3 A_{32}}{0.432 \gamma_{21} A_{21} + 0.269 n_e (S_{21} + S_{23} + S_{24})} \quad (III.55)$$

Similarly, from equation (III.51)

$$n_3 = \frac{0.432 n_e n_1 S_{13} + .269 n_e n_2 S_{23}}{0.269 n_e (S_{31} + S_{32} + S_{34}) + 0.432 (A_{32} + \gamma_{31} A_{31})} \quad (III.56)$$

The computational strategy is to make initial guesses for n_2 and n_3 . The collision frequency ν_e and power balance ω_e are calculated from equation (III.48) and (III.42), followed by new values for n_2 , n_3 , and n_e from equations (III.50), (III.51), and (III.52). The process is iterated until the populations no longer change, and then the electric field and power loss may be computed.

In fact this approach works quite well and is relatively inexpensive. The initial guesses for n_2 and n_3 (analogous to initial conditions in the rate equation formulation of the problem) do not affect the final values achieved for n_2 and n_3 (i.e., the solution appears not to be multivalued); they only affect the number of iterations required for convergence. Information about the transient response is lost. Of course the purpose is not really to calculate the transient response of the PCD without illumination, so the loss is small. Transient behavior with illumination is discussed later.

F. CALCULATED RESULTS FOR STEADY STATE PCD WITHOUT ILLUMINATION

Although the principal goal of this work is to evaluate the optogalvanic effect, the model that has been developed can be used to characterize a hydrogen positive column without external illumination. The prerequisite for credible results is that the input parameters, n_1 , T_e , and I be specified consistently. They are not independent parameters, as noted previously.

1. Level Populations

a) $n = 2$

Figure III-5 below shows the population of the first excited level ($n = 2$) as a function of current for three different pressures. It yields the not altogether surprising result that n_2 increases with pressure and electron temperature.

b) $n = 3$

Figure III-6 is the equivalent plot for $n = 3$; the conclusion is similar.

Fig. III-5 First excited state populations ($n = 2$) as a function of pressure and current (see text)

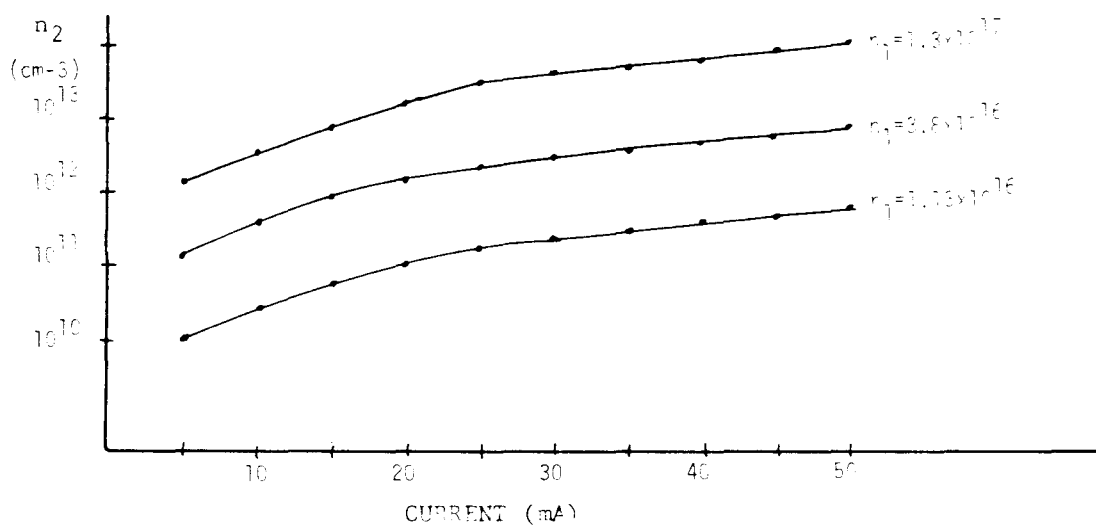
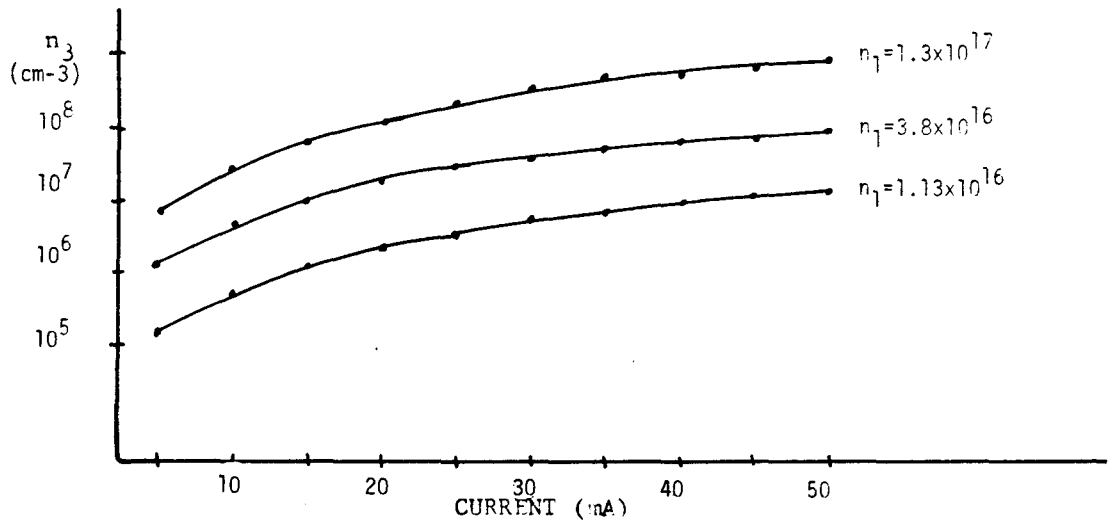


Fig. III-6 Second excited state population as a function of pressure and current.



In both these plots the excited state population is much less than the ground state population, as was expected.

For any level, the net population is determined as a balance between gain and loss. For two levels i and j ,

$$\text{gain} = \text{collisional loss} + \text{radiative loss}$$

$$n_e n_i S_{ij} = n_e n_i S_{ji} + n_j A_{ji} \quad (\text{III.57})$$

Therefore,

$$\frac{n_j}{n_i} = \frac{S_{ij} n_e}{S_{ji} n_e + A_{ji}} \quad (\text{III.58})$$

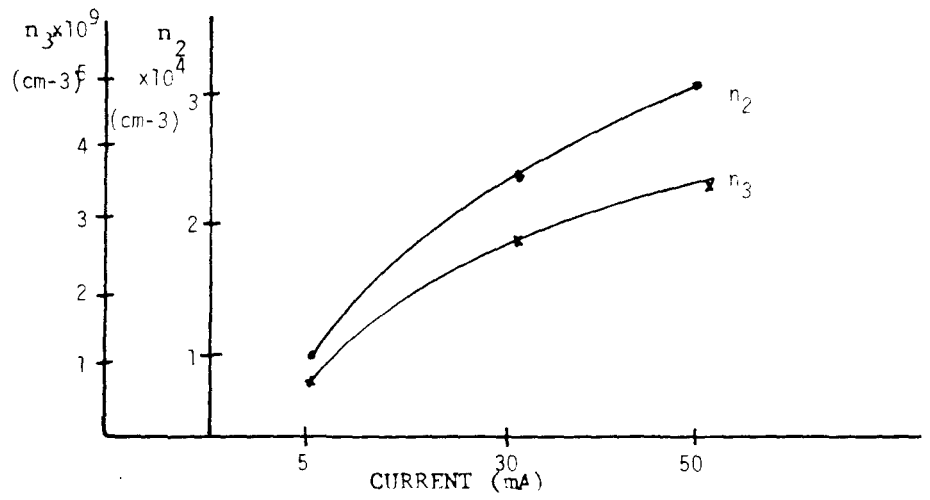
In the absence of radiation (for example, if state b is metastable), $A_{ji} = 0$. From equations (III.24) and (III.29) the simple Boltzmann factor

$$\frac{n_j}{n_i} = \frac{g_j}{g_i} e^{-\epsilon_{ij}/kT_e} \quad (\text{III.59})$$

obtains, where $\epsilon_{ij} = \epsilon_j - \epsilon_i$. Thus the population of metastable levels in a PCD is expected to be much higher than the population of levels where there is radiation and a large A_{ji} decreases n_j/n_i in equation (III.58). Figure III-7 shows the excited level populations of a hydrogen PCD as a fraction of the thermal equilibrium value of equation (III.59). For $n = 3$, the fraction is $\approx 3 \times 10^{-9}$, and for $n = 2$, 2×10^{-4} .

These very low values supply verification of the assumption in Section III-D-4 that the population of excited states does not substantially affect the discharge column, since at these low currents radiative decay dominates excited state losses. For states higher than $n = 3$, as noted, the population falls off very rapidly due to the many radiative

Fig. III-7 Level population as a fraction of thermal equilibrium value
at $p = 1.1$ Torr



de-excitation paths available.

c) Electron density

In Figure III- 8 the electron density is given as a function of current. The electron density was found to vary only about 3% over a factor of 10 in pressure, and is thus not shown on the graph. This verifies the assumption that electron density is determined primarily by current and T_e .

d) Electric field

Finally in Figure III-9 , the electric field is presented as a function of pressure and current (T_e). Not too surprisingly, E increases with both T_e and pressure, which recalls the standard relation $E/p \sim T_e$.

Fig. III-8 Electron density as a function of current (T_e)

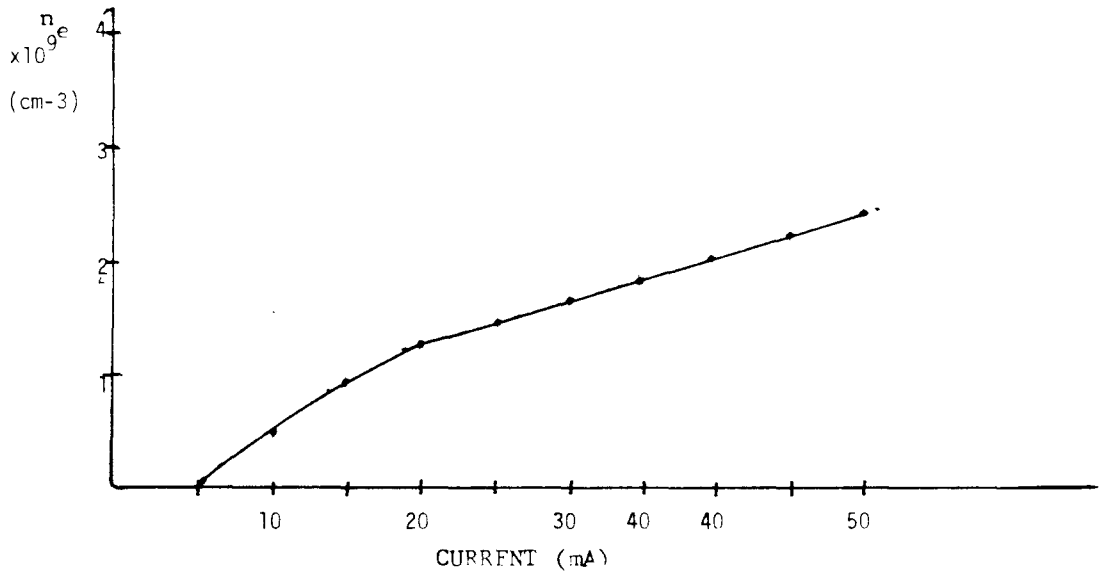
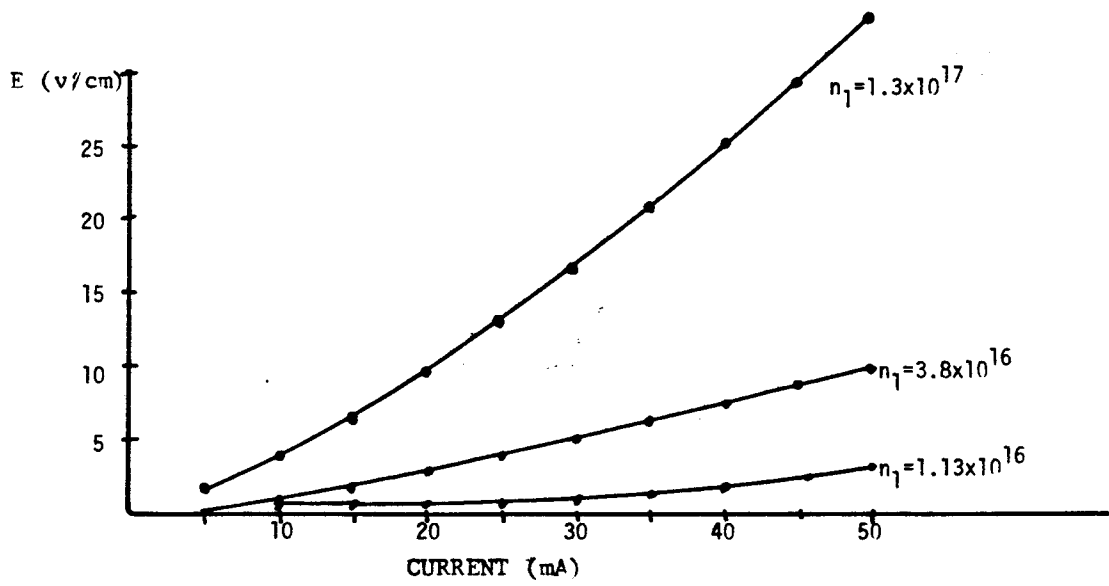


Fig. III-9 Electric field as a function of current (T_e) for several different pressures



REFERENCES - Chapter III

- Acton, J. R. and J. D. Swift, Cold Cathode Discharge Tubes (Academic Press, New York, 1974).
- Ausschnitt, C. P. and G. C. Bjorklund, *Optics Lett.* 4, 4-5 (1979).
- Ausschnitt, C. P., G. C. Bjorklund, and R. R. Freeman, *Appl. Phys. Lett.* 33, 851-853 (1978).
- Bartman, R., 1980, private communication.
- Bates, D. R., A. E. Kingston, and R.W.P. McWhirter, *Proc. Roy. Soc. A* 267, 297-312 (1962); *Proc. Roy. Soc. A* 270, 155-167 (1962).
- Biberman, L. M., I. T. Yakubov, and V. S. Vorob'ev, *Proc. IEEE* 59, 555-572 (1971).
- Brown, S., Basic Data for Plasma Physics (MIT Press, Cambridge, 1965).
- Coffin, F. D., *J. Chem. Phys.* 30, 593 (1959).
- Corrigan, S.J.B. and von Engel, A., *Proc. Roy. Soc. A* 245, 335 (1958).
- Dorgela, H., H. Alting, and J. Boers, *Physica Haag* 2, 959 (1935).
- Goldsmith, J., A. Ferguson, J. Lawler, and A. Schawlow, *Opt. Lett.* 4, 230-232 (1979).
- Goodyear, C. C. and von Engel, A., Proc. 5th Int'l. Conf. Ionization Phenomena in Gases, Munich (1961).
- Grolleau, B. and Y. Catherine, *Phys. Lett.* 45A, 225 (1973).
- Hasted, J., Physics of Atomic Collisions, 2nd Ed. (Amer. Elsevier Publ. Co., New York, 1972).
- Heil, H. and J. Wada, *J. Quant. Electron.* QE-1, 327 (1965).
- Holstein, T., *Phys. Rev.* 72, 1212 (1947); *Phys. Rev.* 83, 1159 (1951).
- Kenty, C., *Bull. Amer. Phys. Soc.* 3, 82 (1958); *J. Appl. Phys.* 38, 4517 (1967).
- Krall, N. and A. Trivelpiece, Principles of Plasma Physics (McGraw-Hill New York, 1973).

- McDaniel, E. W., Collision Phenomena in Ionized Gases (John Wiley, New York, 1964).
- Pepper, D. M., IEEE J. Quant. Electron. 14, 971-977 (1978).
- Persson, K. B. and S. C. Brown, Phys. Rev. 100, 729-733 (1955).
- Reif, F., Statistical and Thermal Physics (McGraw-Hill, New York, 1965).
- Seaton, M. J., Atomic and Molecular Processes, ed. D. Bates (Academic Press, New York, 1962).
- Shaw, T. M., J. Chem. Phys. 30, 1366 (1959); J. Chem. Phys. 31, 1142 (1959).
- Wiese, W., M. Smith, and B. Glennon, Atomic Transition Probabilities I, (NSRDS-NBS-4, U.S. Gov't. Printing Office, Washington, D.C. 1966).
- Wood, R. W., Phil. Mag. 42, 729 (1921).

Chapter IV

EFFECT OF RESONANT ILLUMINATION:
THEORY AND EXPERIMENTAL RESULTS

IV. EFFECT OF RESONANT ILLUMINATION: THEORY AND EXPERIMENTAL RESULTS

A. EFFECT OF RESONANT ILLUMINATION--STEADY STATE

The preceding theory may be extended to include the effect of external resonant illumination on the discharge level populations, and, ultimately, the macroscopic properties of the discharge: voltage, current, or impedance.

1. Rate Equation Changes

Only simple additions need to be made to the preceding model to include the effects of external illumination resonant with the $n=2$ to $n=3$ transition of hydrogen. If the rate per atom of upward transitions induced is R_{23} , and the corresponding downward rate is $R_{32} = g_2/g_3 R_{23}$, then the right side of equation (III.50) is augmented by the term

$$0.432(-R_{23}n_2 + R_{32}n_3)$$

and the right side of equation (III.51) is, of course, diminished by the same term. The spatial form factor of 0.432 assumes uniform illumination of the positive column. The gaussian profile of the laser could be accounted for by changing this constant, but this correction is ignored here.

The logical way to proceed is by adopting the same fixed-current computational scheme as in Section III.E. Experimentally, a fixed current may be achieved by using a ballast resistor in series with the discharge that is large enough to dwarf the small conductivity change caused by the illumination.

The conductivity σ will change in the presence of illumination through the change in n_2 and n_3 which will change through the electron collision

frequency, ν_e (see equation (III.48)). It is found from computation that $\Delta\nu_e/\nu_e$ is less than 10^{-6} for all PCD conditions considered, and laser power up to 400 mW. Thus the illumination does not contribute significantly to the discharge conductivity over the range. The computed change in conductivity, assuming the discharge impedance ($4k\Omega$) is less than $10^{-6} \times (4k\Omega) = 4 \times 10^{-3} \Omega$, which is tiny compared to the 25 k Ω and 40 k Ω ballast resistors used in the experiment. The assumption of fixed current with illumination is thus justified, and the computational strategy of Section (III.E.c) is adopted. Accordingly, equation (III.55) becomes

$$n_2 = \frac{0.432 n_e n_i S_{12} + 0.269 n_e n_3 S_{32} + 0.432 (n_3 A_{32} + n_3 R_{32})}{0.432 (\gamma_{21} A_{21} + R_{23}) + 0.269 n_e (S_{21} + S_{23} + S_{2c})} \quad (IV.1)$$

Equation (III.56) similarly, is now

$$n_3 = \frac{0.432 n_e n_i S_{13} + 0.269 n_e n_2 S_{23} + 0.432 n_2 R_{23}}{0.269 n_e (S_{31} + S_{32} + S_{3c}) + 0.432 (A_{32} + \gamma_{31} + R_{32})} \quad (IV.2)$$

2. Power Balance

The final change that must be made to the model is in the power balance. The electronic power into the discharge is now augmented by the power absorbed from the illumination. Without radiation, the ohmic power was given from (III.53)

$$EI = \frac{1}{e} \frac{I}{\sqrt{.432}} \sqrt{m_e \nu_e \omega_e}$$

With radiation, the net power is

$$EI = \frac{1}{e} \frac{I}{\sqrt{.432}} \sqrt{m_e \nu_e \omega_e} - (R_{23} n_2 - R_{32} n_3) \epsilon_{23} \quad (IV.3)$$

where ν_e and ω_e are written with a prime to emphasize that they will be slightly affected by the presence of illumination; how much they are actually affected comes out of iterating the equations in the model. Dividing this equation by the current yields the expression used with the rate equations to find the voltage change caused by the light, i.e., the optogalvanic effect.

In extending the theory, it has been tacitly assumed that the electron temperature does not change when H_α illumination excites the discharge. Including a change in T_e measured from experiment is trivial; calculating it entails the same problems that plague calculating T_e (discussion in Section III.E). However, the change in T_e induced by the radiation is much less than the error in our ability to measure T_e (see Chapter VII) as limited by the noise present in the tube, so it is quite likely that it is also too small to affect the results significantly.

As it now stands, the model requires four inputs: current I , electron temperature T_e , pressure n_1 , and the per atom rate of optical excitation R_{23} . From these parameters the electric field, excited state populations, radiative loss, and electronic power per unit length of positive column can be calculated. The only task remaining before the model can be compared with experiment is to account for the longitudinal absorption of resonant illumination in the PCD. This is covered in detail in Appendix IV, and is summarized in Section 3 below.

3. Linewidths and Absorption of External Radiation

The detailed derivation of the dependence of the OGE on the laser bandwidth and the absorption coefficient of the gas is contained in Appendix IV. Some results from that appendix are used below.

At low intensities, external monochromatic radiation at frequency is absorbed exponentially in a Doppler-broadened medium:

$$I = I_0 e^{-\gamma(\nu)z} \quad (IV.4)$$

where I is the monochromatic intensity of the external radiation

I_0 is the incident intensity (before any absorption)

z is distance along the discharge

$$\gamma(\nu) = \frac{A_{32}\lambda^2}{8\pi c^2} \left[n_3 - \frac{g_3}{g_2} n_2 \right] g_D(\nu)$$

where $g_D(\nu)$ is the Doppler lineshape of the absorbing gas.

$$g_D(\nu) = \frac{2\sqrt{\ln 2}}{\sqrt{\pi} \Delta\nu_D} \exp\left[-4 \ln 2 \left(\frac{\nu - \nu_D}{\Delta\nu_D}\right)^2\right]$$

where ν_0 is the center frequency of the line

$\Delta\nu_D$, the Doppler linewidth, is given by

$$\Delta\nu_D = 2\nu_D \sqrt{\frac{2k T_n}{Mc^2 \ln 2}}$$

where T_n is the absorbing gas temperature.

As discussed in Appendix IV, the monochromatic low intensity radiation produces a local change in electric field directly proportional to local intensity

$$\Delta E_{\text{local}} \equiv c'' I_{\text{local}} \quad (IV.5)$$

where the constant of proportionality c'' is calculated from the numerical simulation. The OGE voltage measured at the terminals of the discharge is

just the sum of these local voltage changes,

$$\Delta V(\nu) = \int_0^L \Delta E_{\text{local}} dz \quad (\text{IV.6})$$

$$= c'' I_0 \frac{1}{\gamma(\nu)} [1 - e^{-\gamma(\nu)L}] \quad (\text{IV.7})$$

If the illuminating radiation is not monochromatic (as is the case for the Coherent 590 laser with a 40 GHz bandwidth), the OGE voltage must be summed over the beam's spectral components, taking into account the fact that different frequencies are absorbed differently as equation (IV.4) indicates. That is, equation (IV.4) must be integrated over frequency. The "exact" result is

$$\Delta V = c' I_0' \frac{8\pi}{n_2 \lambda^2 A_{32}} \int_{-\infty}^{\infty} d\nu [1 - e^{-\gamma(\nu)L}] \quad (\text{IV.8})$$

where

$$I_0' = I_0 / \Delta\nu_L$$

$$\Delta\nu_L = \text{laser bandwidth}$$

As a simplification, it might be assumed that all of the incident radiation within the absorption linewidth of the medium is absorbed in one folding length, $1/\gamma(\nu_0) \equiv \ell$. In this case, the OGE voltage measured at the terminals of the discharge is

$$\Delta V = \ell c' I_0' [1 - e^{-L/\ell}] \quad (\text{IV.9})$$

This is referred to as the "crude" theory.

B. RESULTS FOR STEADY STATE PCD WITH ILLUMINATION

1. Change in Excited State Populations

The external illumination causing the OGE changes the atomic level populations n_2 and n_3 (most notably n_3) as well as the electron density n_e . Employing the above method of specifying consistent inputs, Figs. IV-1, IV-2, and IV-3 show the induced population changes bandwidth (40 GHz) under different discharge conditions calculated from the rate equation model for an illumination much greater than the absorption linewidth (6 GHz).

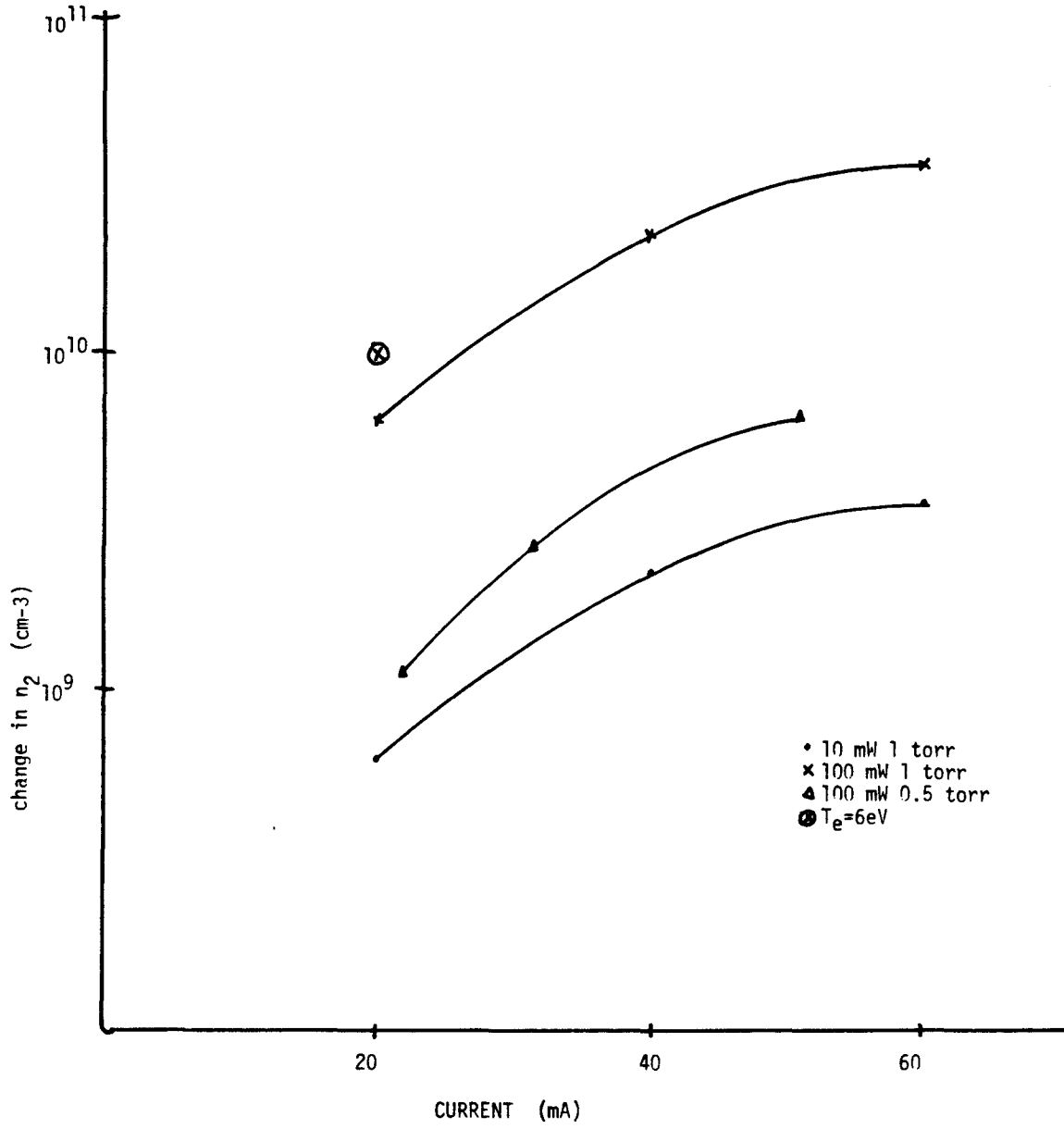
a) $n = 2$

In general, Δn_2 is directly proportional to the illumination intensity within the absorption line. The point marked \otimes indicates Δn_2 calculated for $T_e = 6$ eV at 20 mA instead of the ≈ 4.5 eV indicated by Fig. VI-5, and is a rough gauge of the effect of the inaccuracy inherent in T_e on Δn_2 . The effect on Δn_2 is not large, which augurs well for the model as a whole. Variations in T_e should not affect the outcome of other calculated quantities either. $\Delta n_2/n_2$ was typically 10^{-3} (at 100 mW), justifying the approximation of Section V.C.1 that $\tilde{n}_2 = 0$ (note $n_2(t = \infty) \equiv \Delta n_2$). The perturbation of level $n = 2$ is thus not very large.

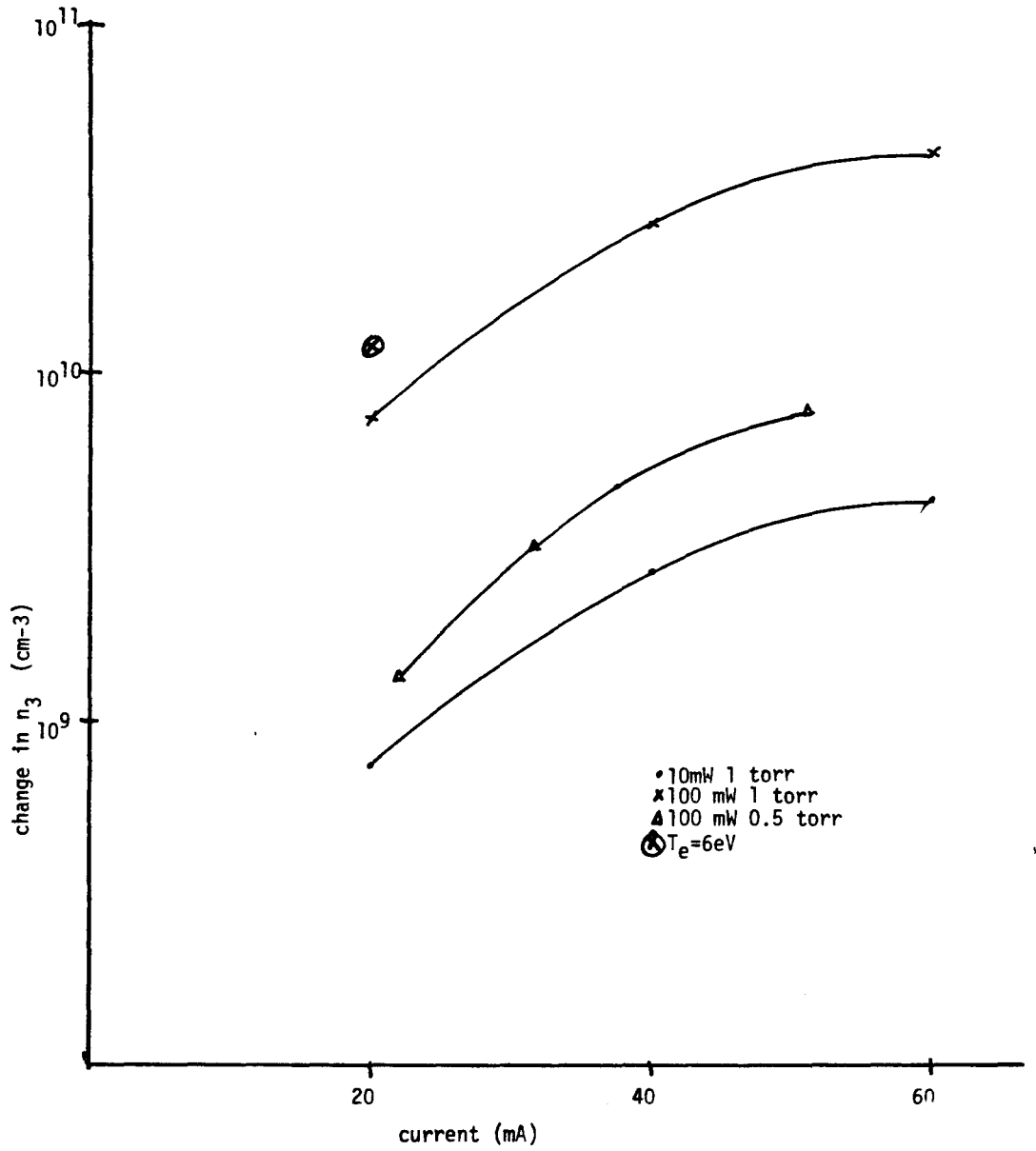
b) $n = 3$

Figure IV-2 gives the calculated results. As expected, $\Delta n_3/n_3 \approx 10^1 \sim 10^2$, meaning n_3 is sparsely populated in the absence of exciting radiation, supporting the previous assumption that higher levels than $n = 3$ are unpopulated. The calculated value of Δn_3 also is directly proportional to laser intensity. Again, the change in n_3 introduced by changing

Fig. IV-1 Calculated change in first excited state ($n=2$) population at $z < 0$ of a hydrogen positive column caused by resonant H_{α} illumination



IV-2 Calculated change in $n=3$ population at $z=0$ of a hydrogen positive column due to resonant H_2 illumination



T_e from 4.5 to 6 eV is indicated by (x), and the previous comments hold, Δn_3 is not dramatically affected by changes in T_e , so the results are credible even in the absence of accurate knowledge of T_e .

c) Electron density

Finally, the calculated change in electron density in the presence of illumination is shown in Fig. IV-3 for some different values of the external parameters. Typically, $\Delta n_e/n_e$ was extremely small, 10^{-4} or less. The "error" introduced by changing T_e is here relatively larger than that for Δn_2 or Δn_3 .

What is remarkable is that Δn_e is negative for all cases calculated. This is the opposite of what might be expected intuitively. The process of exciting electrons in the column to higher states seems as if it should increase electron density by promoting electrons toward the ionization continuum. What the simulation says, however, is quite different. The correct explanation of the microscopic processes is that at constant current the extra power pumped into the discharge from the laser reduces the power required from the electric field, resulting in a reduced electron density. That $\Delta n_e < 0$ is absolutely essential to the discussion of hydrogen-deuterium isotope separation in Chapter VIII. In any application the change in n_e is so small that it is unlikely to be significant.

2. Optogalvanic Effect

The next three sections, 2a, b, and c, show finally the OGE calculated from the model as a function of laser intensity, pressure, and current. In all three, the agreement with experiment is remarkably good, especially considering the simplicity of the model. The same strategy as

Fig. IV-3 Change in electron density n_e from H_α illumination of a hydrogen positive column

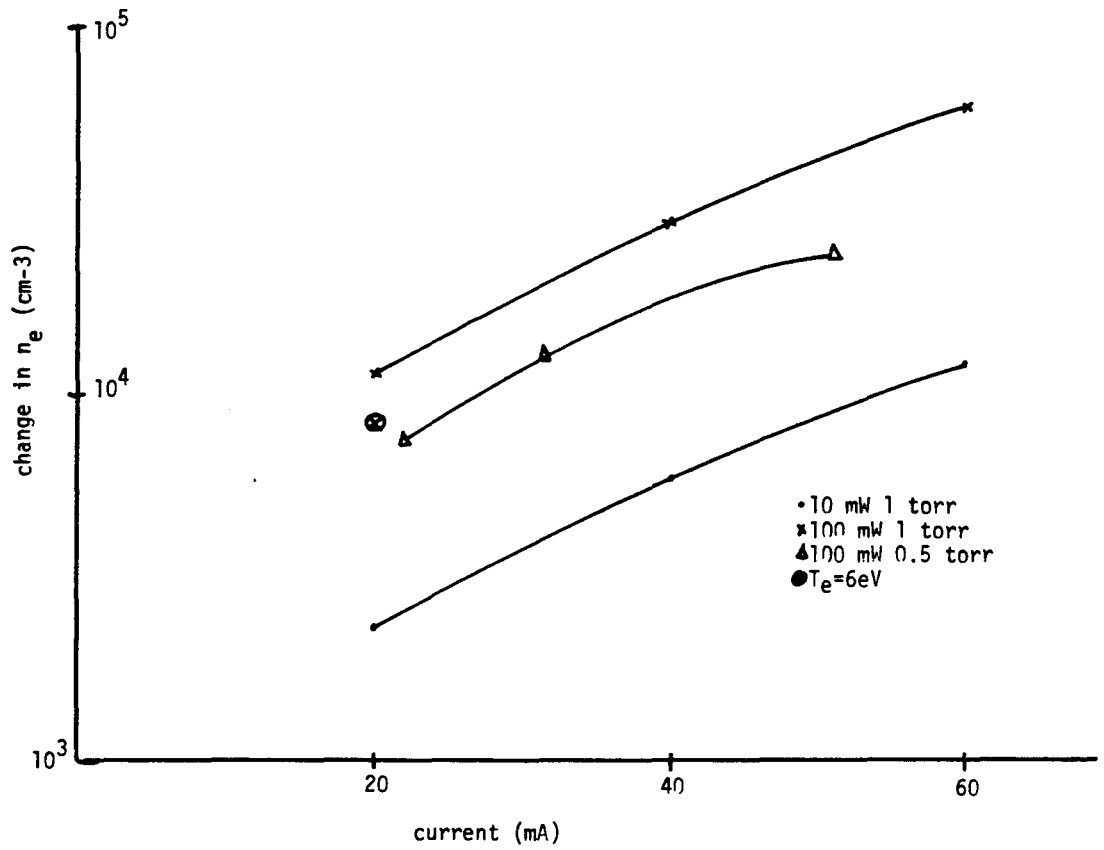
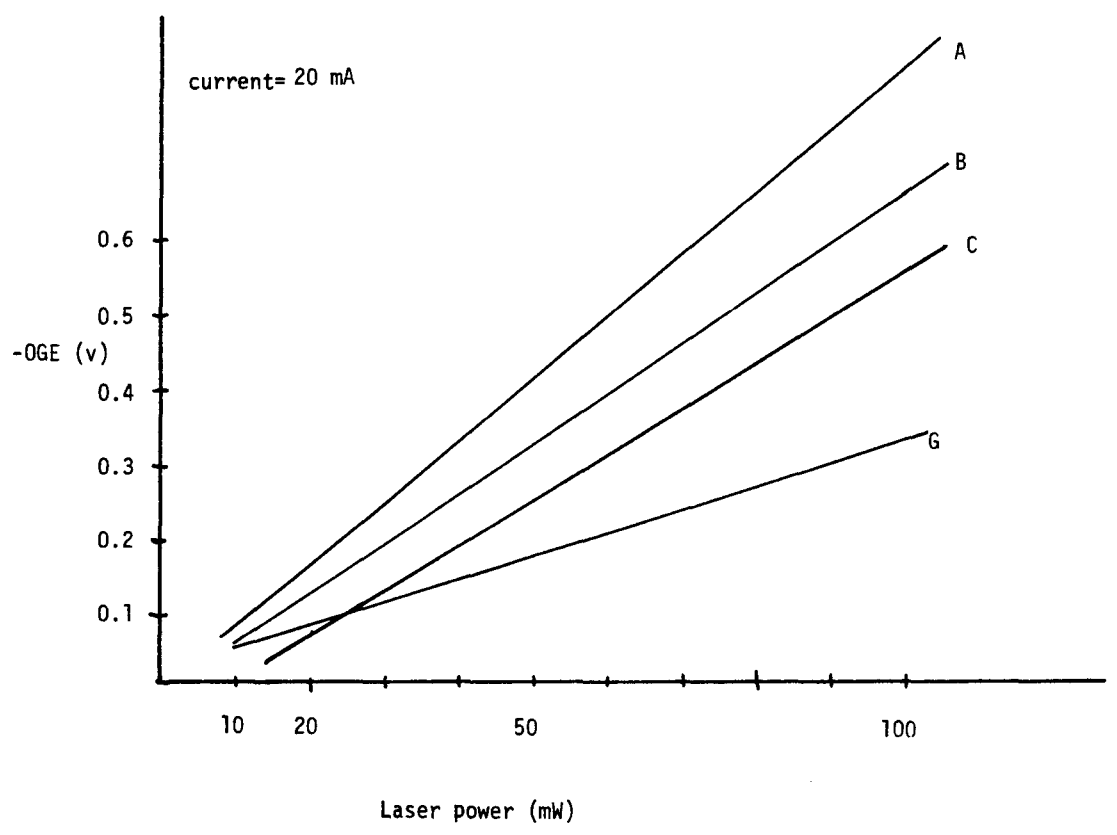
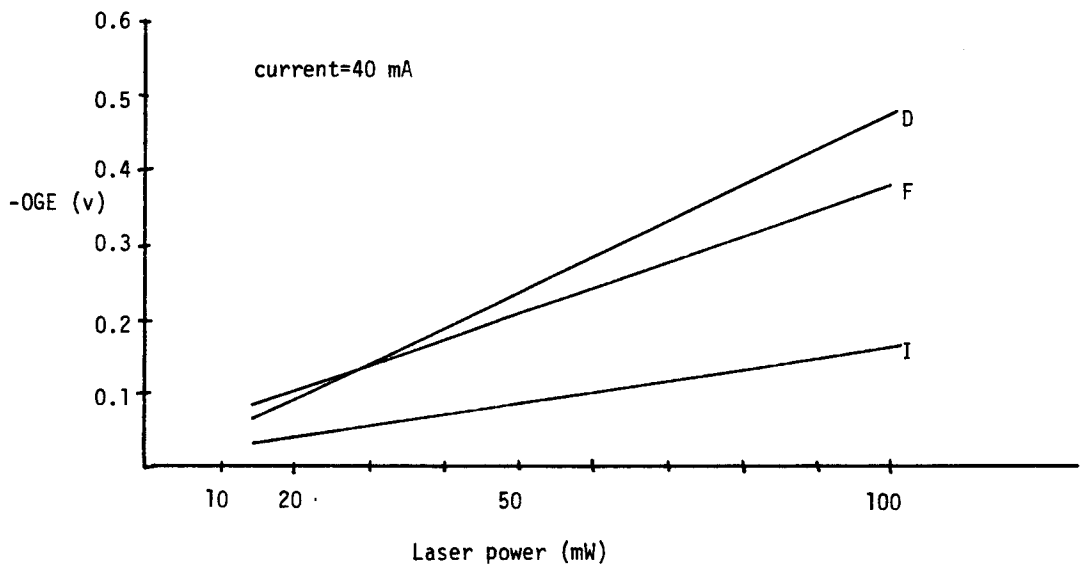
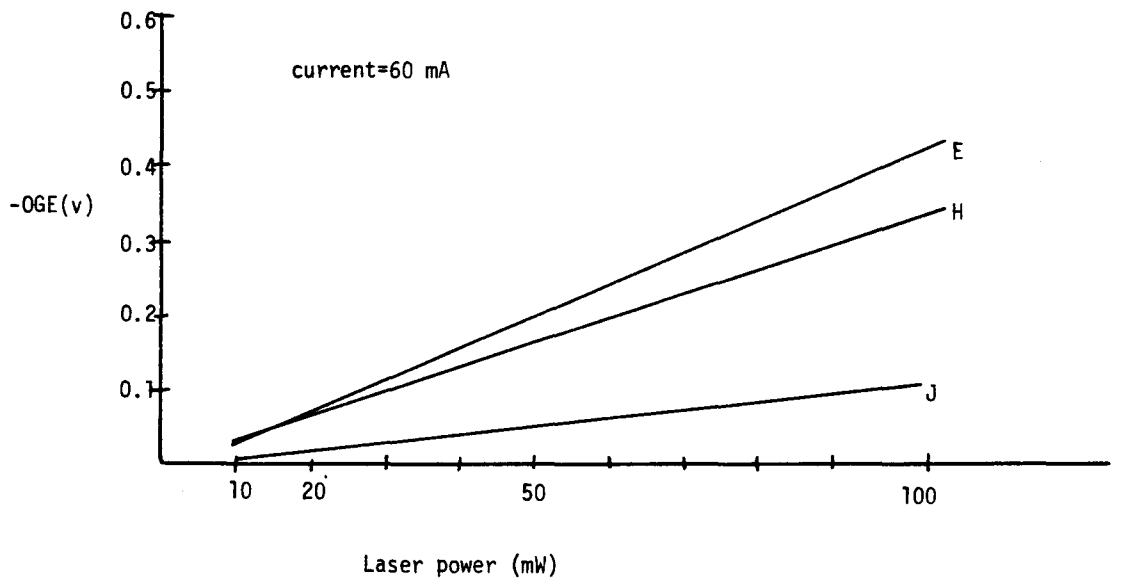


Fig. IV-4 Theoretical and experimental values of OGE in hydrogen as a function of illumination fluence. Errors are typically $\pm 25\%$ in the experimental curves.(least squares fit to data).

- A Exact theory, current = 20 mA
- B Exact theory, $T_e = 6$ eV (see text)
- C Least squares fit to experimental data, current = 24 mA
- D Exact theory, 40 mA
- E Least squares fit to experimental data, current = 60 mA
- F Least squares fit to experimental data, current = 40 mA
- G Crude theory, 20 mA
- H Exact theory, 60 mA
- I Crude theory, 40 mA
- J Crude theory, 60 mA







in Section III.E, using experimental values to specify T_e consistently with pressure and current, is adopted throughout.

a) OGE as a function of illumination intensity

The OGE voltage resulting from H_α illumination of hydrogen is calculated to be (and was observed to be) negative under all conditions. Furthermore, it was observed to be directly proportional to the laser intensity at the available (broadband) powers, $\lesssim 150$ mW; no saturation was observed. Figure IV-4abc shows the theoretical and experimental values of the OGE as a function of laser power for both the "crude" and "exact" theories of Section III with tube current as a parameter. No saturation is predicted from the model, either. It is apparent from Fig. IV-4 that the theory gives remarkably accurate results (note that the vertical scale is linear, not logarithmic).

Neglecting for the moment the current parameter, it will be observed that the crude theory gives results that are too low and the exact theory gives results that are somewhat higher. This was quite predictable: Fig. AIV-2 indicates that the longitudinal absorption integral, when calculated exactly, is always greater than the corresponding crude theory. The fact that the exact theory results are somewhat larger than experiment is probably because no account was taken of any reflection of laser light from the end windows of the discharge (they were not Brewster windows), and the light reaching the column was, therefore, somewhat less than that measured, with a corresponding reduction (perhaps 10%) in the predicted OGE voltage. Additionally, the spatial form factor previously mentioned, accounting for the nonuniform radial illumination, will reduce the

theoretical result slightly. The magnitude of both these corrections is less than that produced by the uncertainty in T_e , and they are considered no further.

Also shown in Fig. IV-4 is the OGE as a function of illumination intensity with (as before) an electron temperature of 6 eV instead of the 4.5 eV given by Fig. VI-5. Two conclusions are apparent; first, the OGE voltage, while depending on T_e , does not depend on it strongly. Any error introduced into the calculation by the uncertainty in T_e is thus insufficient to cause the calculated values of the OGE voltage to be very much different from those of Fig. IV-4, where they are in very good agreement with experiment. Second, the value of T_e at low currents given by Fig. VI-5 is probably too high; the $T_e = 6$ eV curve is closer to the experimental data than is that for $T_e = 4.5$ eV.

Figure IV-4 supplies ample a posteriori justification for the assumption of Section III.E that the OGE, for all cases of experimental interest, is directly proportional to the pumping rate R_{23} . There is no saturation anywhere.

The fact that curve C (experimental data for 20 mA) is everywhere greater than curves E and F (experimental data for 40 mA and 60 mA) indicates that the OGE decreases with current; comparison of the equivalent theoretical curves for 20, 40, and 60 mA confirms this. However, Curve D is greater than E; but D is less than H; however, within the indicated errors, the opposite could be true; there is not enough accuracy to say unambiguously which is greater. Further discussion of this point--and the current dependence--is presented below.

One final result that may be deduced from Fig. IV-4 is an explanation of the failure of the parallel-tube experiment described in Chapter VII. The minimum signal that could be detected with the apparatus was roughly .05 V; anything below that vanished into the discharge noise. The minimum detectable laser power was thus ≈ 10 mW. Estimating from Fig. VII-6, the maximum H_{α} power generated by one U-shaped tube absorbed by the other is approximately 5 mW, which is barely detectable. The Fresnel refractive losses to the two tubes and red cellophane reduce the luminosity further; finally, the U-shaped tubes were considerably noisier than the one used for Fig. IV-4. Thus, in the parallel tube experiment, the signal was just too small.

On several occasions, experiments were conducted to evaluate the effect of reflecting the laser beam back through the discharge. Under no circumstances was it found to produce anything more than a tiny ($< 5\%$) change in the signal. From Fig. AIV-1 after propagating through 20 cm of discharge, the laser beam is almost fully absorbed. Reflecting the beam produces hardly any extra excitation of the column. Invoking once again the argument that the OGE is directly proportional to R_{23} , it is obvious that a significant additional OGE resulting from reflection of the laser beam would be quite unexpected.

It is appropriate to include here one interesting result of applying the model to a narrowband illumination source. It is indicated in Appendix IV that the OGE response resulting from scanning a low power narrowband laser through the Doppler width (6 GHz) of the H atomic line ("OGE lineshape") in a 20 cm discharge would be much "flatter" than the

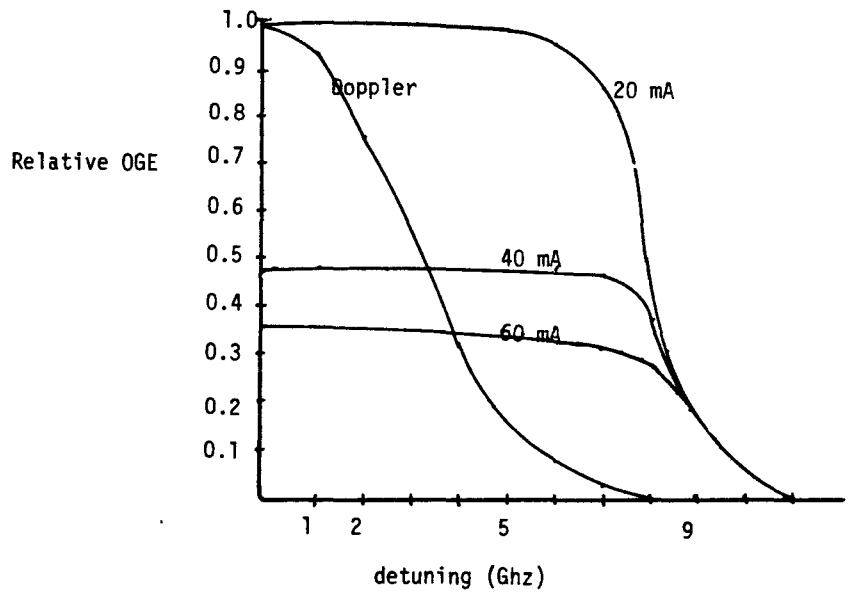
Doppler profile itself. Figure IV-5 below shows the calculated narrowband OGE (normalized to the 20 mA curve), where, as before, T_e is specified consistently with the help of experimental data. The normalized Doppler profile is included for comparison.

In physical terms, what Fig. IV-5 indicates is fairly straightforward. It says that at low intensity monochromatic radiation produces the same OGE voltage even with substantial detuning (greater than $\Delta\nu_D/2$) off line center. This is because all of the incident radiation is absorbed in the 20 cm hydrogen PCD under consideration. Far off line center (7-12 GHz) the absorption coefficient $\gamma(\nu)$ is considerably smaller, and some light is not absorbed, resulting in a reduced OGE voltage. If the external narrowband source illuminated only an infinitesimally short section of the PCD, the OGE voltage would behave like the Doppler lineshape as a function of frequency offset, since there would be only infinitesimal absorption.

b) OGE as a function of pressure

The OGE in hydrogen would not be expected to remain constant as pressure in the column is increased; unfortunately, neither would the electron temperature, which complicates the analysis. As an experimental strategy, the discharge was run at constant current (40 mA) regardless of the pressure. It was necessary to increase the voltage across the tube with increasing pressure (because the electron mean free path was decreasing) to maintain the current. It might be expected that the electron temperature under these circumstances is approximately constant, since E and p are scaled together so $E/p \sim T_e \approx \text{constant}$. A brief examination of Fig. VI-5, electron temperature as a function of current and pressure, shows

Fig. IV-5 Normalized narrowband OGE as a function of frequency. The Doppler profile is included for comparison.



that this is only roughly true; it is, however, true within the experimental error. The analysis, therefore, is done with the same T_e for all pressures, but the caveat must be added that the intrinsic uncertainty in T_e should be considered in the results.

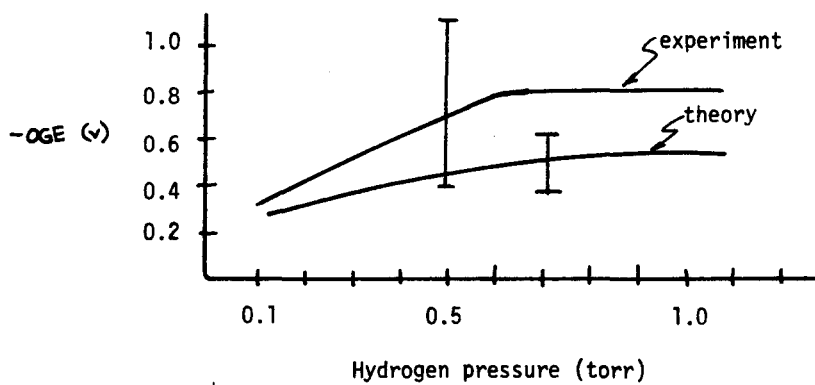
The OGE as a function of pressure for fixed current is presented in Fig. IV-6 . The typical error indicated for the experimental curve represents the observed changes in OGE due to tube noise, gas pumping, instability from situations (especially at higher pressures) and all other effects previously mentioned that hurt reproducibility. The error bar on the theoretical curve shows the variation in predicted OGE when the electron temperature is varied within the error bounds discussed previously.

The results are again remarkably good; even with the linear vertical scale of Fig. IV-6 , both theory and experiment can be drawn, and are in agreement within experimental error (error in both OGE voltage and T_e). Both experiment and theory show saturation at higher pressures. Most probably saturation occurs when the illumination is totally absorbed and a further increase in pressure does not result in more absorption. Similarly, the increase in OGE with pressure corresponds to increasing absorption, an increasing fraction of the discharge power is supplied by the laser and the voltage drops.

c) OGE as a function of current

Except for the recurring problem of electron temperature uncertainty, finding the current dependence of the OGE in hydrogen is relatively simple. In the model for fixed pressure, all that is necessary is a simultaneous (consistent) variation of current I and electron temperature T_e from Fig. VI-5 . Experimentally, all that is involved is increasing the discharge

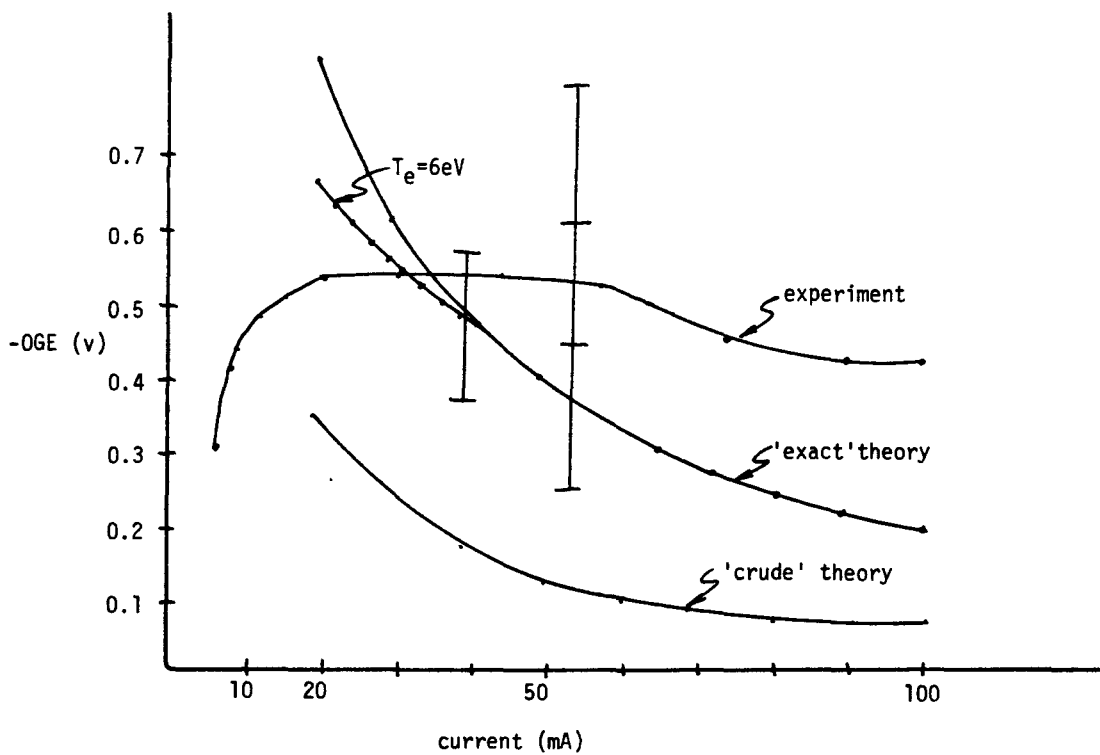
Fig. IV-6 OGE as a function of pressure in a hydrogen positive column at 40 mA current. See text for explanation of error.
Tube diameter = 0.5 cm.



voltage (and current) and measuring the resulting OGE. The results are shown in Fig. IV-7. The agreement between experiment and theory is again good; as before, the OGE predicted ($\sim 0.5V$) is quite close to the experimental values. The errors, as in Section b, arise in the theory from the inaccuracy of T_e , and in the experiment from noise and low reproducibility. The larger error bar indicated on the experiment curve represents the potential change in OGE from experiment to experiment, done on different days with different discharge tubes. The smaller error bars indicate the variation that was observed within the same experiment (i.e., the same measurement taken at different times). The general behavior of increasing and then decreasing OGE is bona fide, however, even though the change is mostly below the uncertainty indicated by the smaller error bar. If the current is changed and the OGE measurement is taken rapidly, the tube has insufficient time to adopt pathological behavior (becoming unstable, striating, outgassing dirt at higher currents, etc.) and the data are more reliable.

At small currents (< 20 mA) Fig. IV-7 shows that the OGE falls off rapidly. This is likely because the population of the $n=2$ excited state is too low to absorb much radiation in the 20 cm of discharge (see Fig. III-5). The theoretical model goes somewhat awry at these low currents because the T_e data become very unreliable. Below 20 mA, the plasma is quite tenuous (the discharge frequently extinguishes spontaneously) because there is only nominally enough voltage to sustain the cathode fall and positive column. The double probe T_e measurement is very hard to make here because practically any voltage applied to the probes disturbs the plasma

Fig. IV-7 OGE as a function of current in a hydrogen discharge. See text for a discussion of errors; error bars apply to the whole curve, not individual points. Tube diameter = 0.5 cm; hydrogen pressure = 0.5 t.



(both between the probes and in the rest of the discharge). The extra curve at 20 mA indicates as before the effect on the OGE of increasing T_e from 4.5 to 6 eV. It is possible to produce better low-current results from the model by adjusting T_e as a function of I , but given the difficulty of good experimental verification, it hardly seems worth while, and it is more truthful to indicate the OGE from errors arising from T_e inaccuracy.

At large currents (> 60 mA) the measured OGE decreases, in agreement with the model. The decrease in OGE is the result of two competing factors, OGE and absorption. At high currents, n_2 has a higher population, and the absorption length decreases. On the other hand, the OGE per unit length increases, since $E_{\text{local}} \sim \sqrt{m_e v_e \omega_e}$, where v_e and ω_e are increasing functions of n_2 . The net OGE measured at the terminals is proportional to $E_{\text{local}} e^{-\gamma Z}$, and decreases.

The above results indicate that the OGE voltage measured at the terminals of a discharge results from a trade-off of two factors, absorption length and local voltage change. At moderate currents, with a relatively long folding length, a small local OGE voltage is generated over a long length; at higher currents and higher excited state populations, a larger voltage is produced over a shorter folding length.

Chapter V
TRANSIENT OPTOGALVANIC EFFECT

V. TRANSIENT OGE

A. INTRODUCTION

The preceding discussion of the optogalvanic effect has been limited to simulation of the steady state conditions in the discharge with and without illumination. However, the OGE does exhibit a transient behavior when the exciting illumination is switched on or off that is more complex than a direct change between the two steady state values. Two methods are presented below for calculating the transient OGE. The first method is straightforward numerical integration of the rate equations, subject to the constraint of power balance. The second method uses perturbation theory to linearize the equations in the model, and then uses the results to calculate the time constants of the OGE.

B. NUMERICAL INTEGRATION

Numerical integration of the rate equations, while not difficult, can be quite expensive due to the multiple time scales involved. A slight improvement in computational efficiency may be had by exploiting the results of the fixed current formulation discussed in Section III.E, that is, electron density is calculated to first order from an assumed current. The computational strategy is then to specify the electron temperature, current and pressure, and calculate first estimates for the level populations, n_2 , n_3 , and n_e from equations (IV.1) and (IV.2). The numerical integrator then integrates equations (III.50) and (III.51) using these estimates as initial values. Each time the levels n_2 and n_3 are computed, n_e is recomputed, too, so that all the equations are solved simultaneously. This procedure may be made slightly more efficient

by using populations computed from the DC model of Section III as starting values; this also serves to check both programs for errors. Once the populations n_2 , n_3 , and n_e have reached steady-state values, the external illumination is "turned on" and the above procedure is repeated. Transient behavior is exhibited by the level populations before they reach their steady state values, and the transient behavior of the discharge voltage (transient OGE) may be deduced exactly as in the DC case of Section III.E.

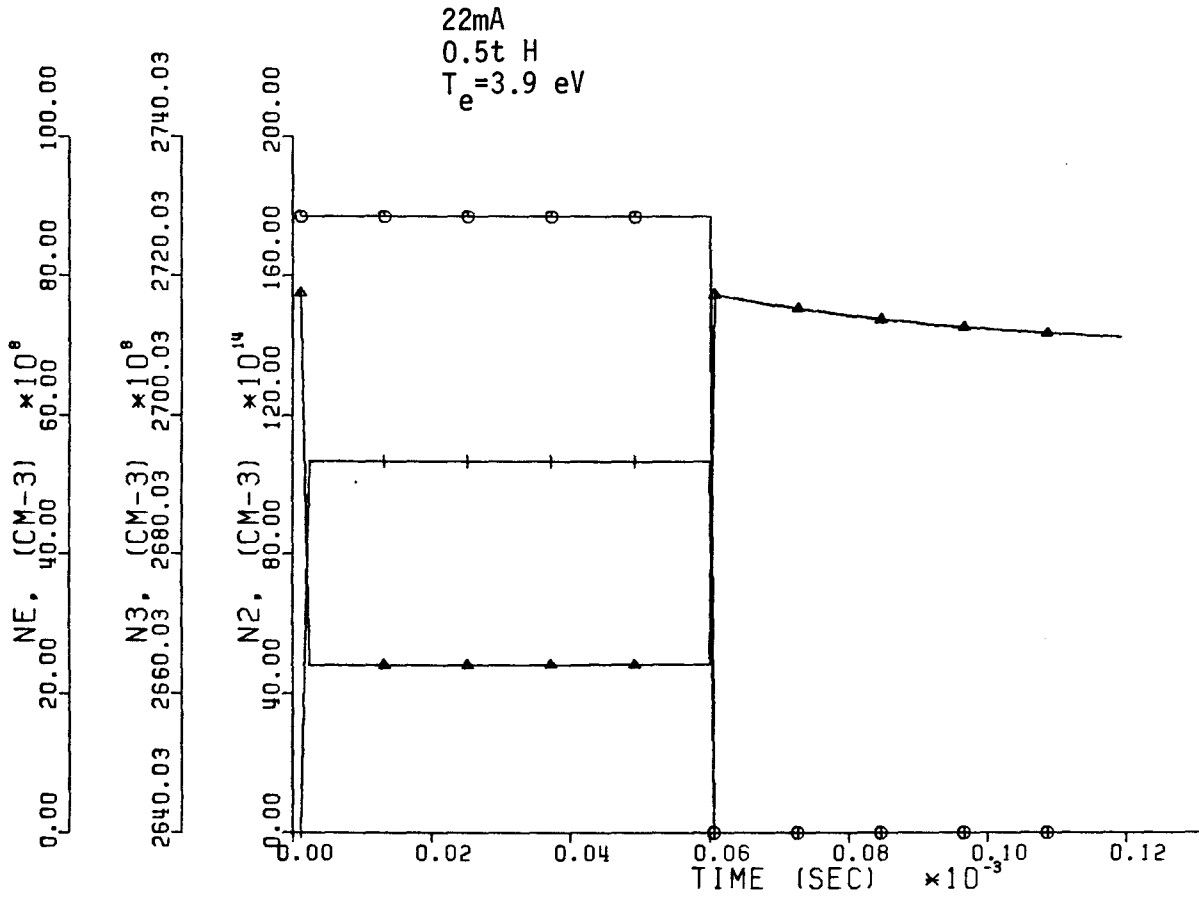
Numerical results for the populations as a function of time are presented in Figure V.1 for one set of typical discharge parameters; electron temperature, $T_e = 3.9$ eV, current $I = 22$ mA, pressure = .105 Torr.

The extreme left-hand side of the plot at $t=0$ shows the populations at $t=0$, i.e., the initial steady state conditions before illumination is added. From there to 6×10^{-5} sec, the laser illumination is turned on, after 2×10^{-5} sec illumination is turned off and the populations relax back to the initial values.

Some previous (and obvious) conclusions about the DC population values are now corroborated. The electron density changes only slightly with illumination. The upper radiative level, $n=3$, is populated strongly by the laser, and the lower level, $n=2$, is slightly depleted by the radiation.

The transient behavior of the discharge populations is very rapid. On the time scale of the computation, only n_2 exhibits transient behavior not tied directly to the radiation, with a time constant $\tau = 2.5 \times 10^{-6}$ sec arising from the trapping of the decay resonance radiation ($n=2$ to $n=1$).

Fig. V-1 Transient behavior of the level populations and electric field from numerical integration of the rate equations



(As noted, the model does not apply for all times, because it requires at least 10^{-7} sec to establish ambipolar diffusion).

C. PERTURBATION THEORY

This numerical integration approach to finding the transient behavior of discharge voltage, while effective, has several significant drawbacks. As noted, it is expensive and cumbersome, but more significantly, it does not easily yield any insight into the physical mechanisms of the OGE; any such insight would have to be deduced from the results of extensive computation. Since from experiment and steady state theory, external illumination only slightly disturbs a hydrogen discharge, it is appropriate to use perturbation theory. Perturbation theory would not, however, be appropriate for discharges which exhibit a large OGE such as the CO₂ laser or the cesium discharge (Bridges, 1978); nor is it appropriate at high illumination intensities where there is a large change in the energy balance (and, perhaps, a change in electron temperature).

The three level populations n_2 , n_3 , n_e are assumed to be perturbed only by the presence of H_α radiation. As a result, the electric field, E , collision frequency ν_e , ambipolar diffusion coefficient D_a , and input power density w_e are also perturbed. In the fixed-current formulation there is no change in I .

First, each level population is written as the sum of a steady state value and a small perturbation:

$$n_2 = \bar{n}_2 + \tilde{n}_2 \quad , \quad n_3 = \bar{n}_3 + \tilde{n}_3 \quad , \quad n_e = \bar{n}_e + \tilde{n}_e \quad (V.1)$$

where \bar{n} indicates steady state value, and \tilde{n} is the perturbation. It is assumed that the switching time of the external radiation is much shorter than the transient behavior of the discharge as determined by the plasma; hence the radiative terms R_{23} and R_{32} may be excluded from the rate equations. Substituting in equations (III.50) and (III.51),

$$\begin{aligned} \frac{d}{dt} (\bar{n}_2 + \tilde{n}_2) &= 0.432 \bar{n}_1 (\bar{n}_e + \tilde{n}_e) S_{12} + (\bar{n}_3 + \tilde{n}_3) (0.269 (\bar{n}_e + \tilde{n}_e) S_{32} + 0.432 A_{32}) \\ &\quad - (0.432 \gamma_{21} A_{21} + 0.269 (\bar{n}_e + \tilde{n}_e) (S_{21} + S_{23} + S_{2c})) (\bar{n}_2 + \tilde{n}_2) \quad (V.2) \end{aligned}$$

$$\begin{aligned} \frac{d}{dt} (\bar{n}_3 + \tilde{n}_3) &= 0.432 \bar{n}_1 (\bar{n}_e + \tilde{n}_e) S_{13} + 0.269 (\bar{n}_e + \tilde{n}_e) S_{23} (\bar{n}_2 + \tilde{n}_2) \\ &\quad - (0.432 (A_{32} + \gamma_{31} A_{31}) + 0.269 (\bar{n}_e + \tilde{n}_e) (S_{31} + S_{32} + S_{3c})) (\bar{n}_3 + \tilde{n}_3) \quad (V.3) \end{aligned}$$

Eliminating DC equations and second order terms,

$$\begin{aligned} \frac{d}{dt} (\tilde{n}_2) &= 0.432 \tilde{n}_e \bar{n}_1 S_{12} + (0.269 \bar{n}_e S_{32} + 0.432 A_{32}) \tilde{n}_3 \\ &\quad + 0.269 \tilde{n}_e \bar{n}_3 S_{32} - (0.432 \gamma_{21} A_{21} + 0.269 \bar{n}_e (S_{21} + S_{23} + \gamma_{2c})) \tilde{n}_2 \\ &\quad - 0.269 \tilde{n}_e \bar{n}_2 (S_{21} + S_{23} + S_{2c}) \quad (V.4) \end{aligned}$$

and

$$\begin{aligned} \frac{d}{dt} (\tilde{n}_3) &= 0.432 \tilde{n}_e \bar{n}_1 S_{13} + 0.269 \bar{n}_e \tilde{n}_2 S_{23} + 0.269 \tilde{n}_e \bar{n}_2 S_{23} \\ &\quad - 0.432 (A_{32} + \gamma_{31} A_{31}) \bar{n}_3 + 0.269 \bar{n}_e (S_{21} + S_{32} + S_{3c}) \tilde{n}_3 \\ &\quad - 0.269 \tilde{n}_e \bar{n}_3 (S_{31} + S_{32} + S_{3c}) \quad (V.5) \end{aligned}$$

1. Simplest Approximation, $\tilde{n}_e = \tilde{n}_2 = \bar{n}_3 = 0$

As indicated previously, the electron density n_e , while weakly coupled to n_2 and n_3 , is determined principally by the current through the external circuit (later computational results show that, in fact, $\Delta n_e/n_e$ due to radiation is quite small, of the order of 10^{-6}). As a first approximation, therefore, it is reasonably credible that $\tilde{n}_e = 0$ for a small perturbation on the discharge from resonant light. An additional approximation is suggested by some of the results of the DC model of Chapter IV. In none of the many computer simulations undertaken was the population of n_2 much changed (depleted) by the presence of illumination; furthermore, the unilluminated value of n_3 was always tiny (10^{-8} the population of the ground state). This suggests that additionally assuming $\tilde{n}_2 = 0$ and $\bar{n}_3 = 0$ are reasonable approximations. With these three assumptions, equation (V.4) yields $\tilde{n}_2 = 0$ and equation (V.5) says

$$\begin{aligned} \frac{d}{dt} \tilde{n}_3 &= -0.432(A_{32} + \gamma_{31}A_{31}) + 0.269 n_e (S_{31} + S_{32} + S_{3c}) \tilde{n}_{3c} \\ &\equiv -\lambda_3 \tilde{n}_3 \end{aligned} \tag{V.6}$$

or

$$\tilde{n}_3 = \tilde{n}_3(0) e^{-\lambda_3 t}$$

The not altogether surprising result is that a perturbation to level 3 decays with a rate constant equal to a sum of the rates "out" of level 3. The decay constant, $0.432(A_{32} + \gamma_{31}A_{31}) + 0.269 n_e (S_{31} + S_{32} + S_{3c})$, is dominated by the radiative terms, especially A_{32} , except at very low pressures ($\lesssim 0.01$ Torr), where $\gamma_{31} \approx 1$. Thus in the simplest theory \tilde{n}_3 (and

\tilde{E}) decay with time constants on the order of $1/A_{32}(.432) \sim 5 \times 10^{-8}$ sec.

The transient OGE may be calculated from equations(III.48, III.49) "perturbing" E , v_e , and ω_e ,

$$E + \tilde{E} = \frac{1}{\sqrt{.432}} \sqrt{m_e(v_e + \tilde{v}_e)(\omega_e + \tilde{\omega}_e)} \quad (V.7)$$

Expanding and eliminating the zero order and second order terms,

$$\tilde{E} = \frac{1}{2} \frac{1}{\sqrt{.432}} (\tilde{v}_e \omega_e + v_e \tilde{\omega}_e) \quad (V.8)$$

Since \tilde{v}_e and $\tilde{\omega}_e$ contain terms linear in \tilde{n}_3 , the transient behavior of E occurs with the same time constant as n_3 . This is shown in Fig. V-2

2. $\tilde{n}_e = \bar{n}_3 = 0$

The approximation that $\tilde{n}_2 = 0$ may be removed; there should now be two time constants in the results.

Equations (V.4) and (V.5) become

$$\begin{aligned} \frac{d}{dt} (\tilde{n}_2) = & -(0.432 \gamma_{21} A_{21} + 0.269 n_e (S_{21} + S_{23} + S_{2c})) \tilde{n}_2 \\ & + (.269 n_e S_{32} + .432 A_{32}) \tilde{n}_3 \end{aligned} \quad (V.9)$$

$$\begin{aligned} \frac{d}{dt} (\tilde{n}_3) = & .269 n_e S_{23} \tilde{n}_2 \\ & - (0.432(A_{32} + \gamma_{31} A_{31}) + 0.269 n_e (S_{31} + S_{32} + S_{3c})) \tilde{n}_3 \end{aligned} \quad (V.10)$$

This is a simple system of first-order linear differential equations for which the solution is easily computed; if each level decays exponentially,

$$\tilde{n}_2 = \tilde{n}_2(0) e^{-\lambda_2 t} \quad (V.11)$$

and

$$\tilde{n}_3 = \tilde{n}_3(0) e^{-\lambda_3 t} \quad (V.12)$$

The level decay constants, λ_2 and λ_3 , are the eigenvalues of the above equations. Using the same argument as in the approximation, the time constants of the level populations are also the time constants associated with E. Thus, equation (V.8) still holds, but it is now computed with \tilde{n}_2 and \tilde{n}_3 . Results and discussion are presented below.

For a typical discharge ($T_e = 6$ eV, $I = 50$ mA, $p = 1$ Torr), the equations are dominated by the radiative decay terms, particularly the untrapped H_α terms; the numerical values are approximately

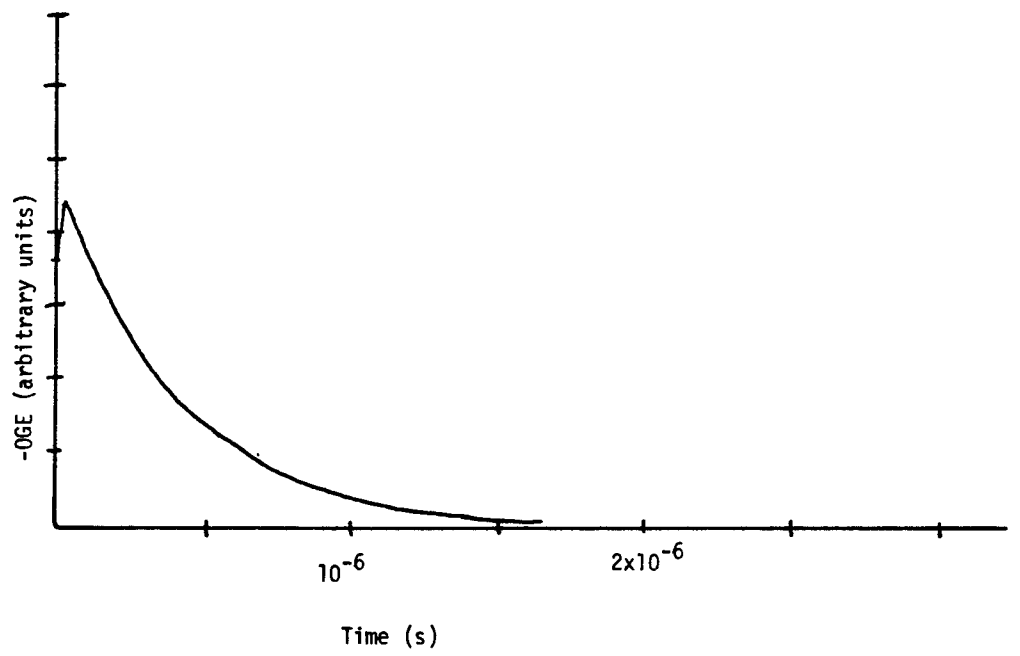
$$\begin{bmatrix} \frac{d\tilde{n}_2}{dt} \\ \frac{d\tilde{n}_3}{dt} \end{bmatrix} = \begin{bmatrix} (-2 \times 10^5) + (1.9 \times 10^7) \\ (2.2 \times 10^2) + (1.9 \times 10^7) \end{bmatrix} \begin{bmatrix} \tilde{n}_2 \\ \tilde{n}_3 \end{bmatrix} \quad (V.13)$$

The two coefficients of \tilde{n}_3 are the same because A_{32} dominates all the other terms; similarly $\gamma_{21}A_{21}$ dominates the first entry. If the lower left entry--by far the smallest--is taken to be zero, the eigenvalues (decay constants) are immediately obvious; they are

$$\begin{aligned} \lambda_2 &= 2 \times 10^5 \text{ sec}^{-1} \\ \lambda_3 &= 1.9 \times 10^7 \text{ sec}^{-1} \end{aligned} \quad (V.14)$$

Level $n = 3$ is (again) found to decay with a time constant equal to $1/.432 A_{32}$, and the level $n = 2$ decays radiatively with a time constant

Fig. V-2 Transient behavior of E , \tilde{E}



$1/\gamma_{21}A_{21}$. The combined behavior of \tilde{n}_2 and \tilde{n}_3 is given in general by the eigenvectors of the equations. In this simple case,

$$\begin{aligned}\tilde{n}_3 &= \tilde{n}_3(0) e^{-.432 A_{31} t} \\ \tilde{n}_2 &= \tilde{n}_2(0) e^{-.432 \gamma_{21} A_{21} t} - \tilde{n}_3(0) e^{-.432 A_{32} t}\end{aligned}\quad (V.15)$$

and the electric field transient, \tilde{E} , may be computed from equation (V.8) \tilde{E} is presented for the same parameters as Fig. V-1. In Fig. V-2 the perturbation is approximated as $\tilde{n}_2(0) = 10^9 \text{ cm}^{-3}$ and $\tilde{n}_3(0) = -\tilde{n}_2(0)$.

While the preceding calculation is for one specific set of discharge parameters, it is easily generalized. At higher pressure the decay constant of \tilde{n}_2 decreases because the trapping factor γ_{21} decreases.

$$\gamma_{21} = \frac{1.6}{k_0 r (\pi \ln(k_0 r))^{1/2}} \quad (V.16)$$

where $k_0 \sim n_1$. At higher electron temperatures the lower left entry $n_e S_{23}$ (0.269) becomes larger, and will have an effect on the decay eigenvalues and eigenmodes, causing the theory to become more complicated. In principle, analytic expressions for the eigenvalues and eigenmodes of equations (V.1) and (V.5) could be derived, but the result is unlikely to be simple enough to yield much insight. Accordingly, it is necessary to invoke numerical results; these are postponed until the next order of approximation ($\tilde{n}_e \neq 0$).

3. No Approximations

Finally, all three assumptions may be removed, although there is the penalty of increased complexity of results.

The perturbation of n_e may be tied to the perturbations \tilde{n}_2 and \tilde{n}_3 through the current equation,

$$n_e = \frac{I}{e} \frac{1}{\pi R^2 \sqrt{.432}} \sqrt{\frac{n_e v_e}{\omega_e}} \equiv C_0 \sqrt{\frac{v_e}{\omega_e}} \quad (\text{V.17})$$

since v_e and ω_e depend on the excited states. Writing the variable quantities as a steady state term plus a perturbation,

$$n_e = \bar{n}_e + \tilde{n}_e, \quad v_e = \bar{v}_e + \tilde{v}_e, \quad \omega_e = \bar{\omega}_e + \tilde{\omega}_e \quad (\text{V.18})$$

$$\begin{aligned} \bar{n}_e + \tilde{n}_e &= C_0 \sqrt{\frac{v_e}{\omega_e}} \sqrt{\frac{1 + \tilde{v}_e/v_e}{1 + \tilde{\omega}_e/\omega_e}} \\ &\approx C_0 \sqrt{\frac{v_e}{\omega_e}} \left(1 + \frac{\tilde{v}_e}{2v_e} - \frac{\tilde{\omega}_e}{2\omega_e}\right) \end{aligned} \quad (\text{V.19})$$

where the assumption that $\frac{\tilde{\omega}_e}{\omega_e}, \frac{\tilde{v}_e}{v_e} \ll 1$ is the justification for the last step. Eliminating \bar{n}_e ,

$$\tilde{n}_e = \frac{C_0}{2} \sqrt{\frac{v_e \bar{\omega}_e}{\omega_e}} \left(\frac{\tilde{v}_e}{v_e} - \frac{\tilde{\omega}_e}{\omega_e}\right) \quad (\text{V.20})$$

Similarly \tilde{v}_e and $\tilde{\omega}_e$ are obtained from equations

$$\tilde{v}_e = .269(S_{23} + S_{2c}) n_2 + 0.269 S_{3c} n_3 \quad (\text{V.21})$$

and

$$\begin{aligned} \tilde{\omega}_e &= (.269(S_{23} \epsilon_{23} + S_{2c} \epsilon_{2c} - S_{21} \epsilon_{12}) + .432 S_{2c} \cdot 5T_e) \tilde{n}_2 \\ &+ (.269(S_{3c} \epsilon_{3c} - S_{32} \epsilon_{23} - S_{31} \epsilon_{13}) + .432 S_{3c} \cdot 5T_e) \tilde{n}_3 \end{aligned} \quad (\text{V.22})$$

Thus, \tilde{n}_e may be written

$$\tilde{n}_e = A\tilde{n} + B\tilde{n}_3 \quad (V.23)$$

where

$$A \equiv \frac{C_0}{2} \sqrt{\frac{\nu_e m_e}{\omega_e}} \frac{.269(S_{23} + S_{2c})}{\nu_e} \quad (V.24)$$

$$- \frac{.269(S_{23}\epsilon_{23} + S_{2c}\epsilon_{2c} - S_{21}\epsilon_{12}) + .432 S_{2c} \cdot 5T_e}{\omega_e}$$

and

$$B \equiv \frac{C_0}{2} \sqrt{\frac{\nu_e m_e}{\omega_e}} \frac{.269 S_{3c}}{\nu_e} \quad (V.25)$$

$$- \frac{.269(S_{3c}\epsilon_{3c} - S_{32}\epsilon_{23} - S_{31}\epsilon_{13}) + .432 S_{3c} \cdot 5T_e}{\omega_e}$$

Using the perturbed rate equations with no approximations,

$$\frac{d\tilde{n}_2}{dt} = \tilde{n}_2 [.432 \gamma_{21} A_{21} + .269 n_e (S_{21} + S_{2c} + S_{23})] + A [.432 n_1 S_{12} + .269 n_3 S_{32} - .269 n_2 (S_{21} + S_{2c} + S_{23})]$$

$$+ n_3 [.269 n_e S_{32} + .432 A_{32} + B (.432 n_1 S_{12} + .269 n_3 S_{32} - .269 n_2 (S_{21} + S_{23} + S_{2c}))] \quad (V.26)$$

and

$$\frac{d\tilde{n}_3}{dt} = \tilde{n}_2 [.269 n_e S_{23} + A (.432 n_1 S_{13} + .269 n_2 S_{23} - .269 n_3 (S_{31} + S_{32} + S_{3c}))]$$

$$+ \tilde{n}_3 [-.432 (A_{32} + \gamma_{31} A_{31}) - .269 n_e (S_{31} + S_{32} + S_{3c})]$$

$$+ B (.432 n_1 S_{13} + .269 n_2 S_{23} - .269 n_3 (S_{31} + S_{32} + S_{3c})) \quad (V.27)$$

Fig. V-3 Decay constant of $n_1 = 2$ as a function of current

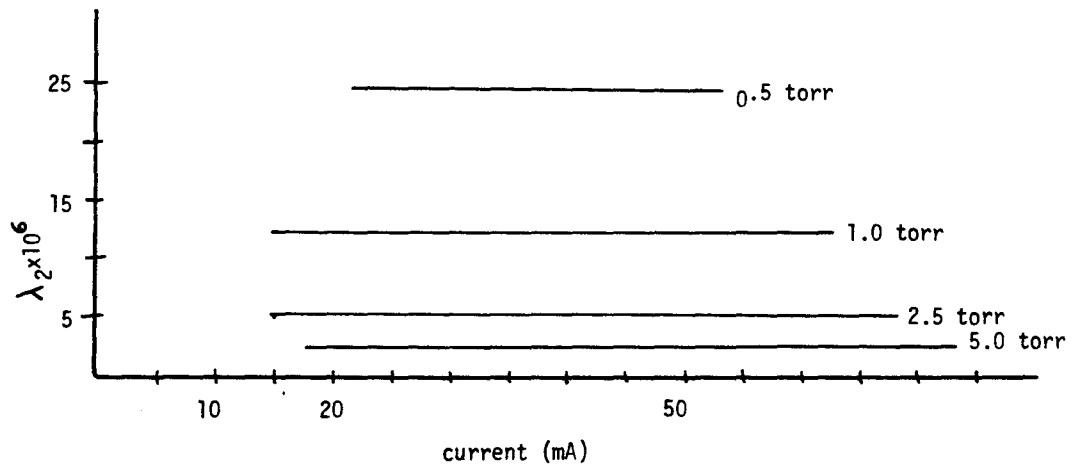
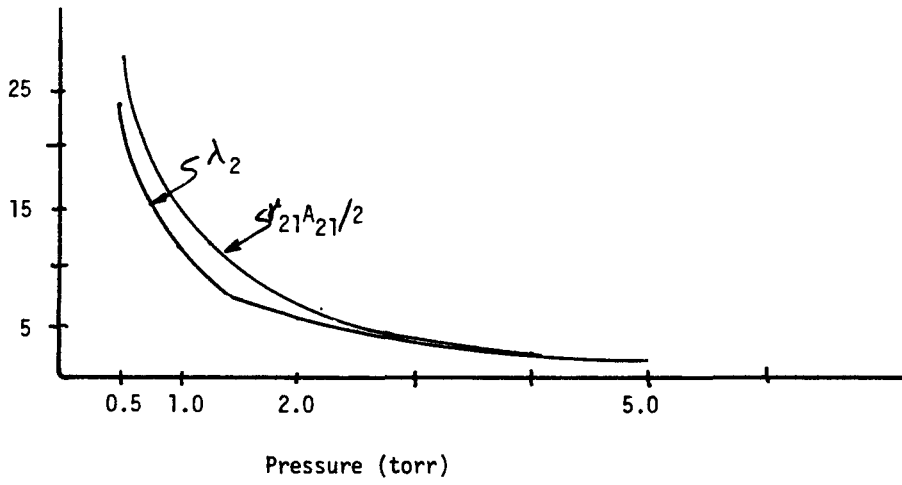


Fig. V-4 Pressure dependence of first entry ($\approx \lambda_2$) and of $\gamma_{21}A_{21}$



The eigenvalues of the above two equations are the desired time constants, as in Section B. The results for this exact treatment do not differ greatly from those of the approximation in the previous sections, which is to be expected, since the change in n_e is tiny.

The rate constant λ_3 is equal to A_{32} within 1% for all currents and pressures considered.

The rate constant λ_2 is shown in Fig. V-3. In all cases, the dominant contribution to λ_2 was from the trapped radiative decay, $\gamma_{21}A_{21}$.

The effect of radiation trapping, which depends strongly on the ground state population (pressure), is made more explicit in Fig. V-4. At high pressures, the decay rate decreases due to stronger resonance trapping.

The transient OGE, E , does not differ much from that shown in Fig. V-4. At higher pressures the transient would become slower (λ_2 would become smaller).

In all cases, the radiative decay is quite fast, and the OGE transients (see Fig. V-2) are also expected to be quite fast. In the experiments conducted to date, no pulsed dye laser was available to corroborate the calculation. Slow transients (10^{-2} sec) were induced by chopping the laser; however, these were assumed to be caused by the external circuit, as they did not change noticeably when different pressures or currents were used. The same slow constant was observed with other gases (helium, neon) in the positive column with the same circuit; they were observed in hollow cathode discharges of neon-lithium and neon-uranium on all lines with the same external circuit with lower voltage. The transient OGE in a neon HCD was measured by Miron et al. (1979) to change with a time constant of

$\sim 5 \mu\text{sec}$, indicating that the slow behavior observed here was the result of the LC time constant of the external circuit.

REFERENCES - Chapter V

Bridges, W. B., J. Opt. Soc. Amer. 68, 352-360 (1978).

Carswell, A. I. and J. I. Wood, J. Appl. Phys. 14, 863 (1963).

Miron, E., I. Smilanski, J. Liran, S. Lavi, G. Erev, IEEE J. Quant. Elec.
1t, 194-196 (1979).

Chapter VI
ELECTRON TEMPERATURE

VI. ELECTRON TEMPERATURE

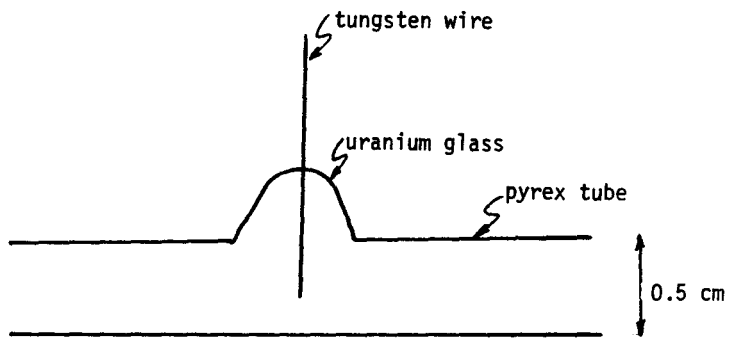
A. INTRODUCTION

It is one of the universal problems in gas discharge physics that even if there is a unique electron temperature, it is very hard to measure accurately. There are basically three techniques for determining T_e : (1) measuring the electron distribution directly in a retarding field with the appropriate electron optics (for example, Heil and Wada, (1963), (2) measuring microwave noise radiation, and (3) Langmuir probes. The first option, an electron velocity spectrometer, is relatively difficult to make and operate. The second possibility, microwave noise measurement, has some potential in the present work. Discharge tubes embedded in microwave waveguides have long been used as microwave noise standards (Bekefi and Brown, 1961; Parzen and Goldstein, 1950). The microwave noise power is simply related to the electron temperature of the discharge (Parzen and Goldstein, 1950). However, this technique was not adopted because the requisite apparatus, a hydrogen discharge inside a microwave waveguide, was deemed harder to construct than the equipment required for Langmuir probe measurements.

B. PROBE TECHNIQUES

The final option is to use an electrostatic probe in the discharge, and this technique was adopted. A narrow tungsten wire is introduced into the positive column as shown in Fig. VI-1 . The current-voltage characteristic of the tube is recorded; it is well known (see Huddleston and Leonard, 1965) that the slope of the positive part of the

Fig. VI-1 Langmuir probe in discharge tube



characteristic is proportional to e^{eV/kT_e} , provided the probe does not perturb the plasma. This technique proved to be impractical experimentally; the ground reference for the probe bias was the discharge tube cathode, and the probe voltage and current tended to exhibit DC drift. This occurred because the probe was "competing" with the anode; the effects of the probe were not confined to one sheath layer, and the result was some instability in probe current.

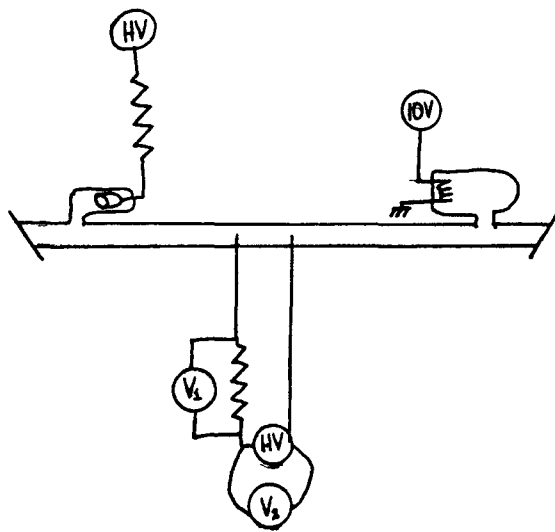
An alternative solution was adopted, that of using a second probe as the ground reference, and floating the probe power supply at this voltage (also a well known technique). The circuit is shown in Fig. VI-2. This arrangement eliminates drift of the DC probe potential relative to ground, and DC measurements may be taken with good reproducibility.

The impedance of a double probe is (Huddleston and Leonard, 1965)

$$I_p = i_+ \tanh (e(V-V_0)/kT_e) \quad (\text{VI.1})$$

where i_+ is the probe current at saturation (see below), V is the probe voltage, V_0 is the voltage at zero current, and I_p is the probe current. This expression is symmetric about $I=0$ as might be expected, since the two probes are identical. With the bias V in either direction, the current asymptotes to i_+ , the "saturation ion current." Physically, this occurs when there are no more ions "available" in the sheath layer to contribute to the current, even when the probe-to-probe voltage is increased. Unfortunately, this means that under any circumstances, only the high energy "tail" of the electron distribution can be sampled; only relatively few "fast" electrons are needed to balance all the "slow" ions

Fig. VI-2 Double probe circuit. V_2 yields the current; $V_2 + V_1$ is the probe voltage. The power supply floats.



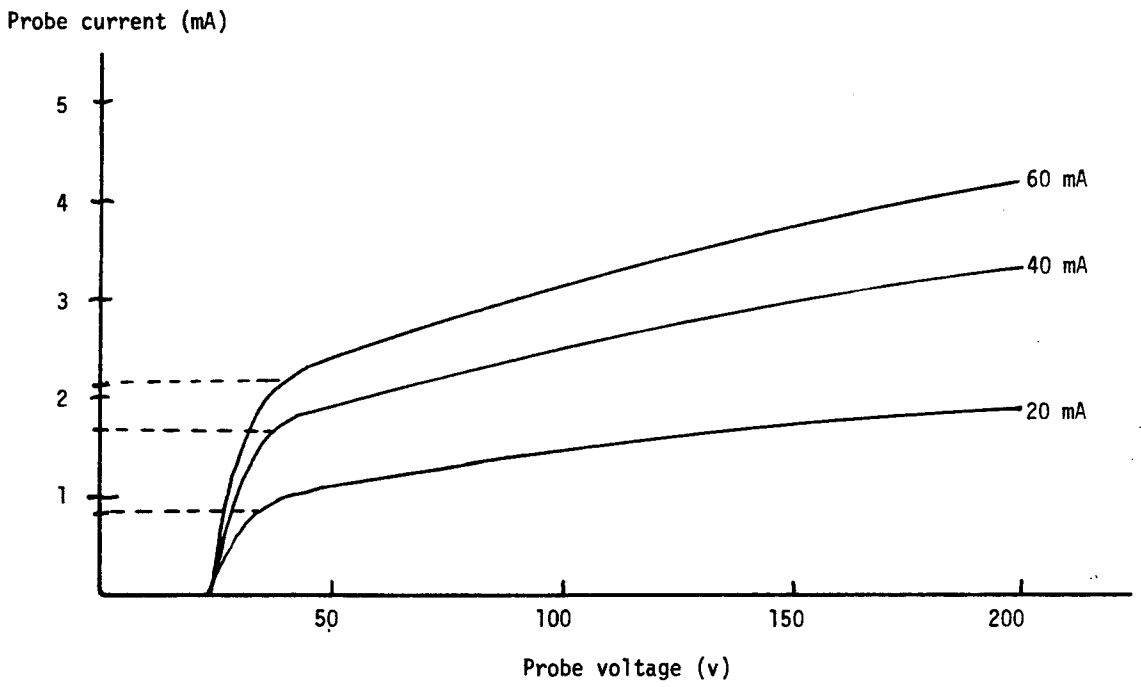
($T_e \gg T_i$). The tail of the electron distribution is what drives the discharge; the first excited state is at 10.2 eV, and a typical electron temperature is ≈ 5 eV. Thus, a double probe measures the electron temperature in exactly the region where it is expected to be non-Maxwellian. Further compounding the inaccuracy is the fact that the probes never exhibit a true saturation current (see Fig. VI-3); at high voltages the plasma between the probes starts to form a "discharge within a discharge" again because the effect of the bias voltage is not confined to a sheath length. This presents a problem in the analysis of the data.

A typical double probe characteristic is presented in Fig. VI-3. The zero current potential V_0 is approximately 24 volts, the probes were separated by ≈ 2 cm, implying an electric field of 12 V/cm in the positive column. The lack of complete current saturation is clearly evident. Further, the probe impedance is affected by the presence of striations, and striations tend to form around any constriction in the column, such as the probes themselves.

The electron temperature is deduced by estimating a saturation current (taken from the point where the probe characteristic turns most sharply) and performing a least squares fit to the data on an HP-34C programmable calculator.[†] The results are presented in the next section; it must be emphasized, however, that any measured value for T_e must be viewed with some suspicion.

[†]The method of least squares is used; the zero of the derivative of the error squared is calculated.

Fig. VI-3 Double probe characteristic

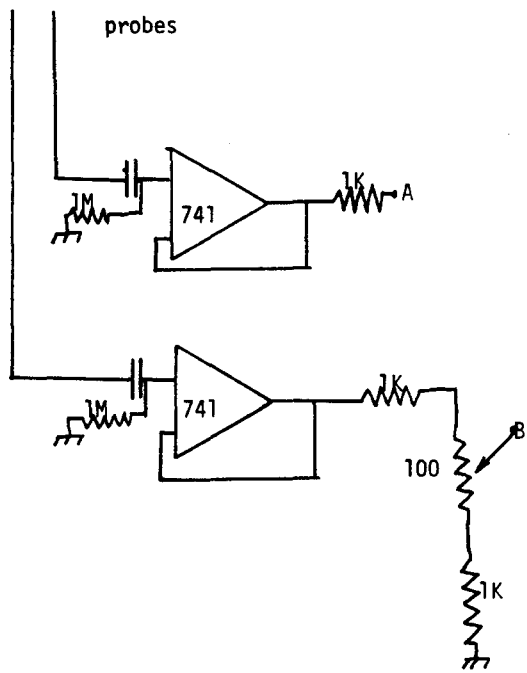


C. EFFECT OF ILLUMINATION ON T_e

The presence of H_α illumination, at sufficient intensity, is probably capable of changing the electron temperature. Experimentally, a change in T_e , ΔT_e could be detected by taking double probe characteristics with and without illumination. With the apparatus previously described, however, no change could be detected. Chopping the laser illumination and using a lock-in amplifier (Princeton Applied Research HR-8) to detect synchronous changes in probe voltage and current showed them both to be present, but small and practically lost in the discharge noise (≈ 0.1 V RMS). The circuit used is shown in Fig. VI-4; even with rejection of common mode noise from the two probes, only a tiny ΔV_p and ΔI_p were seen. The effect of illumination on T_e was certainly far below the "theoretical noise" introduced by the lack of an exact saturation current. It should be noted, however, that the probes, being about half-way down the positive column, are not in the region of maximum absorption of resonant light near the anode. Were the probes nearer the anode, a larger synchronous current and voltage change might be visible; it is not, however, clear that this would result in a larger value for T_e , and beam attenuation between the probes would be a problem.

Experimentally, the double Langmuir probe method suffers from many drawbacks; an intrinsically noisy source and the lack of saturation current are the most serious. Extra helium, added to suppress the striations clinging to the probes, also appears to increase the discharge noise, even to the point where the noise damaged the detection electronics. Synchronous changes in T_e were even more difficult to detect, as the

Fig. VI-4 Synchronous electron temperature probe circuit. The signal is taken between A and B so common mode noise is rejected. The adjustable resistance B is to offset any differential gain.



incremental signal is much smaller. Even in a CO₂ laser which exhibits an enormous voltage change (OGE) when it lases (which might be expected from a high-efficiency laser), the corresponding change in electron temperature is tiny (Garscadden, 1969). Thus, the measured T_e must be assumed somewhat inaccurate, and ΔT_e is assumed to be less than a few percent.

D. EXPERIMENTAL RESULTS--T_e FROM PROBES

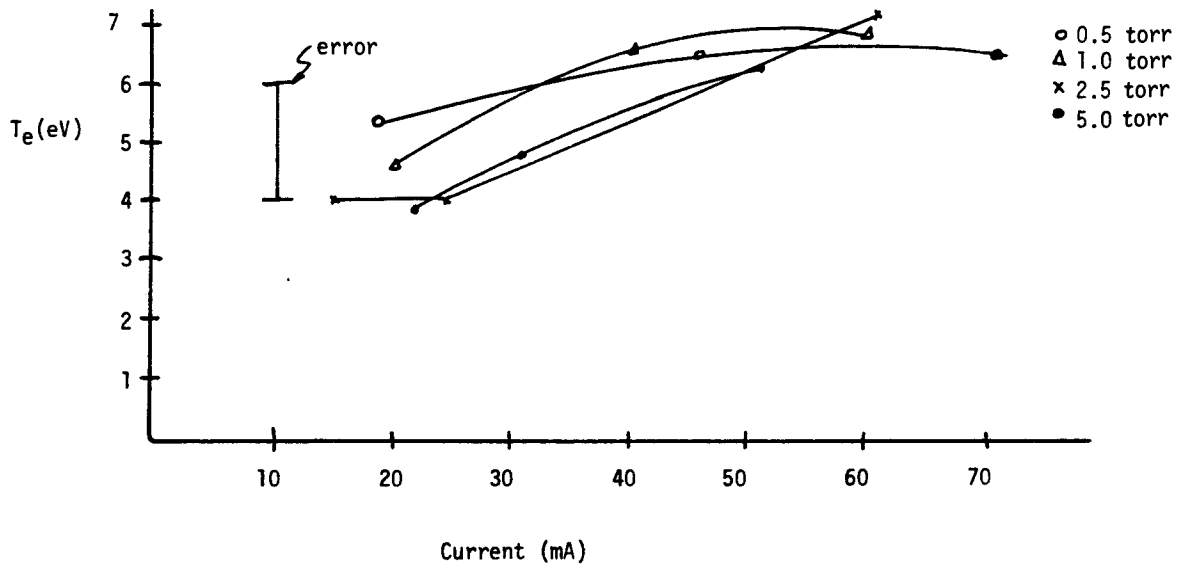
The electron temperature as a function of current is presented below for discharges run with several different partial pressures of hydrogen in a 5 Torr helium buffer. Measurements were taken with the double Langmuir probe. T_e was deduced from a least-squares fit of 5 points of the probe data to the theoretical probe characteristic, equation (VI.1) . Errors, as indicated by the error bars on the figure, were typically ±1 eV on each set of data (experimental double probe characteristic) used.

There were three sources of error in the data. Noise in the discharge tube was always a problem, yielding only fair reproducibility of the probe characteristic. Second, as noted, the ion saturation current was not well defined, and whatever value was chosen affected the T_e found. Finally, the choice of which five data points to fit to the theoretical probe characteristic was important; points chosen at high voltages (above the saturation current voltage) introduced larger mean-square errors. An attempt was made to compensate for this. Since well below the probe current the characteristic is nearly linear, i.e.,

$$\frac{d}{dx} \tanh x = \operatorname{sech}^2 x \approx 1 - x^2 + \dots$$

≈ 1 for small x, (VI.2)

VI-5 Electron temperature as a function of current for several different partial pressures of hydrogen



a linear fit to the data for low voltages should also yield the electron temperature. This approach did not yield any better results than fitting the full curve; the reproducibility of the data was still mediocre, and there is no clear definition of what constitutes "small x " when there is not a well defined saturation current. The electron temperatures deduced from this approach were, however, within the approximate (± 1 eV) errors of fitting to the full curve, and it was concluded that there was no advantage to this method.

With the caveat that the T_e data are somewhat unreliable (particularly at lower discharge currents where the probes can perturb the positive column significantly) the above data are used as input for the OGE simulation, along with current and pressure. The electron temperature depends on these two variables, so it is specified consistently from experiments (within experimental error) rather than independently. Thus the equation relating I and T_e in the characterization of the atomic model is explained, and there is a consistent way to specify the inputs for the rate equation model.

REFERENCES - Chapter VI

Bekefi, G., and S. Brown, Amer. J. Phys. 29, 404 (1961)

Garscadden, A. and P. Bletzinger, Ninth Int'l. Conf. Phenomena in Ionized Gases, Bucharest (1969), p. 251.

Heil and Wada, J. Quant. Electron. QE-1, 327 (1965).

Huddlestone, R. and S. Leonard, Plasma Diagnostic Techniques (Academic Press, New York, 1965).

Parzen, P. and L. Goldstein, Phys. Rev. 79, 190 (1950).

Chapter VII

OPTOGALVANIC EFFECT EXPERIMENTAL APPARATUS

VII. OGE EXPERIMENTAL APPARATUS

A. INTRODUCTION

This chapter contains a description of the experimental apparatus used in making hydrogen OGE measurements. Included are the hydrogen discharge tube and associated gas-handling apparatus. Some discussion is presented of experimental problems that were encountered in developing the experiments.

B. EXPERIMENTAL SETUP AND PROCEDURES

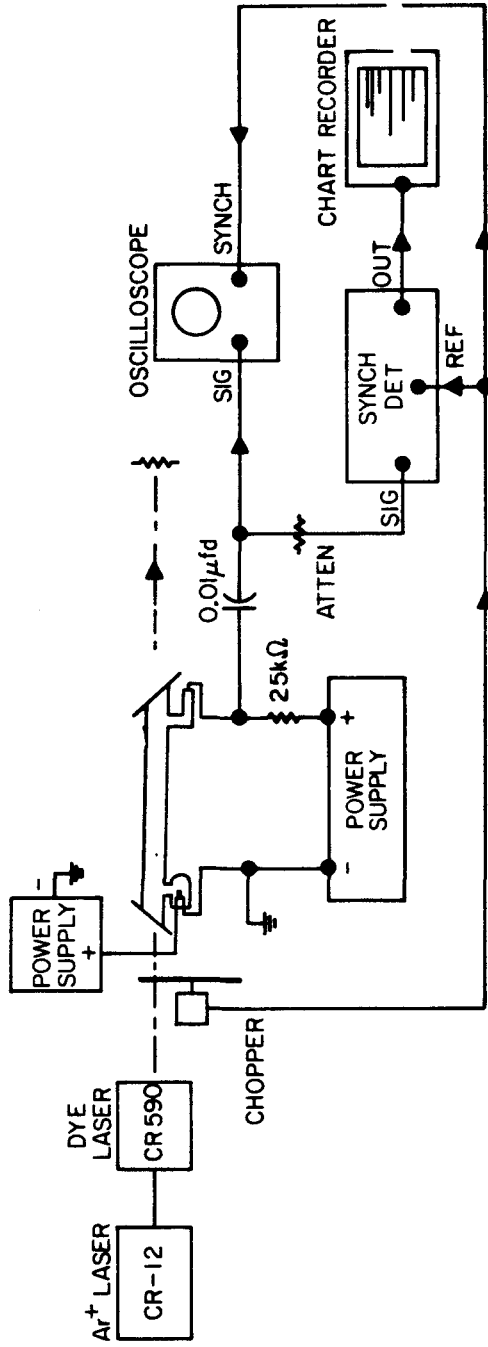
1. Apparatus

The experimental setup for the investigation of illumination of a hydrogen discharge is shown in Fig. VII.1. The illumination source consisted of a CR-590 (Coherent Inc., Palo Alto, CA) dye laser with rhodamine 101 dye (sold as Rh 640 by Exciton Chemical Corp., Dayton, OH) excited by the 5145\AA line of a Coherent CR-12 argon ion laser. The maximum power available was about 150 mW at 6563\AA , with a nominal bandwidth of 40 GHz.

The chopper was typically operated at a frequency of ~ 1 kHz. The magnitude of the OGE signals was found not to depend on the chopping frequency (i.e., the chopping was not exciting any acoustic instabilities of the plasma). The CR-590 dye laser did not drift off the H_{α} line appreciably, and no attempt was made to lock it to the appropriate frequency.

The hydrogen discharge tube consisted of a pyrex tube with microscope slides fastened with Varian Torr-Seal epoxy serving as the end windows. The positive column was approximately 20 cm long. The anode was a conventional neon-sign electrode that had been leached with perchloric acid to remove the barium carbonate coating usually employed to lower the work function in

Fig. VII-1 Basic setup



neon-sign service. The anode was outgassed under vacuum with an RF induction heater. A barium oxide hot cathode consisting of a directly heated coated-nickel strip was used in most of the experiments. A DC current of about 2A raised the temperature to 900°C. Cold cathodes were initially tried, but no amount of cleaning and outgassing could completely remove the impurities (typically CO) sputtered into the discharge.[†] The hot cathode was also found necessary to suppress the noise in the tube. Discharge noise did occur in hot-cathode tubes, but less frequently and more predictably. The OGE signal is sufficiently small in hydrogen that a small amount of noise can obscure the signal entirely. Additionally, strong discharge noise can appear unpredictably (with grim consequences for the front end of the oscilloscope or lock-in amplifier).

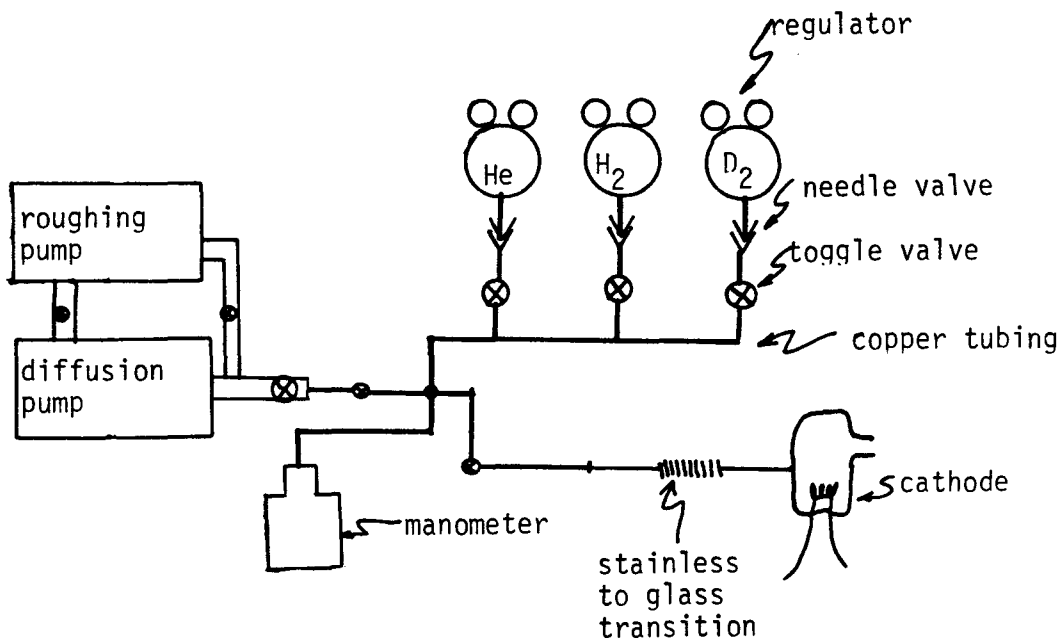
The gas-handling system is diagrammed in Fig. VII.2. Except as noted, it was constructed entirely of 1/4" copper tubing and Swagelok fittings. A stainless-steel-to-glass transition was used to connect the discharge tube; pyrex wool was stuffed into the glass part of the transition to prevent arcing to the material by changing the local pd product. Valves were Teflon-seated; previous attempts with both greased glass valves and greased metal valves introduced impurities into the discharge (CO more often than not).

2. Procedures

A typical experimental procedure was to pump down the entire system for half an hour and heat it simultaneously with either a heat gun or

[†]On one not-so-memorable occasion, an attempt was made to clean a cold cathode by running a high current Ar discharge. The result was a pure C₂ discharge; the spectrum showed clear Swann bands and almost no argon!

Fig. VII-2 Gas handling system



heater tape. Typical bottom-end pressures were $\sim 10^{-7}$ Torr, measured at the ion-gage or the diffusion pump; the limiting factor appeared to be the toggle valve packing. The system was then flushed with ~ 50 -100 Torr He and pumped down to ~ 5 torr (the reason for the buffer was discussed above). Hydrogen was then bled in through a needle valve.

The discharge operates at approximately constant current when excited with resonant illumination. This is because the ballast resistor was quite large (25 k Ω - 40 k Ω) and dwarfed the small resistance change of the PCD ($\sim 1\Omega$) induced by illumination. The OGE signal coupled out through the capacitor was almost entirely a PCD voltage change and not a current change.

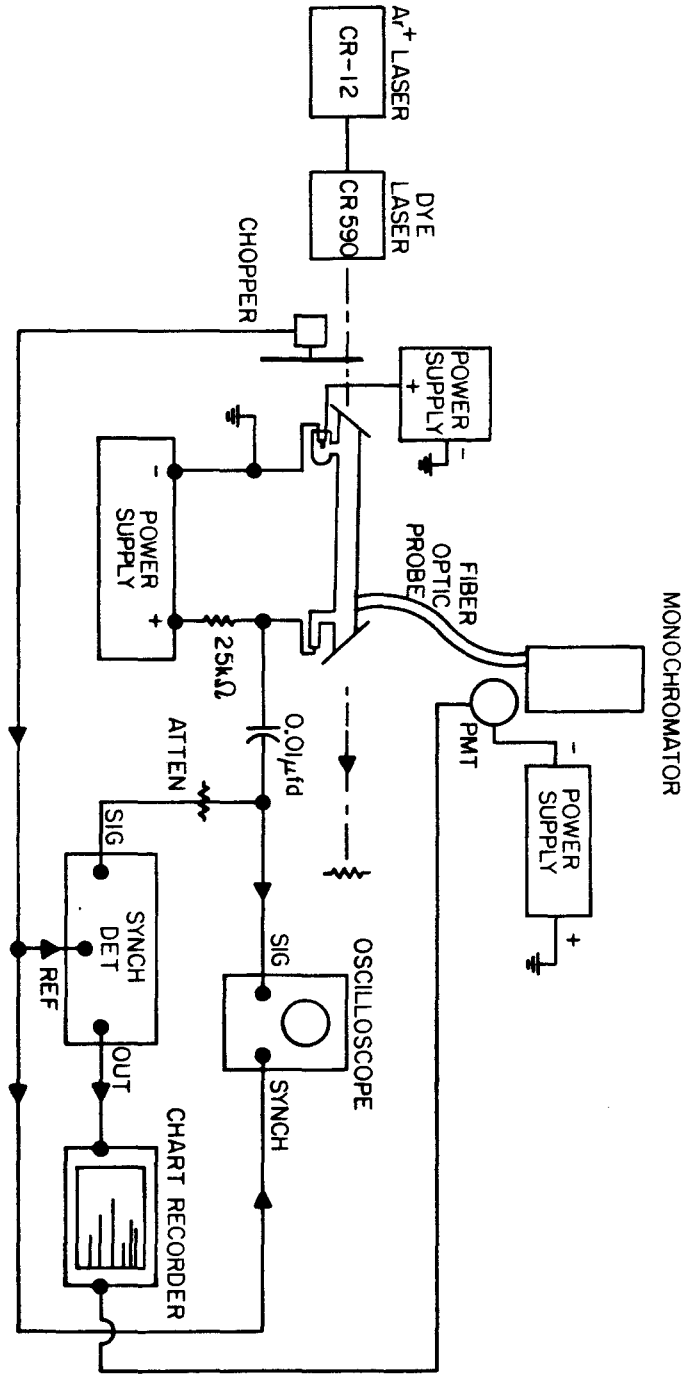
Experimental results were presented in Chapter IV along with the theoretical calculations. For all the OGE measurements, data were taken by measuring the voltage changes directly on the oscilloscope shown in Fig. VII-1. Pressure was read off a digital voltmeter connected to the capacitive manometer (MKS Instruments, type 222AHS), shown in Fig. VII-2. Current was measured directly with a DC ammeter connected in series with the discharge and ballast resistor.

C. STRIATIONS IN THE HYDROGEN DISCHARGE

Pure hydrogen striates very strongly in a discharge; that is, the positive column breaks up into regions of light (strong radiative emission) and dark (negligible radiation). Each striation is several millimeters long.

The presence of striations can affect the magnitude of an optogalvanic signal. An experiment that shows the correlation between striations and OGE was performed to demonstrate this. Figure VII-3 shows the apparatus.

Fig. VII-3 Experiment showing correlation of OGE and striations



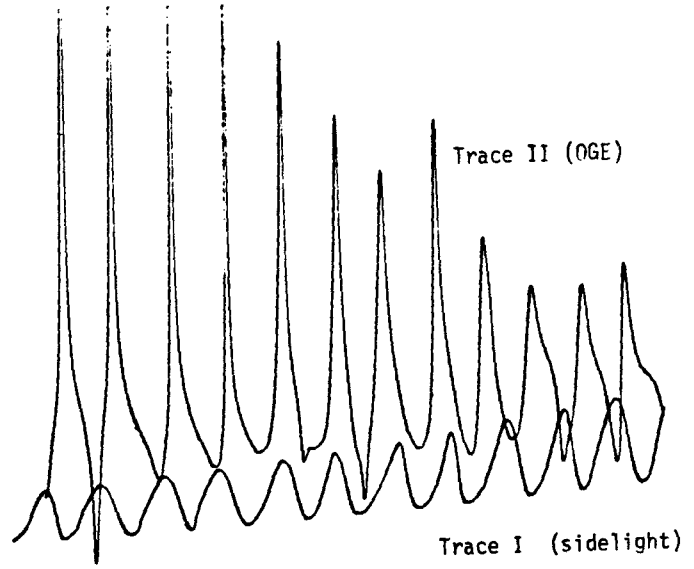
A pure hydrogen discharge was run at a current of ~ 40 mA. The discharge was excited with resonant ($\lambda = 6563\text{\AA}$) radiation from the dye laser, resulting in a voltage change which was measured by a lock-in amplifier. The output of the amplifier was fed to one channel of a strip chart recorder. Simultaneously, a fiber optic probe was placed against the discharge near the anode. The other end of the fiber was placed at the entrance slit of a Jarrell-Ash monochromator tuned to H_{β} ($\lambda = 4861\text{\AA}$), and the photomultiplier tube output of the monochromator was fed to a second channel of the strip chart recorder.

A discharge was struck in the tube at a low pressure (0.2 Torr), and hydrogen was allowed to bleed in through a needle valve, raising the pressure and increasing the number of striations. The resulting traces taken by the strip chart recorder then showed relative OGE and relative sidelight at one location as pressure increased. Figure VII-4 shows the strip-chart traces.

When the pressure increased, the number of striations increased (and the length of each striation decreased slightly). Thus the striations appeared to "move" down the tube until they were "swallowed" by the anode, resulting in the "periodic" sidelight of trace 1. The magnitude of the OGE was strongly affected by the exact positions of the striations in the tube, as is obvious from trace 2.

The relative phase of the OGE signal and the sidelight changes with increasing pressure in Fig. VII-4. This is because the fiber optic sidelight probe was not exactly at the anode. Thus when pressure increased, the number of striations increased, the length of each striation decreased,

Fig. VII-4 OGE and H_{α} sidelight as a function of pressure in the presence of striations



and the fiber optic probe's phase relative to the striations changed.

The helium buffer, introduced primarily to enhance the dissociation of H_2 (Ausschnitt et al., 1978) was also found to suppress striations and yield a more reproducible OGE signal. Sidelight spectra were taken, and almost no H_2 lines were present; they were much weaker than the H atomic lines. Helium lines were also quite weak; since the radiation is generally a small perturbation, it is a fair conclusion that the helium is neither excited nor ionized significantly by the discharge. (This is the standard assumption for a buffer gas in a discharge of a more readily ionized gas; the difference in ionization potentials is ~ 10 eV, so the current is supported almost entirely by electrons from hydrogen ions.)

D. EXPERIMENTAL PROBLEMS

The helium and hydrogen show some tendency to separate in the discharge, with helium preferring the cathode region and hydrogen preferring the anode. This effect was not always observed.

Typical power supply operating voltages were ~ 1500 - 2000 V, most of which (1200 V) was across the ballast resistor. Typical currents were 25-100 mA. Below 25 mA, the discharge was quite unstable and tenuous; above 100 mA, the cathode was overloaded, the discharge walls became so hot that outgassing of impurities was a problem. Typical positive column voltages were ~ 10 - 15 V/cm (measured at zero current through the two Langmuir probes). The apparatus, as noted previously, operates very nearly at constant current.

E. EARLY EXPERIMENT WITH A HYDROGEN RESONANCE LAMP

An earlier and unsuccessful version of this OGE experiment is shown in Fig. VII.5 . A second parallel hydrogen discharge was used as the illumination source instead of the dye laser. The source tube was run with an AC power supply; the passive OGE tube was operated DC. Electrostatic coupling between tubes was found to be a problem, but was eliminated by placing a grounded copper wire screen between the tubes. Blue light from H_{β} was eliminated with red cellophane. Both tubes were wrapped in foil to enhance any radiative coupling. However, even on the infrequent occasions when the DC discharge ran quietly, no OGE was observed. This is, however, in agreement with the theory; the H_{α} luminosities available from a discharge are much too low to produce a signal much above the noise, see Fig. VII-6 and Fig. III-4b.

Fig. VII-5 Parallel tube illumination. Tube radius = 1 cm.

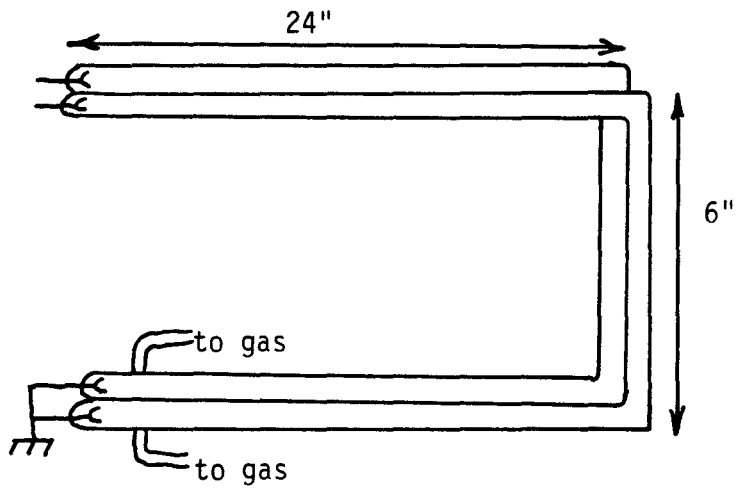
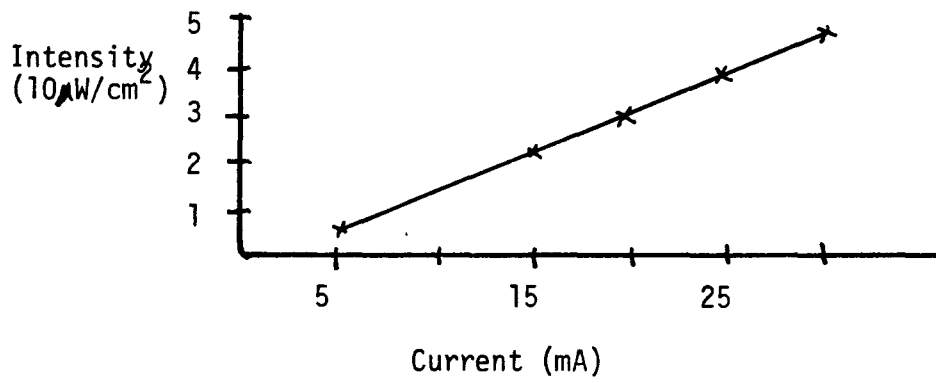


Fig. VII-6 H_{α} luminosity of a 1 cm hydrogen discharge as a function of current at a distance of 5.5 cm



REFERENCES - Chapter VII

Ausschnitt, C. P., G. C. Bjorklund, and R. R. Freeman, Appl. Phys. Lett.
33, 851-853 (1978).

Chapter VIII

OPTICALLY ASSISTED CATAPHORETIC ISOTOPE SEPARATION

VIII. OPTICALLY ASSISTED CATAPHORETIC ISOTOPE SEPARATION

A. INTRODUCTION

The basic idea for isotope separation described in Chapter I was to use a laser to excite one isotope (hydrogen or deuterium) in the body of the discharge and induce increased ionization of that isotope. Preferential ionization would then cause the ions of the excited isotope to be acted on by the discharge electric field for a longer period of time than the other (unexcited) isotope. Thus the excited isotope ions would be preferentially drawn to the cathode, resulting in a physical separation of the two isotopes. A reduced level of ionization caused by illumination (for example, by destroying an important intermediate level) could also be exploited to separate isotopes in the same manner, except the stimulated isotope would drift to the anode.

The purpose of this chapter is to use a model for cataphoresis (Shair and Remer, 1968) in conjunction with the OGE model described in Chapters III-V to try to predict how much isotope separation could be expected with optical excitation. The model of Shair and Remer was chosen over the other models reviewed in Chapter II because it was deemed the most complete. One result of their cataphoresis model is that the degree of cataphoretic separation in a gas discharge depends strongly on the ionization fraction of the preferentially ionized species. The positive column model in Chapter III and the optogalvanic effect model in Chapter IV are sufficient to evaluate the change in

charge fraction induced by external illumination. The unfortunate conclusion is that the average intensities of H_{α} or D_{α} illumination that are available from either resonance lamps or a commercial dye laser are too low to affect the ionization fraction significantly.

B. CATAPHORESIS: THEORY OF SHAIR AND REMER

Shair and Remer (1968) have published the most complete theory of transient and steady state longitudinal cataphoresis. Like other theories (Ch. II), it is based on equating the "preferential flow" of ions to the cathode to the diffusive flux toward the anode caused by the concentration gradient. Assuming the buffer gas is not ionized, ions of the more easily ionized gas are subject to diffusion against the gradient, radial ambipolar diffusion and drag from the electric field. Neutrals of the more easily ionized (impurity) gas are subject only to diffusion in either the longitudinal or radial directions. Thus, in this theory the diffusion equation for the ions of the more easily ionized (impurity) gas reads

$$\frac{\partial n_+}{\partial t} = D_+ \frac{\partial^2 n_+}{\partial z^2} + D_a \nabla_r^2 n_+ + \mu \nabla n_+ + R_c \quad (\text{VIII.1})$$

while for the neutrals of the more easily ionized gas,

$$\frac{\partial n_0}{\partial t} = D \frac{\partial^2 n_0}{\partial z^2} + D \nabla_r^2 n_0 - R_c \quad (\text{VIII.2})$$

where n_0 = concentration of impurity neutrals
 n_+ = concentration of impurity ions

- ∇_r^2 = radial Laplacian
- D_+ = ion diffusion coefficient
- D = neutral diffusion coefficient
- D_a = ambipolar diffusion coefficient
- R_c = production rate of ions
- z = distance from cathode
- μ = mobility of ions

Longitudinal diffusion of atoms in excited states is probably not an important effect, as the populations are quite small for the hydrogen discharges under consideration. Ionization of excited states is unlikely to be an important process for the same reason. While the electron (and ion) density is small, charged species are acted on by the electric field and their longitudinal motion may not be ignored.

Assuming that the ratio of impurity ions to total impurities (the charge fraction) $n_+/(n_0+n_+)$ remains constant, and combining the two equations, a general equation for concentration of the more easily ionized impurity is obtained:

$$\frac{\partial \theta}{\partial \tau} = \frac{\partial^2 \theta}{\partial \eta^2} + \alpha \frac{\partial \theta}{\partial \eta} \quad (\text{VIII.3})$$

where

$$\theta = \frac{n_0 + n_+}{n_0}$$

is the total impurity concentration normalized to the neutral impurity concentration, and

$$\eta = z/L$$

$$L = \text{tube length}$$

$$\alpha = \frac{\mu EL}{D} \frac{n_+}{n_0 + n_+}$$

(which is the charge fraction normalized to $\frac{\mu EL}{D} = \frac{EL}{kT_n} = \frac{V_{\text{total}}}{kT_n}$)

$$E = \text{tube electric field}$$

$$\tau = \frac{tD}{L^2}$$

(the time normalized to the characteristic diffusion time for length L , L^2/D).

Boundary conditions that include the effect of gas reservoirs at the anode and cathode ("endbulbs") are

$$\frac{\partial \theta}{\partial \eta} = \delta(\partial \theta / \partial \tau) - \alpha \theta \quad \text{at } \eta = 0 \quad (\text{VIII.4})$$

where

$$\delta = \frac{\text{cathode bulb volume}}{\text{discharge volume}}$$

$$\epsilon = \frac{\text{anode bulb volume}}{\text{discharge volume}}$$

$$\frac{\partial \theta}{\partial \eta} = -\alpha \theta - \epsilon \left(\frac{\partial \theta}{\partial \tau} \right) \quad \text{at } \eta = 1 \quad (\text{VIII.5})$$

In physical terms, these equations are just continuity equations, saying that an increase or decrease in the atomic concentration in the endbulbs is caused by a net flux of atoms.

Thus

$$\frac{\partial \theta}{\partial \eta} \quad \text{is the flux (divergence) of } \theta$$

$$\frac{\partial \theta}{\partial \tau} \quad \text{is the accumulation of } \theta$$

$$\alpha \theta \quad \text{is the flux of } \theta \text{ due to drift in the electric field}$$

The resulting transient solution is quite complicated and is not given here. However, the steady state part is relatively simple, and is the only result needed in the present work. That is,

$$\theta(\eta, \tau = \infty) = \frac{1 + \delta + \epsilon}{\delta + \epsilon e^{-\alpha} - \frac{e^{-\alpha}}{\alpha} + \frac{1}{\alpha}} e^{-\alpha\eta} \quad (\text{VIII.6})$$

Equation (VIII.6) says that the steady state concentration of impurity atoms has an exponential spatial distribution. The steepness of the profile depends on the charge fraction α .

If the more easily-ionized impurity in the discharge is actually a mixture of isotopes, then each isotope will assume the same exponential profile described above. If they have the same charge fraction, α , which is to be expected, they will have the same spatial distribution. Thus the theory does not predict the cataphoretic separation of isotopes unless, for some reason, one isotope is preferentially ionized or is otherwise preferentially acted on by the discharge. This may be the case in H/D discharges, as explained in Chapter II, because the $\sqrt{2}$ difference in thermal velocities produces quite different molecular recombination rates, which in turn affects the concentrations of the various species.

In the present experimental work, efforts were made to eliminate any formation of H_2 or D_2 molecules, as discussed in Chapter VI. Thus, for these experiments it is appropriate to evaluate the effect of the

H_{α} illumination in stimulating or reducing ionization of one isotope, H or D, without considering the effects of molecules.

C. OPTICAL ASSIST

The OGE model of Chapters III-V may be used to calculate the change in charge fraction with the addition of resonant illumination, which with equation (VIII.6) will yield an estimate of how much external illumination affects cataphoretic separation. For a pure hydrogen discharge, Fig. IV-3 indicates that the relative change in the electron density is negative, and at most $\approx 3 \times 10^{-4}$ for an illumination intensity of several hundred milliwatts (broadband). Accordingly, in a discharge that is a mixture of H and D, the charge fraction of the illuminated isotope (hydrogen or deuterium) will change by less than one percent. This is not sufficient to cause a significant separation; from equation (VIII.6)

$$\theta + \delta\theta \sim e^{(\alpha + \delta\alpha)}$$

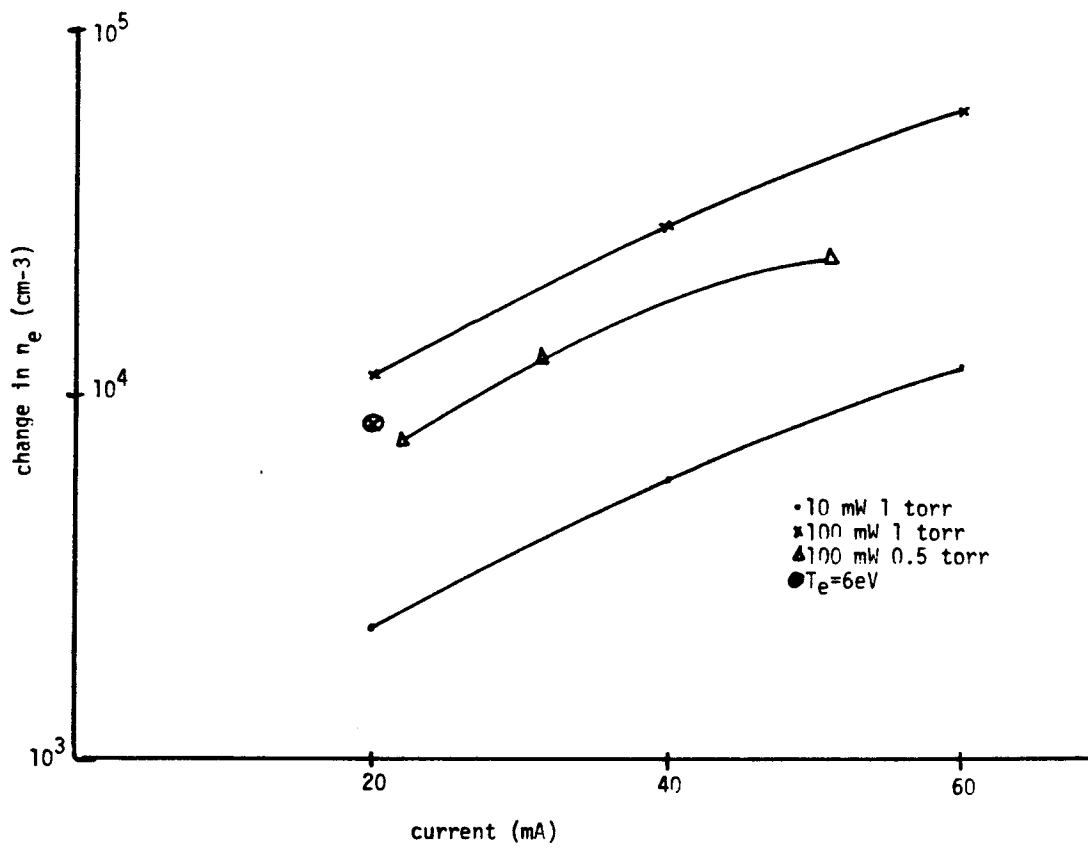
or

$$\delta\theta \sim \eta\delta\alpha$$

so the optically enhanced separation is too small to be significant.

At higher intensities, the electron (and ion) density will be affected more than at lower intensities. However, when the intensity is high enough that the transition is saturated (this occurs at about 12 watts broadband), additional illumination has no effect on the electron density or on any other discharge variable. At this high intensity, the change in ion density will probably still not be enough

Fig. IV-3 Change in electron density n_e from H_α illumination of a hydrogen positive column



to produce a significant separation. Even if Δn_e scaled directly with laser power instead of saturating, Fig. IV-3 indicates that at 10 watts, Δn_e would be $\approx 3 \times 10^7 \text{ cm}^{-3}$, still less than one percent of the total n_e of $\approx 10^{10} \text{ cm}^{-3}$. (Note that at high intensities the model may fail if there is a change in T_e caused by the laser.) Thus, under fully saturated conditions for the hydrogen discharge considered in Fig. IV-3 (1 torr hydrogen, 40 mA current) no laser-assisted cataphoresis is expected. The effect is just too small.

In the foregoing argument, it was assumed that the change in electron density and charge fraction must be the cause of cataphoretic separation, as in Shair and Remer's model. The conclusion that optically assisted separation in H/D mixtures is not possible may also be deduced with somewhat more physical insight from a different viewpoint. In the absence of illumination, the rate at which atoms are ionized from the ground state is

$$Z_{1c} \equiv n_e n_1 S_{1c}$$

From the state $n=3$, the ionization rate is

$$Z_{3c} \equiv n_e n_3 S_{3c}$$

Therefore,

$$\frac{Z_{3c}}{Z_{1c}} = \frac{n_3}{n_1} \frac{S_{3c}}{S_{1c}} \quad (\text{VIII.7})$$

From Table III-2

$$\frac{S_{3c}}{S_{1c}} \approx 5 \times 10^2 \quad \text{at} \quad T_e \approx 5 \text{ eV} \quad (\text{VIII.8})$$

However, Fig. III-7 indicates that at 5 eV or 30 mA, $(n_3/n_1) \approx 10^{-7}$, meaning that Z_{1c} is much greater than Z_{3c} . Even if resonant illumination changes n_3 by two orders of magnitude, which is more than Fig. IV-2 would predict, Z_{3c} will still be less than one percent of Z_{1c} . Thus the H illumination cannot produce a significant change in the gross excitation of the discharge. Even if the $\approx 12\text{W}$ required to saturate the transition were available, this conclusion would be roughly true. At full saturation, $n_3 = n_2$. From Fig. III-5 for the hydrogen discharge parameters under consideration, n_2 would be $\approx 10^{13}$, and thus

$$\frac{Z_{3c}}{Z_{1c}} \approx 10^{-1} \quad (\text{VIII.9})$$

which might be observable.

Thus, unfortunately, the conclusion is that for hydrogen-deuterium discharges with pressure 0.1 to 5.0 Torr and current 20-100 mA, optically assisted cataphoretic isotope separation is unobservably small with H_α powers of the order of 1/2 Watt. The primary difficulty is that the level from which the optical pumping occurs is too sparsely populated. The situation would be more hopeful if that level were the ground state on a well-populated metastable level.

D. COMPARISON WITH EXPERIMENT AND CONCLUSION

1. Comparison

Cataphoretic isotope separation was attempted in the parallel-tube experiment shown in Fig. VIII-5. One tube was filled with a mixture of equal parts H and D, with total pressure 0.1 to 10.0 Torr. The other tube was filled with one gas only (H or D), and the two tubes were wrapped in foil to enhance the radiative coupling. The H/D tube was operated at currents from 20-150 mA; the monoisotopic tube was run at ≈ 100 mA and served as the isotopically selective illumination source. At no current or pressure, with or without the external illumination, was any isotope separation observed by monitoring H_{α}/D_{α} side-light. No separation without illumination (caused by different recombination rates discussed in Chapter II) was really expected; Beckey, Groth, and Welge (1953) found almost no separation for parameters near those listed above. It was indicated in Chapter V that no optogalvanic effect was observed for any discharge parameters with the parallel tube apparatus. If there is no OGE, it is almost certain there will be no optically assisted isotope separation, as both effects require an optically induced change in the discharge kinetics. The requirements for seeing an OGE seem to be less stringent than those for seeing optical isotope separation.

In the smaller hot cathode discharges of the type shown in Fig. VII-1, no separation of H and D was observed, as was expected. Equation (VIII.6) indicates that, all other parameters being equal,

cataphoretic separation is proportional to length, and these tubes were much shorter than the parallel tubes discussed above. (They were designed for OGE experiments.) Using the indicated laser illumination source, optogalvanic signals were measured, however, in H/D mixtures. Signals were produced with the laser tuned to either the H_{α} or the D_{α} line. No separation was observed with the excitation of either isotope, as expected.

2. Comment

The basic conclusion of this chapter is that H/D isotope separation by optically enhanced cataphoresis is not practical; the enhancement is too small at the H_{α} intensities that are available in the laboratory. At very high H_{α} illumination intensities, the prediction of the PCD model may break down because the light may affect the electron temperature. It seems unlikely that this conclusion would be any different if H_2 molecular processes were considered, for two reasons. First, H_2 has a binding energy of only 4.5 eV (compared to 10.2 eV for the first excitation of H), so it is easily dissociated, and it is very unlikely that H_2 will change the discharge kinetics greatly. Second, the change in charge fraction induced by illumination is, as noted, tiny, and the presence of H_2 is very unlikely to change this. The photon flux from an external source is rapidly attenuated; even when a photon is absorbed by a H or D atom, it excites the atom only by $1.89 \text{ eV}/13.6 \text{ eV} = 14\%$ of the ionization potential.

It may be possible to demonstrate optically enhanced cataphoretic isotope separation in discharges with other elements. In addition to

the requirements imposed by experimental feasibility, the PCD model indicates some other requirements. First, the energy of the stimulating photon (or the sum of the energies of the photons, if multi-step or multi-photon excitation is tried) should be a significant fraction of the ionization energy of the atom. Such illumination is very likely to change the electron temperature in the discharge. Second, high illumination intensity will almost certainly be required, since it is desirable to excite every atom of one isotope. Thus the (maximum) power requirement is (neglecting radiation trapping) one photon per atom in state c in the length of time $1/A_{ji}$, where A_{ji} is the A-coefficient of the $j \rightarrow i$ transition. (This does not imply that a small A coefficient is desirable, however; in the limit $A \rightarrow 0$, no excitation would occur.) Low atomic densities reduce the power requirements and also reduce the problem of charge exchange (excitation exchange) between nearly identical levels of isotopes, which usually is huge (200 times typical electronic cross-sections) and would reduce the selective excitation considerably at higher pressures.

REFERENCES - Chapter VIII

Beckey, H., W. Groth, and K. Welge, Naturw. 8a, 556 (1953).

Shair, F. H. and D. S. Remer, J. Appl. Phys. 39, 5762 (1968).

Chapter IX
FUTURE POSSIBILITIES

IX. FUTURE POSSIBILITIES

A. INTRODUCTION

This chapter contains a collection of ideas relating to the preceding thesis that may be pursued by the next investigator. They are, in general, ideas that suggested themselves as the work progressed but probably would not have contributed much to the main goal of understanding the OGE and optically assisted cataphoresis. No claims are made for the viability of any ideas in this section, as they are for the most part untried. Caveat emptor.

B. POSSIBLE EXTENSIONS OF THEORY AND SIMULATION

1. Molecular Model

An interesting extension of the hydrogen PCD and OGE model described in Chapters III, IV, and V would include some molecular kinetics. A H/D discharge in fact will contain H, D, H₂, D₂, HD, and positive ions of each of these species. The important molecular processes include recombination at the walls (proportional to the wall flux $D_a \nabla_r^2 n_e$) excitation of molecular neutral levels and subsequent radiation dissociation of all molecular species and reactions, e.g., H₂ + D₂ → 2HD. Any recombination term in atomic molecular rate equations should include a parameter to account for the fact that recombination may be determined by wall conditions. Power balance must include molecular as well as atomic processes.

2. Bipolar Signal

Another possible extension of the theory would be to simulate a discharge with a gas that has metastable levels. Positive OGE voltage changes (H_{α} illumination of hydrogen always produces a negative signal) are associated with optically pumping electrons from metastable levels to higher excited states that can decay radiatively to the ground state. Even though the external illumination adds energy to the discharge, it causes enhanced emission of photons in the resonance decay, resulting in a net energy loss. At constant current, the electric field must "make up" the loss, hence the OGE voltage is positive. Positive OGE's are seen in neon, for example (Zalewski et al., 1980). In the preceding theory, even though the terms proportional to R in equation (IV.3) represent energy flowing into the plasma and a negative OGE, the energy input ω_e in the first term will be strongly increased, resulting in a positive OGE. It would be very interesting to model a simple system with metastables and try to predict a positive OGE voltage. Unfortunately, any real atom with metastable states is likely to have too many levels to model accurately. Some OGE signals originating from excitation of metastable levels are observed experimentally to be bipolar (Bridges, 1978) as a function of current, since current affects the metastable population. This could be explained as the competition between two effects using equation (IV.3) exactly as above.

3. He-Ne Optogalvanic Lamb Dip

It would be an interesting, if ambitious, project to develop a simulation for the He-Ne laser. Johnston (1978) measured an "optogalvanic Lamb dip" in the He-Ne laser. He found that as he tuned a narrowband dye laser near $6328\overset{\circ}{\text{A}}$ that illuminated a He-Ne discharge from both directions, the optogalvanic signal so produced was reduced on line center from the signal produced off line center. This is due to the fact that both beams were exciting the same atoms, and absorption was reduced. The theory in Chapter IV and Appendix IV is sufficient to give a quantitative evaluation of this effect if a reasonable simulation of a HeNe PCD could be developed.

A more limited approach would be to use the theory of Gordon et al.(1963). An alternative experiment would be to measure the optogalvanic Lamb dip resulting from H_{α} illumination of a hydrogen discharge, since the simulation is relatively simple. The extension of the theory to cover saturation effects, such as the optogalvanic Lamb dip, is given in Appendix IV.

C. POSSIBLE FUTURE EXPERIMENTS

1. Microwave Radiometry and Synchronous T_e Measurements

As noted in Chapter VII, a discharge embedded in a microwave waveguide could be used to measure the electron temperature. Microwave radiation originating from bremsstrahlung generated by electron collisions is simply related to the electron temperature (Parzen and Goldstein, 1950). It would be interesting to measure T_e this way. The

gas in the discharge would be excited with a laser as in Fig. IX-1. Alternatively, the experiment could be conducted in a slotted waveguide (Bridges, 1978, unpublished) and the light from a laser or resonance lamp would excite the discharge through the slot, as in Fig. IX-2.

Spatially averaged changes in T_e could be measured this way. This scheme is obviously amenable to synchronous detection: chopping the illumination and looking for synchronous modulation of the microwave noise would enhance sensitivity considerably. The drawback is that it is somewhat hard to say just what the microwave measurement means if the plasma is non-Maxwellian, which it almost certainly is.

An alternative scheme is to use double Langmuir probes described in Chapter VII inside a laser discharge and look for changes in the probe characteristic when the optical cavity is synchronously "spoiled." This eliminates the problem that occurs in an externally illuminated discharge, that light is absorbed as it propagates between the probes. Alternatively, a high intensity narrowband laser could be used to saturate (bleach) the transition and absorption would be less important. This second method is not expected to yield significant results. A similar experiment performed in the CO_2 laser (Garscadden and Bletzinger, 1969), did not find significant changes in electron temperature due to lasing. Even at low currents in hydrogen, where there is little enough absorption that light can reach the probes, only miniscule ($< 5\%$) changes in the probe characteristic were observed. Combined with the lack of an exact saturation current discussed in

Fig. IX-1 Discharge embedded in microwave waveguide for electron temperature measurement

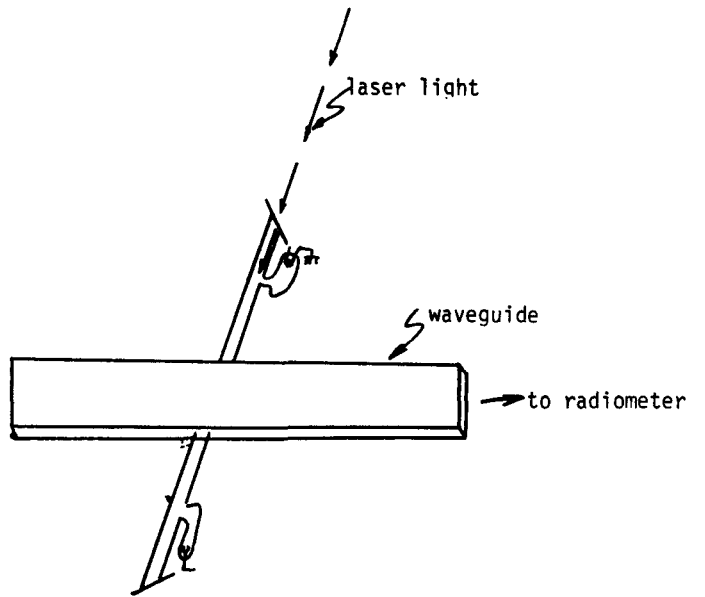
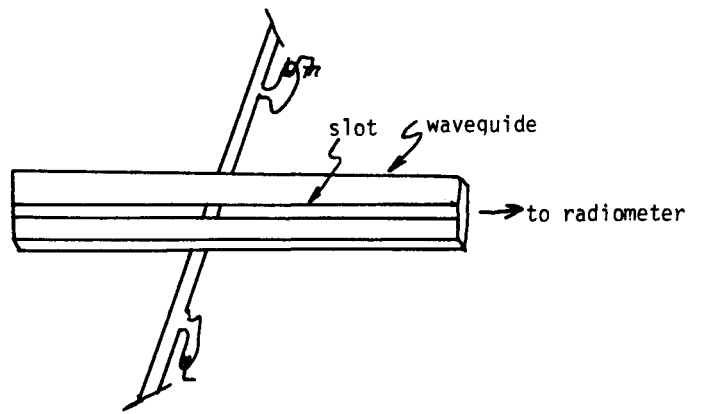


Fig. IX-2 Discharge in slotted waveguide



Chapter VII, the changes were too small to be significant in hydrogen.

3. Optogalvanic Photon Echoes

An interesting experiment would be to use the optogalvanic effect to detect photon echoes. In a conventional photon echo experiment, two pulses of resonant light are used to excite some atoms; a third pulse appears spontaneously when the atoms radiate (for an explanation, see Yariv, 1975). The first two pulses could certainly be detected by optogalvanic means, and the preceding theory would be applicable. However, the third pulse is spontaneously generated from energy contained by the atoms in coherent excited atomic states and might produce an optogalvanic signal.

4. Optically Assisted Cataphoresis of Different Gases

Optically assisted cataphoresis could, in principle, be demonstrated with two different gases instead of two isotopes. The collection of the more easily ionized gas at the cathode could be enhanced by illumination. Cataphoresis, unfortunately, is only a small effect in a HeNe discharge, or a HeNe laser would be an ideal vehicle for demonstrating optically assisted cataphoresis; the laser would serve as the illumination source. A He-Cd laser might be an alternative. This experiment is obviously of limited utility, since the whole point of using the optical "assist" was as a way of distinguishing isotopes.

5. Other Candidates for Optically Enhanced Cataphoretic Isotope Separation

Other gases that might demonstrate optically enhanced isotope

separation are ^3He and ^4He , $^6\text{Li}/^7\text{Li}$, and $^{151}\text{Eu}/^{153}\text{Eu}$. While He is easy to work with and might be a good vehicle for demonstrating isotope separation, it is of little practical importance since ^3He does not occur naturally (it is a decay product of ^3H), thus it does not need to be separated from ^4He . Lithium and europium both have potential for cataphoretic separation. Both appear to have absorption lines with a suitable isotope shift, although experimental documentation is poor, and a sub-Doppler experiment may be necessary to obtain selective excitation. Both require a discharge inside an oven to obtain a significant amount of metal vapor. Two-step excitation of lithium is possible with the first photon at 6708\AA and the second at 6104\AA .

The amount of isotopic cataphoresis in lithium could possibly be measured (Bridges, 1976, unpublished) by allowing the metal to deposit on the cool regions of the discharge walls outside the oven. The tube regions so coated could be removed from the discharge and used as cathodes in hollow cathode lamps. A buffer gas would sputter the lithium cathode and the isotopic abundances could be evaluated by using the same laser that excited the positive column discharge to produce an optogalvanic effect in the hollow cathode lamps.

6. Other Hydrogen Cataphoresis Experiments

If spontaneous H/D cataphoresis occurs because more H than D associates at the discharge walls, as discussed in Chapter VIII, then the degree of cataphoretic separation should be affected by wall properties. A wall which enhances association might also enhance separation;

one that decreases association might decrease separation. There is a certain amount of "black magic" in understanding what wall materials enhance association (see Chapter III), but an interesting experiment would be to vary discharge wall properties and evaluate the effect on cataphoresis.

A related experiment is to measure the radial variation of H and H₂ or a mixture of H and D in a discharge by looking at atomic and molecular lines in the light seen at the end of a discharge. This technique is covered in detail in Webb (1968). For example, if H₂ is produced at the walls, an enhanced H₂ emission would be expected from the regions of gas near the walls. It would be interesting to correlate relative radial species populations with the wall properties and the degree of spontaneous isotope separation.

REFERENCES - Chapter IX

- Bridges, W. B., J. Opt. Soc. Am. 68, 352-359 (1978).
- Garscadden, A. and P. Bletzinger, Proc. Ninth Int. Conf. Phen. Ion. Gas,
Bucharest 1969.
- Gordon, E., A. White, and J. Rigden, Proc. Symp. Optical Masers
(Polytechnic Inst. of Brooklyn, 1963), pp. 309-319.
- Johnston, T. F., Laser Focus, 58 (March 1978).
- Parzen, P., and L. Goldstein, Phys. Rev. 79, 190 (1950).
- Webb, C. E., J. Appl. Phys. 39, 5441-5470 (1968).
- Yariv, A., Quantum Electronics (John Wiley, New York, 1975).
- Zalewski, E., R. Keller, and R. Engleman, J. Chem. Phys., 1980 (accepted
for publication).

Appendix I

HYDROGEN EXCITATION CROSS SECTIONS

Appendix I: HYDROGEN EXCITATION CROSS SECTIONS

A summary of the electron collision excitation cross sections available in the literature is presented in Tables AI-1 to AI-6. Table AI-7, showing the values of σ actually used, is the same as Table III.1 .

AI-1. Ionization from the Ground State

The cross section for the $n=1$ continuum transition is well known for hydrogen; the peak cross section occurs at about 30-50 eV; various values are given in Table 1.

Table 1. Peak cross sections for ionization of ground state hydrogen. E = experimental; T = theoretical

Author	$\sigma(\pi a_0^2)$
Fite (1958, 1959)	.8 (E)
Boksenberg (1961)	.72 (E)
	.8 (T)
Coulter (1978)	.9 (T)
Golden (1971)	.85 (T)

AI-2. Ionization from $n=2$

With the exception of the paper by Dixon et al., who measured the ionization cross section of the 2s metastable level, the values are exclusively theoretical. Results are presented in Table 2.

Table 2. Peak ionization cross sections of $n = 2$ hydrogen. E = experimental; T = theoretical

Author	State	$\sigma_{2c} \max(\pi a_0^2)$
Dixon (1975)	2s	6.5 - 19 (E)
Omidvar (1965)	2s + 2p	18 (T)
Omidvar (1965)	total	14 - 19 (T)
Prasad (1966)	total	13 - 19 (T)

AI-3. Ionization from $n = 3$

A small transition energy makes the $n = 3$ - continuum transition cross sections quite large. No experimental values were found. Results are presented in Table 3.

Table 3. Peak ionization cross section of $n = 3$ hydrogen. E = experimental; T = theoretical

Author	State	$\sigma_{3c} \max(\pi a_0^2)$
Omidvar (1968)	3d $m = 1$	105
	3d $m = 2$	93
Krinberg (1969)	total	95.9

AI-4. n = 1 to n = 2 Excitation

Results are in Table 4.

Table 4. Maximum excitation cross sections for n = 2 to n = 3 transition in hydrogen. E = experimental; T = theoretical; ? = no clear maximum.

Author	Trans.	$\sigma_{12}^{\max}(\pi a_0^2)$
Calloway (1975)	1s - 2s	0.2 (T)
Kaupila (1970)	1s - 2s	0.15 - 0.19 (E)
Kochsmeider (1973)	1s - 2s	0.23 (E)
McDowell et al. (1973)	1s - 2s	0.11 (T)?
Pindzola (1975)	1s - 2s	.35 (T)
Calloway (1975)	1s - 2p	0.75 (E)?
McGowan (1969)	1s - 2p	0.8 ?
Long (1968)	1s - 2p	0.80 (T)?
Pindzola (1975)	1s - 2p	1.0 (T)
Golden (1971)	1 - 2 total	.88 (T)

AI-5. n = 1 to n = 3 Excitation

Results are in Table 5.

Table 5. Maximum excitation cross sections for n = 1 to n = 3 transitions in hydrogen. E = experimental; T = theoretical; ? = no clear maximum

Author	Transition	$\sigma_{13}(\pi a_0^2)$
Mahan (1976)	1s - 3s	$2 - 2 \times 10^{-2}$ (E)
McDowell et al. (1973)	1s - 3s	3×10^{-2} (T)?
Mahan (1976)	1s - 3p	$1 - 2 \times 10^{-1}$ (E)
Mahan (1976)	1s - 3d	$3 - 5 \times 10^{-2}$ (E)
Syms (1975)	1 - 3 total	1.25×10^{-2}

Table 6. Maximum cross sections for n = 2 to n = 3 transitions in hydrogen. T = theoretical; ? = no clear maximum

Author	Transition	$23_{\max}(\pi a_0^2)$
Blerkom (1968)	2s - 3s	19 (T)
Burke (1967)	2s - 3s	10 (T)
Blerkom (1968)	2s - 3p	14 (T)
Burke (1967)	2s - 3p	14 (T)
Blerkom (1968)	2s - 3d	8 (T)
Burke (1967)	2s - 3d	22 (T)?
Burke (1967)	2p - 3s	0.8 (T)
Blerkom (1968)	2p - 3p	33 (T)
Burke (1969)	2p - 3p	13 (T)
Blerkom (1968)	2p - 3d	43 (T)
Burke (1967)	2p - 3d	37 (T)?
Blerkom (1968)	2 - 3 total	55 (T)
Burke (1967)	2 - 3 total	47 (T)

Table AI-7 Peak cross sections used for computing excitation rates.
 a_0 is the Bohr radius.

Principal Quantum Number of Transition	Peak Cross Section, σ_{ij} πa_0^2
1-c	.75
2-c	18.0
3-c	95.9
1-2	.88
1-3	1.25×10^{-2}
2-3	50.0

REFERENCES - Appendix I

- Blerkom, J. V., J. Phys. B 1, 423-427 (1968).
- Boksenberg, A., Thesis, University of London, 1961; Data from Golden op cit.
- Burke, P., S. Ormonde, and W. Whitaker, Proc. Phys. Soc. 92, 319-335 (1964).
- Burke, P., A. Taylor, and S. Ormonde, Proc. Phys. Soc. 92, 345-350 (1967).
- Burke, P., D. Gallagher, and S. Geltman, J. Phys. B 2, 1142 (1969).
- Calloway, J., M.R.C. McDowell, and L. A. Morgan, J. Phys. B 8, 2181-2190 (1975).
- Coulter, P. W. and W. R. Garrett, Phys. Rev. A 18, 1902-1907 (1978).
- Dixon, A. J., A. von Engel, and M.F.A. Harrison, Proc. Roy. Soc. Lond. A 343, 333-349 (1975).
- Fite, W. and R. Brackman, Phys. Rev. 112, 1141 (1958); Phys. Rev. 113, 1151 (1956).
- Fite, W., R. Stebbings, and R. Brackmann, Phys. Rev. 116, 356 (1959).
- Golden, L. B. and D. H. Sampson, Astrophys. J. 163, 405-410 (1971).
- Kauppila, W., P. Burke, and W. Fite, Phys. Rev. A 1, 1099-1108 (1970).
- Kauppila, W., W. Oh, and W. Fite, Phys. Rev. A 1, 1099 (1970).
- Kochsmeider, H., V. Raible, and H. Klinpoppen, Phys. Rev. A 8, 1355-1358 (1973).
- Krinberg, I. A., Sov. Astron-AJ 12, 840-843 (1969).
- Long, R., D. Cox, and S. Smith, J. Res. NBS 72, 521-535 (1968).
- Mahan, A. H., A. Gallagher, and S. J. Smith, Phys. Rev. A 13, 156-166 (1976).
- McDowell, M.R.C., L. A. Morgan, and V. P. Myerscough, J. Phys. B 6, 1441-1451, (1973).
- McGowan, J., J. Williams, and E. Curley, Phys. Rev. 180, 132-138 (1969).

- Omidvar, K. and E. Sullivan, Proc. Conf. Ionized Gases, 1965, p. 263-273.
- Omidvar, K., Phys. Rev. 140, A26-A27 (1965); Phys. Rev. 140, A38-A46 (1965).
- Pinzola, M. S. and H. P. Kelly, Phys. Rev. A 11, 221-229 (1975).
- Prasad, S. S., Proc. Phys. Soc. 87, 393-398 (1966).
- Syms, R. F., M.R.C. McDowell, L. A. Morgan, and V. P. Myerscough, J. Phys. B 8, 2817-2834 (1975).

Appendix II
COMPUTER PROGRAMS

Appendix II: COMPUTER PROGRAMS

This appendix contains one version of each of the three principal computer programs used in the thesis. The first program is for the calculation of the steady state OGE by iteration of equations (III.55 and III.56). The second program calculates the explicit temporal response of a hydrogen discharge plasma to resonant H_{α} optical stimulation by numerical integration of the rate equations. The third program is for the calculation of the time constants in the perturbation theory of Chapter V.

Program #1

This program computes the level populations in a hydrogen discharge by iterating equations (III.55 and III.56) until stable populations result. The array DATAIN contains the experimentally determined values for current, electron temperature as a function of pressure; these values serve as "inputs" to the equations. Other input variables are specified, and then the subroutine WEBB is called to calculate the excitation rate as a function of peak cross section (see Chapter III). Initial guesses are made for the level populations, and the subroutine HOLST is called to calculate the radiation trapping factors GAM21 and GAM31. Expressions for the level populations, collision frequency, energy input, and electric field are then iterated until they stabilize. The radiative excitation terms (proportional to the radiation density WBAR) are then added to the expressions for the level populations, and the iteration process is repeated. Results are stored in the arrays ARN2, ARN3, ARNE, and AREE, and the differences in the level populations due to the excitation are calculated. The results agree

exactly with the more formal numerical integration presented in Program #2.

Program #2

The second program calculates the temporal response of a hydrogen plasma to optical excitation by integrating the rate equations directly. The initial setup is much the same as Program #1. Input data for I , T_e , and p are specified (note this program treats one set of these three input parameters only, unlike Program #1). Initial guesses are made for the populations and stored in the array POPO. The numerical integrator GEAR calculates the behavior of the populations (with no illumination) up until the time TOUTS. The illumination is then "added" to the rate equations and the integration is repeated.

The subroutines HOLST and WEBB are the same as in Program #1, calculating respectively the radiation trapping and excitation rates. The subroutine DIFFUN contains the rate equations called by GEAR; each time DIFFUN is called, the electron density NE, collision frequency ANUE, power input OMEGEP and electric field EE are calculated with a call to the subroutine ELDEN. The level populations are stored in the PLOT arrays and fed to a plotter. The results agree exactly with those of Program #1

Program #3

This program calculates the time constants in equations (V.26, V.27) derived from perturbation theory in Chapter V. The input variables are initialized exactly as in Program #1, and the level populations are found by iterating algebraic equations (III.55), (III.56) again, as in Program

#1. The coefficients of \tilde{n}_2 and \tilde{n}_3 , the perturbations to the level populations induced by resonant illumination are calculated as ALPHA, BETA, GAMMA, and DELTA, which all contain the constants AAA and BBB. These numbers are printed out, and the calculation is repeated for all the sets of input data in DATAIN.

Program #1

IV G LEVEL 20.7 VS MAIN DATE = 6/27/80 14:55:44

```
IMPLICIT REAL*8(A-Z)
REAL*8 LASER,NE
INTEGER*4 ITE,JN1,ILOOP,ISAT
C
C
C
DIMENSION ARN2(3,4),ARN3(3,4),ARNE1(3,4)
& ,AREE(3,4)
& ,ARN2N(3,4),ARN3N(3,4),ARNE1N(3,4)
& ,AREEN(3,4)
& ,DATAIN(2,3,4),PRESS(4)
C
C
PRESS(1)=0.5
PRESS(2)=1.0
PRESS(3)=2.5
PRESS(4)=5.0
C
C
DATAIN(1,1,1)=22.0
DATAIN(1,2,1)=31.5
DATAIN(1,3,1)=51.0
DATAIN(2,1,1)=3.9
DATAIN(2,2,1)=4.9
DATAIN(2,3,1)=6.35
DATAIN(1,1,2)=20.0
DATAIN(1,2,2)=40.0
DATAIN(1,3,2)=60.0
DATAIN(2,1,2)=4.6
DATAIN(2,2,2)=6.6
DATAIN(2,3,2)=7.0
DATAIN(1,1,3)=15.
DATAIN(1,2,3)=24.
DATAIN(1,3,3)=62.
DATAIN(2,1,3)=4.1
DATAIN(2,2,3)=4.0
DATAIN(2,3,3)=5.6
DATAIN(1,1,4)=18.5
DATAIN(1,2,4)=48.
DATAIN(1,3,4)=72.
DATAIN(2,1,4)=5.5
DATAIN(2,2,4)=6.5
DATAIN(2,3,4)=6.62
WRITE(6,444)((DATAIN(1,ITE,JN1),ITE=1,3),JN1=1,4)
444 WRITE(6,444)((DATAIN(2,ITE,JN1),ITE=1,3),JN1=1,4)
FORMAT( 4( E12.5,2X),//)
C
C
DC 966 ISAT=1,10
C
C
INPUT VARIABLES
C
TE IS ELECTRON TEMPERATURE IN EV IEV=1.6E-12 ERGS
DC 999 ITE=1,3
DC 999 JN1=1,4
C
C
IV G LEVEL 20.7 VS MAIN DATE = 6/27/80 14:55:44
C
N1=PRESS(JN1)*3.54E16
TL=DATAIN(2,ITE,JN1)
C
IN IS NEUTRAL TEMP, IN EV
IN=.6322DC
```

```
C      R IS TUBE RADIUS IN CM
      R=0.500
C      ALALW IS LASER LINEWIDTH, HZ
      ALALW=40.04
C      ALI IS TOTAL LASER POWER, WATTS
      ALI=0.01
C
C      ALI=ALI*ISAT
C
C      PHE IS BUFFER PRESSURE, TORR
      PHE=5.00
C      PH IS HYDROGEN PRESSURE, TORR
      PH=0.500
C      PTOT=TOTAL PRESSURE, TORR
      PTOT=PH+PHE
      A31H=5.57507
      A32H=4.4107
      A21H=4.65406
      WBAR=ALI*1.67/(3.141600*R**2*ALALW*3.010)
      WBARM=WBAR
      B32H=A32H*(6563.D-8)**3/(8.D0*3.141600*6.626D-27)
      B23H=B32H*18.00/8.00
C      WRITE(6,2) TN,R,ALALW,ALI,WBAR,B32H,B23H,A31H,
C      & A32H,A21H,PH,PHE
2  FORMAT( ' NEUTRAL TEMP =',D10.3,'EV',//,
& ' TUBE RADIUS=',D10.3,'CM',//,
& ' LASER LINEWIDTH=',D10.3,'GHZ',//,
& ' LASER INTENSITY=',D10.3,'WATTS',//,
& ' ENERGY DENSITY=',D10.3,'ERGS/HZ/CM3',//,
& ' B32H=',D10.3,'SEC-1/WBAR',//,
& ' B23H=',D10.3,'SEC-1/WBAR',//,
& ' A31H=',D10.3,'SEC-1',//,
& ' A32H=',D10.3,'SEC-1',//,
& ' A21H=',D10.3,'SEC-1',//,
& ' HYDROGEN PRESS=',D10.3,'TORR',//,
& ' HE BUFFER PRESS=',D10.3,'TORR')
C      COMPUTE COEFFICIENTS FOR RATE EQUATIONS
C      HYDROGEN
      CALL WEBB(1.7500,13.600,TE,SIGAV)
      S14H=SIGAV
      CALL WEBB(15.00,3.400,TE,SIGAV)
      S24H=SIGAV
      CALL WEBB(95.900,1.5100,TE,SIGAV)
      S34H=SIGAV
      CALL WEBB(1.000,10.200,TE,SIGAV)
      S12H=SIGAV
      S21H=S12H*.2500*DEXP(10.200/TE)
      CALL WEBB(60.00,1.8900,TE,SIGAV)
      S23H=SIGAV
      IV G LEVEL 20.7 VS      MAIN      DATE =      6/27/80      14:55:44
      S32H=S23H*8.00/18.00*DEXP(1.8900/TE)
      CALL WEBB(1.00000,12.0900,TE,SIGAV)
      S13H=SIGAV
      S31H=S13H/9.00*DEXP(12.0900/TE)
      WRITE(6,3) TE
3  FORMAT( ' ELECTRON TEMPERATURE =',D10.3,'EV')
C      WRITE(6,5) S14H,S24H,S34H,S12H,S21H,S13H,S31H,S23H,S32H
5  FORMAT( ' S14H=',D10.3,//,
& ' S24H=',D10.3,//,
& ' S34H=',D10.3,//,
& ' S12H=',D10.3,//,
```



```

C      DA=(R/2.405)**2*(N1*S14H+N2*S24H+N3*S34H)
C      PIG=0.
C      OMEGEP=0.432*N1*(S14H*E14+S13H*E13+S12H*E12)
E      +0.269*N2*(S23H*E23+S24H*E24-PIG*S21H*E12)
E      +0.269*N3*(S34H*E34-PIG*(S32H*E23+S31H*E13))
C      E      +7.85*DA*.5.*TE/(3.1416*R**2)

```

```

C      NE=CUR/(3.1416*R**2*DSQRT(0.432D0))
E      *DSQRT(ANUE*.511D6/OMEGEP)
E      /(3.010*1.6D-19)

```

```

C      N2=(0.432*NE*N1*S12H+0.539*NE*N3*S32H
E      +0.432*N3*(A32H+B32H*WBAR))
E      /(0.432*LAM21*A21H+0.269*NE*(S21H+S23H+S24H)
E      +0.432*B23H*WBAR)

```

```

C      N3=(0.432*NE*N1*S13H+0.269*NE*N2
E      *S23H+0.432*N2*B23H*WBAR)
E      /(0.269*NE*(S31H+S32H+S34H)
E      +0.432*(B32H*WBAR+A32H*GAM31*A31H))

```

```

C      EE=DSQRT(ANUE*OMEGEP*.511E6)/(3.E10*SQRT(.432))
E      +1.6E-19/CUR*
E      (-B23H*WBAR*N2*E23*0.432*3.1416*R**2
E      +B32H*WBAR*N3*E23*0.432*3.1416*R**2)

```

IV G LEVEL 20.7 VS MAIN DATE = 6/27/80 14:55:44

```

C      112 CCNTINUE
C      IF(WBAR.EQ.WBARM) GO TO 955

```

```

C      ARN2(ITE,JN1)=N2
C      ARN3(ITE,JN1)=N3
C      ARNE1(ITE,JN1)=NE
C      AREE(ITE,JN1)=EE
C      WBAR=WBARM
C      GO TO 108

```

```

C      955 ARN2N(ITE,JN1)=N2
C      ARN3N(ITE,JN1)=N3
C      ARNEIN(ITE,JN1)=NE
C      AREEN(ITE,JN1)=EE
C      999 CCNTINUE

```

```

C      JC 998 JN1=1,4
C      DC 998 ITE=1,5

```

```

ARN2N(ITE,JN1)=ARN2N(ITE,JN1)-ARN2(ITE,JN1)
ARN3N(ITE,JN1)=ARN3N(ITE,JN1)-ARN3(ITE,JN1)
ARNE1N(ITE,JN1)=ARNE1N(ITE,JN1)-ARNE1(ITE,JN1)
AREEN(ITE,JN1)=AREEN(ITE,JN1)-AREE(ITE,JN1)
998 C CONTINUE

```

```

WRITE(6,91)((ARN2(ITE,JN1),ITE=1,3),JN1=1,4)
WRITE(6,915)((ARN2N(ITE,JN1),ITE=1,3),JN1=1,4)
WRITE(6,92)((ARN3(ITE,JN1),ITE=1,3),JN1=1,4)
WRITE(6,925)((ARN3N(ITE,JN1),ITE=1,3),JN1=1,4)
WRITE(6,93)((ARNE1(ITE,JN1),ITE=1,3),JN1=1,4)
WRITE(6,935)((ARNE1N(ITE,JN1),ITE=1,3),JN1=1,4)
WRITE(6,96)((AREE(ITE,JN1),ITE=1,3),JN1=1,4)
WRITE(6,965)((AREEN(ITE,JN1),ITE=1,3),JN1=1,4)
91 FORMAT( ' N2N2N2',//,4(1X,3D10.3,1X),//)
915 FORMAT( ' DELTA N2N2N2',//,4(1X,3D10.3,1X),//)
92 FORMAT( ' N3N3N3',//,4(1X,3D10.3,1X),//)
925 FORMAT( ' DELTA N3N3N3',//,4(1X,3D10.3,1X),//)
93 FORMAT( ' NE1NE1',//,4(1X,3D10.3,1X),//)
935 FORMAT( ' DELTA NE1NE1',//,4(1X,3D10.3,1X),//)
96 FORMAT( ' EEEEE',//,4(1X,3D11.5,2X),//)
965 FORMAT( ' DELTA EEEEE',//,4(1X,3D11.5,2X),//)
966 C CONTINUE

```

C
C

STOP
END

IV G LEVEL 20.7 VS MAIN DATE = 6/27/80 14:55:44 PAGE 0006

SUBPROGRAMS CALLED							
LOCATION	SYMBOL	LOCATION	SYMBOL	LOCATION	SYMBOL	LOCATION	SYMBOL
118	WEBB	11C	HCLST	120	DEXP	124	DSQRT
12C							128

SCALAR MAP							
LOCATION	SYMBOL	LOCATION	SYMBOL	LOCATION	SYMBOL	LOCATION	SYMBOL
1F8	TE	200	TN	208	R	210	ALALM
220	PHE	228	PH	230	PIOT	238	A31H
248	A21H	250	WBAR	258	WBARM	260	B32H
270	SIGAV	278	S14H	280	S24H	288	S34H
298	S21H	2A0	S23H	2A8	S32H	280	S13H
2C0	N2	2C8	N3	2D0	NE	2D8	GAMMA
2E8	GAM21	2F0	E12	2F8	E13	300	E14
310	E24	318	E34	320	CUR	328	DA
338	OMEGEP	340	EE	348	PIG	350	ITE
35C	ISAT	360	ILOOP	364			358

ARRAY MAP							
LOCATION	SYMBOL	LOCATION	SYMBOL	LOCATION	SYMBOL	LOCATION	SYMBOL
368	ARN3	3C8	ARNE1	428	AREE	488	ARN2N
548	ARNE1N	5A8	AREEN	608	DATAIN	668	PRESS

FORMAT STATEMENT MAP							
LOCATION	SYMBOL	LOCATION	SYMBOL	LOCATION	SYMBOL	LOCATION	SYMBOL
748	2	757	3	892	5	885	50
943	91	940	915	968	92	991	925
904	935	9F2	96	A17	965	A35	9AF

STATEMENT NUMBER MAP							
STATEMENT LOCATION	STATEMENT LOCATION	STATEMENT LOCATION	STATEMENT LOCATION	STATEMENT LOCATION	STATEMENT LOCATION	STATEMENT LOCATION	STATEMENT LOCATION
D2C	6	D34	7	D3C	8	D44	9
D54	11	D5C	12	D64	13	D6C	14
D7C	16	D84	17	D8C	18	D94	19

```

LA4 21 LAC 22 DB4 23 DBC 24 DC4
DCC 26 DD4 27 DDC 28 DE4 29 DEC 30
D14 31 DFC 32 E04 33 E0C 34 E78 35
EE4 37 EEC 38 F00 39 F12 40 F1E 41
F26 42 F2E 43 F36 44 F3E 45 F46 46
F6A 47 F7A 48 F7E 49 F86 50 F8E 51
F96 52 F9E 53 FBE 54 FC6 55 FE6 56
FF6 58 F00 59 100C 60 101A 61 1022 62
1030 63 1038 64 1046 65 104E 66 107C 67
108A 68 1092 69 10C4 70 10D2 71 10DA 72
1108 75 1124 76 112C 77 1134 78 113C 79
114A 80 1152 81 1160 82 1168 83 1170 84
1178 86 1180 87 1184 88 1190 89 1198 90
11A4 91 11AC 92 11B4 93 118C 94 11C4 95
11CC 96 11D4 98 11E2 99 11E2 100 121E 101
124A 102 12F0 103 134A 104 138C 105 1428 106
148E 107 14D2 108 14E0 109 14E8 110 14F0 111
N IV G LEVEL 20.7 VS MAIN DATE = 6/27/80 14:55:44 PAGE 0007
14F8 112 1500 113 1508 114 150E 115 1516 116
151E 117 1526 118 152E 119 1572 120 157E 121
1588 122 1594 123 15A0 124 15AC 125 1588 126
15E8 127 1650 128 1688 129 1720 130 1788 131
17F0 132 1858 133 18C0 134 1928 135 193C 136

```

```

IONS IN EFFECT* ID,EBCDIC,SOURCE,NOLIST,NODECK,LOAD,MAP
ICNS IN EFFECT* NAME = MAIN LINECNT = 58
TISTICS* SOURCE STATEMENTS = 144,PROGRAM SIZE = 6474
TISTICS* NO DIAGNOSTICS GENERATED
N IV G LEVEL 20.7 VS MAIN DATE = 6/27/80 14:55:44 PAGE 0001
C
C
C
CC

```

```

SUBROUTINE WEBB(SIGMAX,ETRANS,TE,SIGAV)
IMPLICIT REAL*(A-Z)
SIGAV=6.69D7*7.854D-17*(SIGMAX*DSQRT(ETRANS)
& *DSQRT((ETRANS/TE)**3)**(3.0D0+ETRANS/TE)
& /((1.0D0+ETRANS/TE)**3)*DEXPI(-ETRANS/TE)
RETURN
END
N IV G LEVEL 20.7 VS WEBB DATE = 6/27/80 14:55:44 PAGE 0002

```

```

LOCATION 90 SUBPROGRAMS CALLED SYMBOL LOCATION LOCATION
DEXP 94 SCALAK MAP SYMBOL LOCATION LOCATION
A8 80 80 88
LOCATION 18E STATEMENT NUMBER MAP STATEMENT LOCATION STATEMENT LOCATION
3 18E 4 252
ICNS IN EFFECT* ID,EBCDIC,SOURCE,NOLIST,NODECK,LOAD,MAP
ICNS IN EFFECT* NAME = WEBB LINECNT = 58
TISTICS* SOURCE STATEMENTS = 5,PROGRAM SIZE = 602
TISTICS* NO DIAGNOSTICS GENERATED
N IV G LEVEL 20.7 VS MAIN DATE = 6/27/80 14:55:44 PAGE 0001
C
C
C
C

```

```

SUBROUTINE HOLSTR, BLAMDA, TN, AM, G2, G1, AN, A, GAMMA)
  IMPLICIT REAL*(A-Z)
  NOTE INPUT MASS IS IN AMU
  DNUD=2.*3.010718252*(BLAMDA*1.D-8)*
  6 DSQRT(2.00*TN*DLCG(2.00)/(AM*9.3908))
  6 AKO=2.00/DNUD*DSQR(DLOG(2.00)/3.141600)*(BLAMDA*1.D-8)**2
  6 /18.00*3.141600/G2/G1*AN*A
  DUM=AKC*
  IF(DUM.LT.1.78900) GO TO 10
  GAMMA=1.6/(AKO*DSQRT(3.141600*DLOG(AKO*R)))
  RETURN
  10 GAMMA=1.0D0
  RETURN
  END
  I IV G LEVEL 20.7 VS          HOLST          DATE = 6/27/80  14:55:44          PAGE 0002

```

LOCATION 9C SUBPROGRAMS CALLED

SYMBOL	LOCATION	SYMBOL	LOCATION	SYMBOL	LOCATION
DLOG	A0				

SCALAR MAP

SYMBOL	LOCATION	SYMBOL	LOCATION	SYMBOL	LOCATION
BLAMDA	C8	TN	DO	AM	08
G1	F0	AN	F8	A	100
GAMMA	118				

IT LOCATION STATEMENT NUMBER MAP

STATEMENT LOCATION	STATEMENT LOCATION	STATEMENT LOCATION	STATEMENT LOCATION
294	3	4	5
364	8	9	10
	294	2EC	34A
	3AE	386	38E

IONS IN EFFECT* ID, EDCIC, SOURCE, NOLIST, NODECK, LCAD, MAP
 GNS IN EFFECT* NAME = HCLST , LINECNT = 58
 LISTICS* SOURCE STATEMENTS * 11, PROGRAM SIZE = 966
 LISTICS* NO DIAGNOSTICS GENERATED
 LISTICS* NO DIAGNOSTICS THIS STEP

USED - PRINT, MAP, NOLET, CALL, RES, NOTERM, SIZE=243760, NAME=**GO

TYPE	ADDR	NAME	TYPE	ADDR	NAME	TYPE	ADDR
SD	8010	WEBB	SD	89960	HOLST	SD	898C0
LR	89FA0	IHCSSQRT*	SD	8A188	SQRT	LR	8A188
SD	8A430	DEXP	LR	8A430	IHCCECOMH*	SD	8A688
LR	88C98	IHCCECOMH2*	SD	8B620	SEQDASD	LR	8B998
SD	8CAAC	IHCJOPT	SD	8C258	IHCFFINTH*	SD	8C558
LR	8DE90	FIDCS#	LR	8CAA0	FIDCSBEP*	LR	8CAA6
LR	8E9CA	FCVOUTP*	LR	8DF3A	FCVOUTP*	LR	8DFCA
LR	8F668	ERRINA	LR	8EBE4	INT65WCH*	LR	8EECB
78E8	HEX		30952	DEC			
LENGTH	88010						

NAME TYPE ADDR

DLOG10	LR	89F88
DSQRT	LR	8A2D0
FIDCS#	LR	8A774
ERRON	LR	8BC80
ADJSMWCH*	LR	8C8F4
IHCFCVTH*	SD	8DE90
FCVOUTP*	LR	8E4C8
IHCETRCH*	SD	8F668

NAME TYPE ADDR

IHCLLOG*	SD	89F88
IHCSSQRT*	SD	8A2D0
IBCDB*	LR	8A688
IHCERRM*	SD	8B688
ARITH*	LR	8C558
IHCFCIS2*	SD	8D96C
FCVOUTP*	LR	8E4C8
IHCUTBL*	SD	8F030

NAME TYPE ADDR

IHCLLOG	SD	898C0
IHCSSQRT	LR	8A188
IBCDB	SD	8A688
IHCERRM	LR	8B998
ARITH	SD	8C558
IHCFCIS2	LR	8D96C
FCVOUTP	LR	8E4C8
IHCUTBL	LR	8F030

STATEMENT LOCATION

6	356
---	-----

Program #2

```

IV G LEVEL 20.7 VS          MAIN          DATE = 6/24/80
IMPLICIT REAL*8(A-Z)
INTEGER*4 K,J,N,MF,IND,MC,NO
REAL*4 PLOT1,PLOT2,PLOT3,PLOT4,PLOT5
COMMON R,TE,TN,S14H,S24H,S34H,S12H,S21H,S13H,S31H,
& S23H,S32H,A31H,A21H,A32H,B23H,B32H,WBAR
& ,POPDOX,GAM31,GAM21,LASER
& ,ANUE,DA,OMEGEP,NE,EE,CUR

C
C
C
DIMENSION POP(3,13),POPDOT(3),POPO(3)
& ,POPDOX(3)
& ,PLOT1(102),PLOT2(102),PLOT3(102),PLOT4(102),PLOT5(102)
C INPUT VARIABLES
C TE IS ELECTRON TEMPERATURE IN EV IEV=1.6E-12 ERGS
TE=2.500
C TN IS NEUTRAL TEMP, IN EV
TN=.0322
C R IS TUBE RADIUS IN CM
R=0.5
C ALALW IS LASER LINEWIDTH, HZ
ALALW=40.E9
C ALI IS TOTAL LASER POWER,WATTS
ALI=0.5
C PHE IS BUFFER PRESSURE, TORR
PHE=5.
C PH IS HYDROGEN PRESSURE,TORR
PH=0.5
C PTOT=TOTAL PRESSURE,TORR
PTOT=PH+PHE
A31H=5.575E7
A32H=4.41E7
A21H=4.699E8
LASER=0.
WBAR=ALI*1.E7/(3.1416**2*ALALW*3.F10)
B32H=A32H*(6563E-8)**3/(8.*3.1416*6.626E-27)
B23H=B32H*18./8.
WRITE(6,2) TN,R,ALALW,ALI,WBAR,B32H,B23H,A31H,
& A32H,A21H,PH,PHE
2 FORMAT( ' NEUTRAL TEMP =',E10.3,'EV',//,
& ' TUBE RADIUS=',F10.3,'CM',//,
& ' LASER LINEWIDTH=',E10.3,'GHZ',//,
& ' LASER INTENSITY=',F10.3,'WATTS',//,
& ' ENERGY DENSITY=',E10.3,'ERGS/HZ/CM3',//,
& ' B32H=',E10.3,'SEC-1/WBAR',//,
& ' B23H=',F10.3,'SFC-1/WBAR',//,
& ' A31H=',E10.3,'SEC-1',//,
& ' A32H=',E10.3,'SEC-1',//,
& ' A21H=',E10.3,'SFC-1',//,
& ' HYDROGEN PRESS=',E10.3,'TORR',//,
& ' HE BUFFER PRESS=',E10.3,'TORR')
C COMPUTE COEFFICIENTS FOR RATE EQUATIONS
C HYDROGEN
CALL WFHR(.75,13.6,TE,SIGAV)
S14H=SIGAV
CALL WEBB(15.,3.4,TE,SIGAV)
IV G LFVFL 20.7 VS          MAIN          DATE = 6/24/80 13:16:09
S24H=SIGAV
CALL WEHR(95.9,1.51,TE,SIGAV)
S34H=SIGAV
CALL WEHR(.88,10.2,TE,SIGAV)
S12H=SIGAV
S21H=S12H*.25*DI XP(10.,P/TE)

```



```
TOUT=TOUT+TOUTS/50.
WRITE(6,30)TOUT,(POPO(J),J=1,3),NE,DA,OMEGEP,CUR,EE
PLOT1(K)=POPO(1)
PLOT2(K)=POPO(2)
PLOT3(K)=POPO(3)
PLOT4(K)=TOUT
C PLOT5(K)=EE
TOUT=TOUT+TOUTS/50.
LASFR=1.
25 CONTINUE
30 FORMAT(9(E12.5,1X))
TO=TOUT-TOUTS/50.
TOUTS=2.*TOUTS
HO=1.E-10/360.
LASER=0.
DO 60 K=1,50
50 CALL GEARDR(N,TO,HO,POPO,TOUT,EPS,MF,IND,MC,POP,NO)
IF(IND.LT.0) GO TO 100
WRITE(6,30)TOUT,(POPO(J),J=1,3),NE,DA,OMEGEP,CUR,EE
PLOT1(K+50)=POPO(1)
PLOT2(K+50)=POPO(2)
PLOT3(K+50)=POPO(3)
PLOT4(K+50)=TOUT
C PLOT5(K+50)=EE
TOUT=TOUT+TOUTS/50.
60 CONTINUE
99 CONTINUE
C
C
C CALL SCALES(PLOT4,8.,100,1)
CALL SCALES(PLOT1,5.,100,1)
CALL SCALES(PLOT2,5.,100,1)
CALL SCALES(PLOT3,5.,100,1)
C CALL SCALES(PLOT5,5.,100,1)
C
C
C CALL PLOTS(0,0,6)
CALL PLOT(2.,1.,-3)
CALL AXIS(0.,0.,10HTIME (SEC),-10,8.,0.,PLOT4(101),PLOT4(102))
IV G LEVEL 20.7 VS MAIN DATE = 6/24/80 13:16:09
CALL AXIS(-.8,0.,10HN3, (CM-3),10,5.,90.,PLOT2(101),PLOT2(102))
CALL AXIS(-1.6,0.,10HNE, (CM-3),10,5.,90.,PLOT3(101),PLOT3(102))
C CALL AXIS(-2.4,0.,10HEF, (V/CM),10,5.,90.,PLOT5(101),PLOT5(102))
C
C CALL LINE(PLOT4,PLOT1,100,1,10,1)
CALL LINE(PLOT4,PLOT2,100,1,10,2)
CALL LINE(PLOT4,PLOT3,100,1,10,3)
C CALL LINE(PLOT4,PLOT5,100,1,10,4)
CALL PLOT(0.,0.,+999)
C
C STOP
C
C
C ERROR DUMP
100 CONTINUE
DO 110 J=1,3
WRITE(6,120) TOUT,POPO(J),POPDOX(J),J,IND,NE
110 CONTINUE
120 FORMAT( ' ERROR T=',E10.3,3X,' POP=',E10.3,3X,' POPDOT=',
E10.3,3X,I3,3X,I3,3X,' NE=',F12.5)
C STOP
```

```

SUBROUTINE WEBB(SIGMAX,ETRANS,TE,SIGAV)
IMPLICIT REAL*(A-Z)
SIGAV=6.69E7*7.85E-17*SIGMAX*DSQRT(ETRANS)
C *DSQRT((FTRANS/TE)**3)*(3.+ETRANS/TE)
C /(1.+FTRANS/TE)**3*DEXP(-ETRANS/TE)
RETURN
END
    
```

IV G LEVEL 20.7 VS WFBF DATE = 6/24/80 13:16:09 PAGE 0002

SUBPROGRAMS CALLED									
LOCATION	SYMBOL	LOCATION	SYMBOL	LOCATION	SYMBOL	LOCATION	SYMBOL	LOCATION	SYMBOL
90	DEXP	94							
SCALAR MAP									
LOCATION	SYMBOL	LOCATION	SYMBOL	LOCATION	SYMBOL	LOCATION	SYMBOL	LOCATION	SYMBOL
A8	SIGMAX	B0	ETRANS	B8	TE	C0			
STATEMENT NUMBER MAP									
T LOCATION	STATEMENT	LOCATION	STATEMENT	LOCATION	STATEMENT	LOCATION	STATEMENT	LOCATION	STATEMENT
186	3	186	4	24F					

IONS IN EFFECT* ID,EBCDIC,SOURCE,NOLIST,NODECK,LOAD,MAP
IONS IN EFFECT* NAME = WEBB , LINECNT = 58
ISTICS* SOURCE STATEMENTS = 5, PROGRAM SIZE = 598
ISTICS* NO DIAGNOSTICS GENERATED

IV G LEVEL 20.7 VS MAIN DATE = 6/24/80 13:16:09 PAGE 0001

C
C
C
C

```

SUBROUTINE HOLST(R,BLAMDA,TN,AM,G2,G1,AN,A,GAMMA)
IMPLICIT REAL*(A-Z)
NOTE INPUT MASS IS IN AMU
DNUD=2.*3.E10/(BLAMDA*1.E-8)*
C DSQRT(2.*TN*ALOG(2.)/(AM*9.39E8))
AKO=2./DNUD*SQRT(ALOG(2.)/3.1416)*(BLAMDA*1.E-8)**2
C /(8.*3.1416)*G2/G1*AN*A
DUM=AKO*R
IF(DUM.LT.1.789) GO TO 10
GAMMA=1.6/(AKO*R*DSQRT(3.1416*DLOG(AKO*R)))
RETURN
10 GAMMA=1.0
RETURN
END
    
```

IV G LEVEL 20.7 VS HOLST DATE = 6/24/80 13:16:09 PAGE 0002

SUBPROGRAMS CALLED									
LOCATION	SYMBOL	LOCATION	SYMBOL	LOCATION	SYMBOL	LOCATION	SYMBOL	LOCATION	SYMBOL
9C	ALOG	A0	SQRT	A4	DLOG	A8			
SCALAR MAP									
LOCATION	SYMBOL	LOCATION	SYMBOL	LOCATION	SYMBOL	LOCATION	SYMBOL	LOCATION	SYMBOL
C9	BLAMDA	D0	TN	D8	AM	E0	AKO	E8	
F0	G1	F8	AN	100	A	108	DUM	110	
118	GAMMA	120							
STATEMENT NUMBER MAP									
T LOCATION	STATEMENT	LOCATION	STATEMENT	LOCATION	STATEMENT	LOCATION	STATEMENT	LOCATION	STATEMENT
244	3	244	4	304	5	36A	6	376	
384	8	3CE	9	3D6	10	3DE			

IONS IN EFFECT* ID,EBCDIC,SOURCE,NOLIST,NODECK,LOAD,MAP
IONS IN EFFECT* NAME = HOLST , LINECNT = 58
ISTICS* SOURCE STATEMENTS = 11, PROGRAM SIZE = 998
ISTICS* NO DIAGNOSTICS GENERATED

C
C
C

```

SUBROUTINE DIFFUN(N,T,POP,POPDOT)
IMPLICIT REAL*8(A-Z)
INTEGER*4 K,J
REAL*8 LASER,NE
COMMON R,TE,TN,S14H,S24H,S34H,S12H,S21H,S13H,S31H,
& S23H,S32H,A31H,A21H,A32H,B23H,B32H,WBAR
& ,PCPDOX,GAM31,GAM21,LASER
& ,ANUE,DA,OMEGEP,NE,EE,CUR
DIMENSION POPDOT(3),POP(3)
& ,POPDOX(3)
CALL ELDEN(POP)

```

C
C
C
C
C

```

WRITE (6,51) NE
51 FORMAT(' ELECTRON DENSITY NE =',E12.5,'CM-3')

```

C
C
C

```

T1=0.432*POP(1)*NE*(S12H+S13H+S14H)
T2=DA*NE*7.85/(3.1416*R**2)
T3=0.519*NE*(POP(3)*S31H+POP(2)*S21H)
T4=0.432*GAM21*A21H*POP(2)
T5=0.432*GAM31*A31H*POP(3)
POPDOT(1)=-T1+T2+T3+T4+T5

```

C
C
C

```

T10=0.432*NE*PCP(1)*S12H
T11=0.519*NE*POP(2)*(S21H+S23H+S24H)
T12=0.519*NE*POP(3)*S32H
T13=0.432*A32H*POP(3)
T14=0.432*B32H*WBAR*POP(3)*LASER
T15=0.432*B23H*WBAR*POP(2)*LASER
T16=0.432*GAM21*A21H*POP(2)
POPDOT(2)=T10-T11+T12+T13+T14-T15-T16

```

C
C
C
C
C

```

T17=NE*(POP(1)*S13H*0.432+POP(2)*S23H*0.519)
T18=0.519*NE*POP(3)*(S31H+S32H+S34H)
T19=0.432*A32H*POP(3)
T20=0.432*GAM31*A31H*POP(3)
T21=0.432*B23H*WBAR*POP(2)*LASER
T22=0.432*B32H*WBAR*POP(3)*LASER
POPDOT(3)=T17-T18-T19-T20+T21-T22

```

```

WRITE(6,333)T1,T2,T3,T4,T5,T10,T11,T12,T13,T14,T15,
& T16,T17,T18,T19,T20,T21,T22
333 FORMAT(3(6(E12.5,1X),/))

```

```

DO 100 J=1,3
POPDOX(J)=POPDOT(J)
100 CONTINUE

```

IV G LFVEL 20.7 VS DIFFUN DATE = 6/24/80 13:16:09 PAGE 0002
RETURN
END

IV G LEVEL 20.7 VS DIFFUN DATE = 6/24/80 13:16:09 PAGE 0003

LOCATION	SYMBOL	COMMON BLOCK / LOCATION	/ MAP SIZE	FO	SYMBOL	LOCATION	SYMBOL	LOCATION
0	TF	8	TN	10	S14H	18	S24H	20
24	S12H	30	S21H	38	S14H	40	S31H	48

```
*OPTIONS IN EFFECT* ID,FRCNIC,SOURCE,NOLIST,NODFCK,LOAD,MAP
*OPTIONS IN EFFECT* NAME = PEDERV , LINECNT = 58
*STATISTICS* SOURCE STATEMENTS = 3,PROGRAM SIZE = 372
*STATISTICS* NO DIAGNOSTICS GENERATED
FORTRAN IV G LEVEL 20.7 VS MAIN DATE = 6/24/80 13:16:09 PAGE 0001
```

```
C
C
C
0001 SUBROUTINE ELDEN(POPS)
0002 IMPLICIT REAL*8(A-Z)
0003 REAL*8 LASER,NE
0004 COMMON R,TF,TN,S14H,S24H,S34H,S12H,S21H,S13H,S31H,
& S23H,S32H,A31H,A21H,A32H,B23H,B32H,WBAR
& ,POPDOX,GAM31,GAM21,LASER
& ,ANUF,DA,OMEGEP,NE,FE,CUR
0005 DIMENSION POPS(3),POPDOX(3)
```

```
C
C
C
0006 ARG1=POPS(1)
0007 CALL HOLST(R,1025.72,TN,1.,18.,2.,ARG1,A31H,GAMMA)
0008 GAM31=GAMMA
0009 CALL HOLST(R,1215.67,TN,1.,8.,2.,ARG1,A21H,GAMMA)
0010 GAM21=GAMMA
C
0011 50 WRITE(6,50) GAM21,GAM31
0012 FORMAT(' GAM21=',E10.3,'GAM31=',E10.3)
0013 E12=10.2D0
0014 E13=12.09D0
0015 F14=13.6D0
0016 E23=1.89D0
0017 E24=3.4D0
0018 F34=1.51D0
```

```
C
0018 N1=POPS(1)
0019 N2=POPS(2)
0020 N3=POPS(3)
C
0021 ANUE=0.432*N1*(S12H+S13H+S14H)
0022 & +0.519*N2*(S23H+S24H)+0.519*N3*S34H
C
0023 & DA=(R/2.405)**2*(N1*S14H)
C
& +(R/2.405)**2*(N2*S24H+N3*S34H)
C
PIG=0.
OMEGEP=0.432*N1*(S14H*E14+S13H*E13+S12H*E12)
& +0.519*N2*(S23H*E23+S24H*E24-PIG*S21H*E12)
& +0.519*N3*(S34H*E34-PIG*(S32H*E23+S31H*E13))
& +7.85*DA*5.*TE/(3.1416*R**2)
```

```
C
C
0024 NE=CUR/(3.1416*R**2*DSQRT(0.432D0))
0025 & *DSQRT(ANUE*.511E6/OMEGEP)
& /(3.D10*1.6D-19)
& EE=DSQRT(ANUE*OMEGEP*.511E6)/(3.E10*SQRT(.432))
```

```
C
0026 RETURN
0027 END
FORTRAN IV G LEVEL 20.7 VS ELDEN DATE = 6/24/80 13:16:09 PAGE 0002
```

COMMON BLOCK /		/ MAP SIZE		FO					
SYMBOL	LOCATION	SYMBOL	LOCATION	SYMBOL	LOCATION	SYMBOL	LOCATION	SYMBOL	LOCATION
R	0	TF	8	TN	10	S14H	18	S24H	20
S34H	28	S12H	30	S21H	38	S13H	40	S31H	48
S23H	50	S32H	58	A31H	60	A21H	68	A32H	70
B23H	78	B32H	80	WBAR	88	POPDOX	92		


```

C      ALI IS TOTAL LASER POWER,WATTS
      ALI=0.01
C
C      ALI=ALI*ISAT
C
C      PHE IS BUFFER PRESSURE, TORR
      PHE=5.00
C      PH IS HYDROGEN PRESSURE,TORR
      PH=0.500
C      PTOT=TOTAL PRESSURE,TORR
      PTOT=PH+PHE
      A31H=5.57507
      A32H=4.4107
      A21H=4.69908
      WBAR=ALI*1.D7/(3.141600*R**2*ALALW*3.D10)
      WBAR=0.
      B32H=A32H*(6563.D-8)**3/(8.00*3.141600*6.6260-27)
      B23H=B32H*18.00/8.00
      WRITE(6,2) TN,R,ALALW,ALI,WBAR,B32H,B23H,A31H,
C      A32H,A21H,PH,PHE
2      FORMAT( ' NEUTRAL TEMP =',D10.3,'EV',/,
C      & ' TUBE RADIUS=',D10.3,'CM',/,
C      & ' LASER LINEWIDTH=',D10.3,'GHZ',/,
C      & ' LASER INTENSITY=',D10.3,'WATTS',/,
C      & ' ENERGY DENSITY=',D10.3,'ERGS/HZ/CM3',/,
C      & ' B32H=',D10.3,'SEC-1/WBAR',/,
C      & ' B23H=',D10.3,'SEC-1/WBAR',/,
C      & ' A31H=',D10.3,'SEC-1',/,
C      & ' A32H=',D10.3,'SEC-1',/,
C      & ' A21H=',D10.3,'SEC-1',/,
C      & ' HYDROGEN PRESS=',D10.3,'TORR',/,
C      & ' HE BUFFER PRESS=',D10.3,'TORR')
C      COMPUTE COEFFICIENTS FOR RATE EQUATIONS
C      HYDROGEN
      CALL WEBB(.7500,13.600,TE,SIGAV)
      S14H=SIGAV
      CALL WEBB(15.00,3.400,TE,SIGAV)
      S24H=SIGAV
      CALL WEBB(95.900,1.5100,TE,SIGAV)
      S34H=SIGAV
      CALL WEBB(1.000,10.200,TE,SIGAV)
      S12H=SIGAV
      S21H=S12H*.2500*DEXP(10.200/TE)
      CALL WEBB(60.00,1.8900,TE,SIGAV)
      S23H=SIGAV
      S32H=S23H*8.00/18.00*DEXP(1.8900/TE)
      CALL WEBB(1.00000,12.0900,TE,SIGAV)
      S13H=SIGAV
      S31H=S13H/9.00*DEXP(12.0900/TE)
N IV G LEVEL 20.7 VS      MAIN      DATE =      7/08/80      12:30:33
      WRITE(6,3) TE
3      FORMAT( ' ELECTRON TEMPERATURE =',D10.3,'EV')
      WRITE(6,5)S14H,S24H,S34H,S12H,S21H,S13H,S31H,S23H,S32H
5      FORMAT ( ' S14H=',D10.3,/,
C      & ' S24H=',D10.3,/,
C      & ' S34H=',D10.3,/,
C      & ' S12H=',D10.3,/,
C      & ' S21H=',D10.3,/,
C      & ' S13H=',D10.3,/,
C      & ' S31H=',D10.3,/,
C      & ' S23H=',D10.3,/,

```

```

C      & * S32H=*,D10.3)
C
C
C
C      *****
C
C
C
C      *****
C      N2=.1F10
C      N3=.1E4
C      NE=.1E10
C
C      CALL HOLST(R,1025.7200,TN,1.00,18.00,2.00,N1,A31H,GAMMA)
C      GAM31=GAMMA
C      CALL HOLST(R,1215.6700,TN,1.00,8.00,2.00,N1,A21H,GAMMA)
C      GAM21=GAMMA
C      WRITE(6,50) GAM21,GAM31
50  FORMAT( ' * GAM21=*,D10.3, *GAM31=*,D10.3)
C
C
C
C      E12=10.200
C      E13=12.0900
C      E14=13.600
C      E23=1.8900
C      E24=3.400
C      E34=1.5100
C
C
C      CUR IS THE CURRENT,AMPS
C      MUST BE SPECIFIED CONSISTENTLY WITH CURRENT
C      CUR=DATAIN(1,ITE,JN1)*1.E-3
C
C
C      DA=0.
C      ANUE=0.
C      OMEGEP=0.
C      EE=0.
C      WBAR=0.0
C
N IV G LEVEL 20.7 VS          MAIN          DATE =    7/08/80    12:30:33
C
C
C
C      DO 112 1LOOP=1,100
C      IF(ITE.GE.2) GO TO 110
C      WRITE(6,109) N1,N2,N3,NE,DA,ANUE,OMEGEP,WBAR,EE
109  FORMAT( 9(E12.5,2X))
110  CONTINUE
C
C      ANUE=0.432*N1*(S12H+S13H+S14H)
C      +0.269*N2*(S23H+S24H)+0.269*N3*S34H
C      DA=(R/2.405)**2*(N1*S14H+N2*S24H+N3*S34H)
C      PIG=0.
C      OMEGEP=0.432*N1*(S14H*E14+S13H*E13+S12H*E12)
C      +0.269*N2*(S23H*E23+S24H*E24-PIG*S21H*E12)

```

```

C      E +0.269*N3*(S34H*F34-PIG*(S32H*E23+S31H*F13))
C      E -0.432*(B23H*WBAR*E23*N2-B32H*WBAR*E23*N3)/NE
C      E +7.85*DA*5.*TE/(3.1416*R**2)
C
C      NE=CUR/(3.1416*R**2*DSQRT(0.432D0))
C      E *DSQRT(ANUE*.511D6/OMEGEP)
C      E /(3.010*1.6D-19)
C
C      N2=(0.432*NE*N1*S12H+0.269*NE*N3*S32H
C      E +0.432*N3*(A32H+B32H*WBAR))
C      E /(0.432*GAM21*A21H+0.269*NE*(S21H+S23H+S24H)
C      E +0.432*B23H*WBAR)
C
C      N3=(0.432*NE*N1*S13H+0.269*NE*N2
C      E *S23H+0.432*N2*B23H*WBAR)
C      E /(0.269*NE*(S31H+S32H+S34H)
C      E +0.432*(B32H*WBAR+A32H+GAM31*A31H))
C
C      EE=DSQRT(ANUE*OMEGEP*.511E6)/(3.E10*SQRT(.432))
C      E +1.6E-19/CUR*
C      E (-B23H*WBAR*N2*E23*0.432*3.1416*R**2
C      E +B32H*WBAR*N3*E23*0.432*3.1416*R**2)
C
C 112 CONTINUE
C
C      WRITE(6,665) N1,N2,N3,NE,ANUE,OMEGEP,EE
C 665 FORMAT(7(E12.5,3X),//)
C
C      CO=CUR/(1.6E-19*3.1416*R**2*SQRT(.432))
C      AAA=CO/2.*DSQRT(ANUE*.511E6/OMEGEP)/3.E10
N IV G LEVEL 20.7 VS      MAIN      DATE =      7/08/80      12:30:33
C      E *(.269*(S23H+S24H)/ANUE-(.269*(S23H*E23+S24H*E24-S21H*E12)
C      E +.432*S24H*5.*TE)/OMEGEP)
C
C      BBB=CO/2.*DSQRT(ANUE*.511E6/OMEGEP)/3.E10
C      E *(.269*S34H/ANUE-(.269*(S34H*E34-S32H*E23-S31H*E13)
C      E +.432*S34H*5.*TE)/OMEGEP)
C
C      ALPHA=-(.432*GAM21*A21H+.269*NE*(S21H+S24H+S23H))
C      E +AAA*(.432*N1*S12H+.269*S32H*N3-.269*N2*(S21H+S24H+S23H))
C
C      BETA=-.269*NE*S32H+.432*A32H+
C      E BBB*(.432*N1*S12H+.269*N3*S32H-.269*N2*(S21H+S23H+S24H))
C
C      GAMMA=-.269*NE*S23H
C      E +AAA*(.432*N1*S13H+.269*N2*S23H-.269*N3*(S31H+S32H+S34H))
C
C      DELTA=-.432*(A32H+GAM31*A31H)-.269*NE*(S31H+S32H+S34H)
C      E +BBB*(.432*N1*S13H+.269*N2*S23H-.269*N3*(S31H+S32H+S34H))

```

```

C
C
666 WRITE(6,666) AAA,BBB,ALPHA, BETA,GAMMA,DELTA
999 FORMAT(6(E12.5,3X))
CONTINUE
C
C

```

STOP
END
IV G LFVEL 20.7 VS MAIN DATE = 7/08/80 12:30:33 PAGE 0006

SUBPROGRAMS CALLED

LOCATION	SYMBOL	LOCATION	SYMBOL	LOCATION	SYMBOL	LOCATION	SYMBOL	LOCATION
88	WEBB	8C	HOLST	CO	DEXP	C4	DSQRT	C8
CC								

SCALAR MAP

LOCATION	SYMBOL	LOCATION	SYMBOL	LOCATION	SYMBOL	LOCATION	SYMBOL	LOCATION
1A0	TE	1A8	TN	1B0	R	1B8	ALALW	1C0
1C8	PHE	1D0	PH	1D8	PTOT	1E0	A31H	1E8
1F0	A21H	1F8	WBAR	200	B32H	208	B23H	210
218	S14H	220	S24H	228	S34H	230	S12H	238
240	S23H	248	S32H	250	S13H	258	S31H	260
268	M3	270	NE	278	GAMMA	280	GAM31	288
290	E12	298	E13	2A0	E14	2A8	E23	280
288	E34	2C0	CUR	2C8	DA	2D0	ANUE	2D8
2E0	EE	2E8	WBARM	2F0	PIG	2F8	CO	300
308	BBB	310	ALPHA	318	BETA	320	DELTA	328
330	JN1	334	ISAT	338	ILOOP	33C		

ARRAY MAP

LOCATION	SYMBOL	LOCATION	SYMBOL	LOCATION	SYMBOL	LOCATION	SYMBOL	LOCATION
340	PRESS	400						

FORMAT STATEMENT MAP

LOCATION	SYMBOL	LOCATION	SYMBOL	LOCATION	SYMBOL	LOCATION	SYMBOL	LOCATION
420	2	42F	3	56A	5	58D	50	602
61B	665	625	666	631				

STATEMENT NUMBER MAP

LOCATION	STATEMENT	LOCATION	STATEMENT	LOCATION	STATEMENT	LOCATION	STATEMENT	LOCATION
8FC	6	904	7	90C	8	914	9	91C
924	11	92C	12	934	13	93C	14	944
94C	16	954	17	95C	18	964	19	96C
974	21	97C	22	984	23	98C	24	994
99C	26	9A4	27	9AC	28	984	29	98C
9C4	31	9CC	32	9D4	33	9DC	34	A48
AB4	37	ACO	38	ACE	39	ADA	40	AE2
AEA	42	AF2	43	AFA	44	B02	45	B26
B2E	47	B36	48	B42	49	B4A	50	B52
B5A	52	B7A	53	B82	54	BA2	55	BB2
C28	58	C36	59	C3E	60	C4C	61	C54
C62	63	C6A	64	C78	65	C80	66	CAE
C8C	68	CC4	69	CF6	70	DO4	71	DOC
D3A	74	D58	76	DB4	77	DBC	78	DC4
DCC	80	DDA	81	DE2	82	DF0	83	DF8
E1C	86	E24	87	E2C	88	E34	89	E3C
E44	91	E4C	92	E58	93	E60	94	E68
E70	96	E78	97	E80	98	E88	99	E96
EF4	102	EF4	103	F30	104	F5C	105	1002
105C	107	10CE	108	113A	109	11D0	110	11E4
1230	113	1268	114	12EA	115	1368	116	13CA

IV G LFVEL 20.7 VS MAIN DATE = 7/08/80 12:30:33 PAGE 0007

```

141E          118          1468          119          14CE          121          1514          122          1548
IONS IN EFFECT* ID,EBCDIC,SOURCE,NOLIST,NODECK,LOAD,MAP
IONS IN EFFECT* NAME = MAIN , LINECNT = 58
TISTICS* SOURCE STATEMENTS = 123,PROGRAM SIZE = 5462
TISTICS* NO DIAGNOSTICS GENERATED
AN IV G LEVEL 20.7 VS MAIN DATE = 7/08/80 12:30:33 PAGE 0001
C
C
C
CC

```

```

SUBROUTINE WEBB(SIGMAX,ETRANS,TE,SIGAV)
IMPLICIT REAL*8(A-Z)
SIGAV=6.69D7*7.854D-17*SIGMAX*DSQRT(ETRANS)
& *DSQRT((ETRANS/TE)**3)*(3.DO*ETRANS/TE)
& /(1.DO*ETRANS/TE)**3*DEXP(-ETRANS/TE)
RETURN
END
AN IV G LEVEL 20.7 VS WEBB DATE = 7/08/80 12:30:33 PAGE 0002

```

```

SUBPROGRAMS CALLED
LOCATION SYMBOL LOCATION SYMBOL LOCATION SYMBOL LOCATION SYMBOL LOCATION
90 DEXP 94

SCALAR MAP
LOCATION SYMBOL LOCATION SYMBOL LOCATION SYMBOL LOCATION SYMBOL LOCATION
A8 SIGMAX B0 ETRANS B8 TE C0

STATEMENT NUMBER MAP
ENT LOCATION STATEMENT LOCATION STATEMENT LOCATION STATEMENT LOCATION STATEMENT LOCATION
1BE 3 1BE 4 252

```

```

IONS IN EFFECT* ID,EBCDIC,SOURCE,NOLIST,NODECK,LOAD,MAP
IONS IN EFFECT* NAME = WEBB , LINECNT = 58
TISTICS* SOURCE STATEMENTS = 5,PROGRAM SIZE = 602
TISTICS* NO DIAGNOSTICS GENERATED
AN IV G LEVEL 20.7 VS MAIN DATE = 7/08/80 12:30:33 PAGE 0001
C
C
C
C

```

```

SUBROUTINE HOLST(R,BLAMD,TN,AM,G2,G1,AN,A,GAMMA)
IMPLICIT REAL*8(A-Z)
NOTE INPUT MASS IS IN AMU
DNUD=2.*3.D10/(BLAMDA*1.D-8)*
& DSQRT(2.DO*TN*DLOG(2.DO)/(AM*9.39D8))
AKO=2.DO/DNUD*DSQRT(DLOG(2.DO)/3.1416DO)*(BLAMDA*1.D-8)**2
& /(8.DO*3.1416DO)*G2/G1*AN*A
DUM=AKO*R
IF(DUM.LT.1.789D0) GO TO 10
GAMMA=1.6/(AKO*R*DSQRT(3.1416DO*DLOG(AKO*R)))
RETURN
10 GAMMA=1.0D0
RETURN
END
AN IV G LEVEL 20.7 VS HOLST DATE = 7/08/80 12:30:33 PAGE 0002

```

```

SUBPROGRAMS CALLED
LOCATION SYMBOL LOCATION SYMBOL LOCATION SYMBOL LOCATION SYMBOL LOCATION
9C DLOG A0

SCALAR MAP
LOCATION SYMBOL LOCATION SYMBOL LOCATION SYMBOL LOCATION SYMBOL LOCATION

```

Appendix III

POSITIVE COLUMN SIMULATION WITH
FIXED DIFFUSION COEFFICIENT

Appendix III: POSITIVE COLUMN SIMULATION WITH FIXED DIFFUSION
COEFFICIENT

A. INTRODUCTION

The simulation of a positive column discharge is quite difficult without the assumption of an ambipolar diffusion dominated plasma. In the formulation of the problem given in Section III, it was assumed that all ions were lost to diffusion, i.e.,

$$D_a/\Lambda^2 = n_1 S_{1c} + n_2 S_{2c} + n_3 S_{3c}$$

In a previous formulation of this problem, a different strategy was attempted, one that seemed initially to be more logical and straightforward. In that formulation, D_a was taken as a fixed quantity independent of the plasma parameters (as might be appropriate for a very weakly ionized plasma where electrons collide solely with ground-state neutrals). Then D_a is varied along with the recombination coefficient α to yield credible level populations and power consumption.

B. COMPUTATIONAL STRATEGY

When D_a is fixed, equation (III.21c) no longer collapses, and there are four rate equations which may be numerically integrated. Four time-dependent differential equations and four initial conditions are sufficient to determine a steady state solution. (If only the steady state problem were being considered, three equations and a density for any one state would be required, as the right hand side of the four equations sum to zero; they are not independent equations.) One approximation that may be made is that for low values of n_2 , n_3 , and n_e the ground state is

constant; this reduction to three equations also reduces the cost of computation. The resulting three equations, including a volume-recombination term, are:

$$\begin{aligned} \frac{dn_2}{dt} = & -n_2 n_e S_{23} - n_2 n_e S_{2c} - n_2 n_e S_{21} - n_e n_3 S_{32} + n_e n_1 S_{12} \\ & + \gamma_{32} A_{32} n_e - \gamma_{21} A_{21} n_2 \end{aligned} \quad (\text{AIII.1})$$

$$\begin{aligned} \frac{dn_3}{dt} = & -n_e n_3 (S_{32} + S_{3c} + S_{31}) + n_1 n_e S_{13} + n_2 n_e S_{23} \\ & - A_{32} n_3 - \gamma_{31} A_{31} n_3 \end{aligned} \quad (\text{AIII.2})$$

$$\frac{dn_e}{dt} = n_e (n_1 S_{1c} + n_2 S_{2c} + n_3 S_{3c}) - D_a / \Lambda_2 n_e - \alpha n_e^2 \quad (\text{AIII.3})$$

where charge neutrality has been assumed; $n_e = n_c$.

C. RECOMBINATION

The volume recombination coefficient α is determined by several effects: Electrons and ions can recombine in a discharge plasma in a variety of ways. The two most important are radiative recombination and three-body recombination. In the former case, radiation is emitted as an electron is captured into the bound states of a positive ion; in the latter, the kinetic energy of a third particle (besides the electron and ion) is increased by an amount equal to the binding energy liberated by recombination. Alternately, the three-body recombination may be accompanied by photon emission. The third body is generally a second electron or a neutral atom. (For an overview, see McDaniel, 1964).

Electron three-body recombination rates can be approximated by (Hinnov and Hirschberg, 1962)

$$\alpha \approx 1.09 \times 10^{-26} n_e T_e^{-9/2} \text{ cm}^3/\text{sec} \quad (\text{AIII.4})$$

but the values calculated from this formula are at odds with those calculated from the more sophisticated collisional-radiative models (see below) and its reliability is suspect. Typical values of α for low temperature plasmas are, according to Mitchner and Kruger (1972), $10^{-3} - 10^{08}$.

There appears to be little independent information available on cross sections for three-body recombination and radiative recombination (neutral atom or ion). Mitchner (1972) estimates typical rates at $10^{-7} - 10^{-11}$, but notes that the paucity of experimental results makes them questionable. There is considerable uncertainty on the whole topic of recombination. Experiments (typically measurements on afterglows in pulsed discharges) are difficult to do, and as noted by Drawin (1969), it is not really possible to specify excitation and recombination rates independently of the details of the experiments. Additionally, the presence of impurities may alter recombination rates substantially (Persson et al., 1955), and ultrahigh purity gases and clean apparatus are of paramount importance.

Collisional radiative models (Bates et al., 1962; Biberman et al., (1970; Fujimoto et al., 1972; Hogarth and McElwain, 1975; Johnson and Hinnov, 1973) calculate rate constants for variable electron densities. Typical total recombination rates in those theories vary from 10^{-12} to $10^{-6} \text{ cm}^3/\text{sec}$, and depend as well on the optical thickness of the plasma.

D. COMPUTATIONAL RESULTS

1. Characterization of Model for α and D_a

Given the uncertainty of the numbers α and D_a , it is apposite to treat them as parameters, i.e., to vary them until satisfactory level populations result. T_e is also fixed in this model, and its effect on the steady state populations is evaluated. It was found that the three-level model yielded essentially the same results as the four-level model; hence, all results below are for three levels. The ground state density is taken throughout as 10^{16} cm^{-3} .

a) Effect of α on level populations

The steady state solutions to the rate equations for different values of α are presented in Fig. AIII-1. It should be noted that the electron density is extremely sensitive to α ; this is expected, since α moderates a term quadratic in n_e . Also, the excited state and electron populations are only realistic for a low-pressure discharge ($\sim 10^{10}$) for very large values of α .

b) Effect of D_a on level populations

The effect of varying D_a on the electron density is given in Fig. AIII-2 for two different values of α . When D_a is fixed at the value given by equation (III.34) as might be expected, the rate equations become unstable. Adding a small perturbation (e.g., resonant light) would cause the populations to change by several orders of magnitude.

c) Effect of electron temperature on level populations

The excited state populations found for the rate equations are presented as a function of electron temperature in Fig. AIII-3.

Fig. AIII-1 Steady state solutions for the $n = 2$, $n = 3$, and electron density rate equations for a hydrogen discharge as a function of the recombination coefficient, α

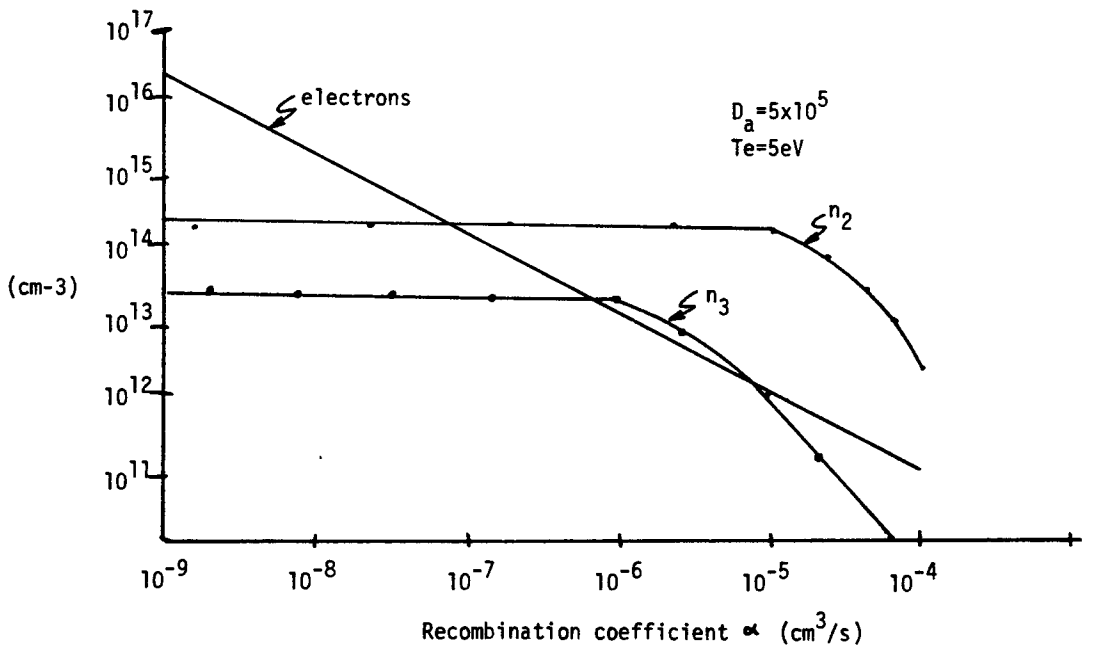


Fig. AIII-2 Effect of D_a on electron density solution of hydrogen rate equations. D_a has only a minor effect on the electron density and excited state populations.

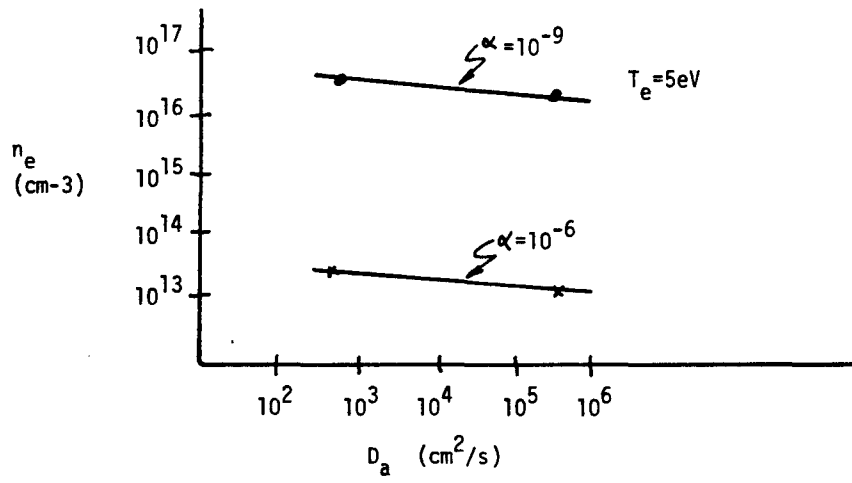
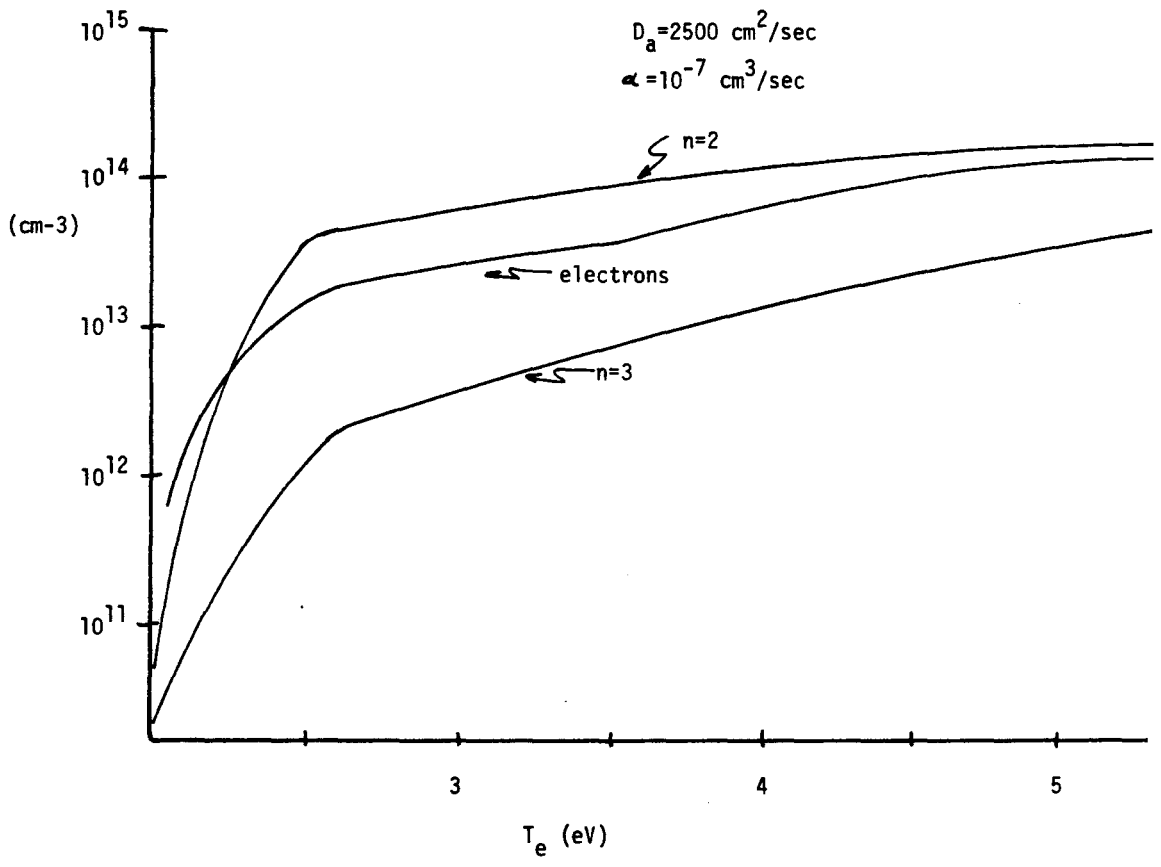


Fig. AIII-3 Excited state populations and electron density solutions to hydrogen rate equations as a function of electron temperature



E. DISCUSSION

From the above results, it may be concluded that the rate equations are sensitive to α but not to D_a , and that a relatively high value of α is required to obtain realistic populations at 5 eV. At lower electron temperatures, smaller values of α will yield acceptable populations. This result is at odds with the $T_e^{-9/2}$ dependence of α given by the Hinnoy-Hirschberg formula; α decreases with T_e in the collisional-radiative models as well.

The 5 eV modelling was undertaken to describe a hydrogen-plus-helium-buffer discharge wherein the electron temperature was measured at approximately 5 eV. It is possible that the large value required for α is accounted for by the presence of the helium; no literature on recombination cross-sections for H^+ -He was found. Additionally, as noted previously, impurities can affect α dramatically.

The drawbacks of the fixed- D_a computation are now manifest. The column must be assumed recombination dominated, the electron temperature is wrong, the values for α and D_a available in the literature are plagued by uncertainty, and power balance (conservation of energy) is not assured. Accordingly, it is assumed that this approach is incomplete, and that a variable D_a resulting in a discharge model that "balances" populations for self-consistency must be invoked as in Section III.

REFERENCES - Appendix III

- Bates, D. R., A. E. Kingston, and R.W.P. McWhirter, Proc. Roy. Soc. A 267, 297-312 (1962); Proc. Roy. Soc. A 270, 155-167 (1962).
- Biberman, L. M., I. T. Yakubov, and V. S. Vorob'ev, Proc. IEEE 59, 555-572 (1971).
- Drawin, H. W., Z. Physik 225, 471-493 (1969).
- Fujimoto, F., Y. Ogata, I. Sugiyama, K. Tachibana, and K. Fukuda, Jap. J. Appl. Phys. 11, 718-725 (1972).
- Hinnov, E., and J. Hirschberg, Phys. Rev. 125, 795 (1962).
- Hogarth, W. L. and D.L.S. McElwain, Proc. Roy. Soc. Lond. A 345, 265-276 (1975).
- Johnson, L. C., and E. Hinnov, J. Quant. Spectrom. Rad. Transfer 13, 333-358 (1973).
- Mitchner, M., and C. H. Kruger, Partially Ionized Gases (John Wiley, New York, 1973).
- McDaniel, E. W., Collision Phenomena in Ionized Gases (John Wiley, New York, 1964).
- Persson, K. B. and S. C. Brown, Phys. Rev. 100, 729-733 (1955).

Appendix IV
LINESHAPES AND ABSORPTION

Appendix IV: LINESHAPES AND ABSORPTION

A. INTRODUCTION

The rate equations (III.50) and (III.51) in Chapter III are somewhat misleading in that they do not depend on the frequency of the external radiation. For example, a monochromatic external H_{α} source would excite only a small fraction of the Doppler-broadened atoms in states 2 and 3. The exact details of the interaction depend on the intensity and frequency of the radiation, and the collisional and Doppler linewidths of the hydrogen in the discharge. This appendix discusses in detail the interaction of the radiation and the atoms, and the relationship to the OGE.

B. GENERAL STATEMENT OF THE PROBLEM

To include the dimension of frequency in the rate equations, (III.50) and (III.51), and the power balance equation, (III.47), the following substitutions are made:

The terms representing collisional pumping are multiplied by Doppler lineshape functions to reflect the fact that atoms have a thermal velocity when they are pumped into excited states:

$$Z_{ij} = n_e n_i S_{ij}$$

becomes

$$Z_{ij} = \frac{2 \sqrt{\ln 2}}{\sqrt{\pi} \Delta v_D} e^{-4 \ln 2 \frac{(\nu - \nu_D)^2}{\Delta v_D^2}}$$

where

$$\Delta\nu_D = 2\nu_D \sqrt{\frac{2kT_n}{Mc^2 \ln 2}}$$

and

ν_D = center frequency of the transition

T_n = gas temperature

M = atomic mass

This accounts for the Doppler shift of atomic frequencies due to thermal motion of the atoms.

The rates R_{23} and R_{32} are the stimulated emission rates. That is,

$$R_{23} = \frac{g_3}{g_2} R_{32} = B_{23} \bar{W}$$

where B_{23} is the Einstein B coefficient[†], and \bar{W} is the spectral density of exciting radiation. To include the frequency dependence of the stimulated radiative processes, the B coefficient must reflect collisional broadening:

$$B_{32} \rightarrow B'_{32}(\nu', \nu) = \frac{B_{32} (2/\pi\Delta\nu_c)}{1 + [2(\nu-\nu')/\Delta\nu_c]^2}$$

where ν is the radiation frequency, ν' is the center frequency of the collisionally broadened transition, and $\Delta\nu_c = 1/\tau_c$ is the collision

[†]Note these B's differ by $c/4\pi$ from those in the previous text. The notation here is consistent with Mitchell and Zemansky, 1971.

frequency.

Finally, the spectral density of the radiation \bar{W} is a function of both frequency ν and, in the case of longitudinal illumination of the discharge, distance z .

$$\bar{W} \rightarrow \bar{W}(\nu, z)$$

The resulting equations are more complicated than the original rate equations, and correspondingly more difficult to solve. While it is probably possible to solve this more general case with elaborate numerical techniques, it is more illuminating to make some approximations and derive analytic solutions.

1. Approximations

In Chapter III, radial diffusion modes of electrons and ions were calculated by treating a simpler version of the electron rate equation which was called the Schottky model. The results were then used in the complete rate equations. In this section, this same technique of deriving partial solutions and applying them to the full problem is used.

It was noted in Chapter III that if the hydrogen PCD is operated at constant current, the electron density is very nearly independent of external illumination. Thus only the equations for n_2 and n_3 [(III.50) and (III.51)] need to be considered.

Following Gordon, White, and Rigden (1963), these rate equations are written:

$$\begin{aligned} \frac{d}{dt} n_3(v', z) = & Z_3(v') - n_3(v', z)[A_3 + B'_{32}(v', \nu) I(\nu, z)/4\pi + Z_{32}^*] \\ & + n_2(v', z)[B'_{23}(v', \nu) I(\nu, z)/4\pi + Z_{23}^*]. \end{aligned} \quad (\text{AIV.1})$$

$$\begin{aligned} \frac{d}{dt} n_2(v', z) = & Z_2(v') + n_3(v', z)[A_{32} + B'_{32}(v', \nu) I(\nu, z)/4\pi + Z_{32}^*] \\ & - n_2(v', z)[A_2 + B_{23}(v', \nu) I(\nu, z)/4\pi + Z_{23}^*] \end{aligned} \quad (\text{AIV.2})$$

where the connection to previous notation is

$$\begin{aligned} Z_2 &\equiv \text{total rate electrons are pumped into } n_2 \\ &\equiv \sum_{j \neq 3} n_e n_j S_{j2} \end{aligned}$$

$$\begin{aligned} Z_3 &\equiv \text{total rate electrons are pumped into } n_3 \\ &\equiv \sum_{j \neq 2} n_e n_j S_{j3} \end{aligned}$$

$$\left. \begin{aligned} Z_{23}^* &\equiv n_e S_{23} \\ Z_{32}^* &\equiv n_e S_{32} \end{aligned} \right\} \begin{array}{l} (* \text{ indicates dimensions are not the same} \\ \text{as } Z_2 \text{ and } Z_3) \end{array}$$

$$B_{ij} I/4\pi \equiv B_{ij} \bar{W}$$

The electron collision terms $n_2 Z_{23}^*$ and $n_3 Z_{32}^*$ are included separately from Z_2 and Z_3 in order to account for the effect of radiation on electron pumping. That is, if n_2 is depleted by radiation, the pumping rate $n_2 Z_{23}^*$ is also decreased. Similarly, $n_3 Z_{32}^*$ increases if n_3 is populated by radiation.

The absorption rate for the intensity I of a single spectral component can be written

$$\frac{dI(\nu, z)}{dz} = \frac{h\nu}{4\pi} I(\nu, z) \int [B'_{32}(\nu', \nu) n_3(\nu', z) - B'_{23}(\nu', \nu) n_2(\nu', z)] d\nu' \quad (\text{AIV.3})$$

Setting

$$\frac{dn_2}{dt} = \frac{dn_3}{dt} = 0$$

the two rate equations, (AIV.1) and (AIV.2), may be rearranged to yield the integrand:

$$B'_{32}n_3 - B'_{23}n_2 = \frac{B_{32} \left[\frac{Z_3}{A_3 + Z_{32}^*} - \frac{\frac{g_3}{g_2} [Z_2(A_3 + Z_{32}^*) + Z_3(A_{32} + Z_{32}^*)]}{(A_3 + Z_{32}^*) A_2} + \frac{(Z_2 + Z_3)Z_{23}^*}{A_2(A_3 + Z_{32}^*)} \right]}{1 + \left[\frac{g_3}{g_2} (A_3 - A_{32}) / ((A_3 + Z_{32}^*) A_2) + \frac{1}{A_3 + Z_{32}^*} \right] \frac{B_{32} I}{4\pi} + \frac{Z_{23}^* (A_3 - A_{32})}{(A_3 + Z_{32}^*) A_2}} \quad (\text{AIV.4})$$

Noting again that atoms born into n_2 or n_3 have a thermal velocity, the pump terms may be written[†]

[†]It is assumed that levels 2 and 3 both have the same temperature as the neutral gas, and that both have the standard thermal (Gaussian) profiles. The latter is not strictly true, for example, in the case of "hole burning" discussed below.

$$Z_i \equiv Z_{i0} \cdot \exp\{-2(\nu-\nu_0)/\Delta\nu_D \sqrt{\ln 2}\}^2\}$$

where

$$Z_{i0} = \frac{2\sqrt{\ln 2}}{\Delta\nu_D \sqrt{\pi}} \sum n_e n_j S_{jo}$$

Defining two new constants,

$$k_0 \equiv \frac{h\nu B_{32}}{4\pi} \times$$

$$\frac{\left[\frac{Z_{30}}{A_3 + Z_{32}^*} - \frac{g_3}{g_2} \frac{[Z_{20}(A_3 + Z_{32}^*) + Z_{30}(A_{32} + Z_{32}^*)]}{(A_3 + Z_{32}^*) A_2} + \frac{(Z_{20} + Z_{30})Z_{23}^*}{A_2(A_3 + Z_{32}^*)} \right]}{1 + Z_{23}(A_3 - A_{32}) / ((A_3 + Z_{32}^*) A_2)} \quad (\text{AIV.5})$$

$$\eta \equiv \frac{\left[\frac{g_3 (A_3 - A_{32})}{g_2 A_2 (A_3 + Z_{32}^*)} + \frac{1}{A_3 + Z_{32}^*} \right] \frac{B_{32}}{4\pi}}{1 + Z_{23}(A_3 - A_{32}) / ((A_3 + Z_{32}^*) A_2)} \quad (\text{AIV.6})$$

and including the explicit lineshape functions, the absorption integral may be written:

$$\frac{1}{I(\nu, z)} \frac{dI(\nu, z)}{dz} = k_0 \int d\nu' \frac{2}{\pi \Delta\nu_c} \times \frac{\exp\{-[2(\nu-\nu_0)/\Delta\nu_D]^2 \ln 2\}}{1 + [2(\nu-\nu')/\Delta\nu_n]^2 + \eta I(\nu, z) \frac{2}{\pi \Delta\nu_c}} \quad (\text{AIV.7})$$

This is the general form of the absorption, using the approximations discussed above.

2. General Solution

The above integral must be rearranged slightly to arrive at a standard form. Let

$$C_1 \equiv \frac{2k_0}{\pi \Delta v_c}$$

$$C_2 \equiv \frac{2I\eta}{\pi \Delta v_c}$$

$$\delta \equiv v - v'$$

The integral is then

$$\frac{1}{I(v,z)} \frac{dI(v,z)}{dz} = C_1 \int d\delta \frac{\exp[-(2(v - v_0 - \delta)/\Delta v_D)^2 \ln 2]}{1 + C_2 + (\frac{2\delta}{\Delta v_c})^2} \quad (\text{AIV.8})$$

which may be written

$$= \frac{C_1}{1 + C_2} \int d\delta \frac{\exp[-(2(v - v_0 - \delta)/\Delta v_D)^2 \ln 2]}{1 + (2\delta/\Delta v_c)^2} \quad (\text{AIV.9})$$

where $\Delta v_c \equiv \Delta v_c \sqrt{1 + C_2}$

The integral is evaluated in Zemansky (1930) in the following manner:

Let

$$q \equiv \frac{2(v - v_0)}{\Delta v_D} \sqrt{\ln 2}$$

$$p \equiv \frac{\Delta v_c}{\Delta v_D} \sqrt{\ln 2}$$

$$x \equiv \frac{2\delta}{\Delta v_D} \sqrt{\ln 2}$$

Then

$$\begin{aligned}
 (1 + c_2)^{1/2} \frac{1}{I} \frac{dI}{dz} &= \frac{2k_0}{\pi \Delta v_c} \int_{-\infty}^{\infty} d\delta \frac{\exp - [[2(v - v_0 - \delta) / \Delta v_D]^2 \ln 2]}{1 + \left(\frac{2\delta}{\Delta v_c} \right)^2} \\
 &= k_0 \frac{p}{\pi} \int_{-\infty}^{\infty} \frac{e^{-(q-x)^2}}{p^2 + x^2} dx \\
 &= \frac{2p}{\pi} k_0 e^{-q^2} \int_0^{\infty} \frac{e^{-x^2} \cos(2iqx) dx}{p^2 + x^2}
 \end{aligned}$$

Noting that

$$\begin{aligned}
 \frac{1}{p^2 + x^2} &= \int_0^{\infty} e^{-(p^2 + x^2)u} du \\
 (1 + c_2)^{1/2} \frac{1}{I} \frac{dI}{dz} &= k_0 \frac{2p}{\pi} e^{-q^2} \int_0^{\infty} e^{-p^2 u} du \int_0^{\infty} e^{-(1+u)x^2} \cos 2iqx dx \\
 &= k_0 \frac{2p}{\pi} e^{-q^2} \int_0^{\infty} e^{-p^2 u} du \left[\frac{1}{2} \left(\frac{\pi}{1+u} \right)^{1/2} e^{q^2 / (1+u)} \right]
 \end{aligned}$$

Letting

$$1 + u \equiv t^2 / p^2,$$

$$(1 + c_2)^{1/2} \frac{1}{I} \frac{dI}{dz} = k_0 \frac{2}{\sqrt{\pi}} e^{p^2 - q^2} \int_p^{\infty} e^{-t^2 + p^2 q^2 / t^2} \quad (\text{AIV.10})$$

Denoting

$$I_n(p) = \frac{2}{\sqrt{\pi}} e^{p^2} p^{2n} \int_p^\infty e^{-t^2} \frac{dt}{t^{2n}}, \text{ thus}$$

$$k_0 \sum_{n=0}^\infty I_n(p) \frac{e^{-q^2} q^{2n}}{n!} = (1+C_2)^{1/2} \frac{1}{I} \frac{dI}{dz} .$$

Integrating by parts, I_n becomes

$$I_n(p) = \frac{p}{2n-1} \left(\frac{2}{\sqrt{\pi}} - 2p I_{n-1}(p) \right)$$

and

$$I_0(p) = e^{p^2} \frac{2}{\sqrt{\pi}} \int_p^\infty e^{-t^2} dt = e^{p^2} (1 - \text{erf}(p))$$

where erf is the error function. The integral may be computed recursively.

Thus, in general,

$$\frac{(1 + \frac{2nI}{\pi\Delta v_c})^{1/2}}{k_0} \frac{1}{I} \frac{dI}{dz} = \sum I_n(p) \frac{e^{-q^2} q^{2n}}{n!} \tag{AIV.11}$$

Some values of the right hand side of this expression are given in Table AIV-1 (Zemansky, 1930) for the low intensity case $C_2 \ll 1$ and $\Delta v_c = \Delta v_c$

3. Special Cases

It is useful to consider some specialized cases of the above derivation.

(a) Pure inhomogeneous broadening

Repeating equation (AIV-10),

$$\sqrt{1+C_2} \frac{1}{I} \frac{dI}{dz} = \frac{2}{\sqrt{\pi}} k_0 e^{p-q^2} \int_p^\infty e^{-t^2 + p^2 q^2/t^2} dt$$

Table AIV-1. Values of right hand side of equation (AIV.11). From Zemansky (1930).

$\begin{array}{c} p \\ \backslash \\ q \end{array}$	0	0.5	1.0	1.5
0	1.0000	0.6157	0.4276	0.3216
0.2	.9608	.6015	.4215	.3186
.4	.8521	.5613	.4038	.3097
.6	.6977	.5011	.3766	.2958
.8	.5273	.4294	.3425	.2779
1.0	.3679	.3547	.3047	.2571
1.2	.2369	.2846	.2662	.2349
1.4	.1409	.2233	.2297	.2123
1.6	.0773	.1728	.1954	.1902
1.8	.0392	.1333	.1657	.1695
2.0	.0183	.1034	.1402	.1504

For small homogeneous linewidth,

$$p = \sqrt{\ln 2} \frac{\Delta\nu_c}{\Delta\nu_D} \approx 0$$

and

$$\begin{aligned} \frac{1}{I} \frac{dI}{dz} &= k_0 e^{-q^2} \frac{1}{\sqrt{1 + \frac{2\text{Im}}{\pi\Delta\nu_c}}} \\ &= \frac{k_0 e^{[-(2(\nu-\nu_0/\Delta\nu_D))^2 \ln 2]}}{\sqrt{1 + \frac{I}{\frac{\pi\Delta\nu_c}{2\eta}}}} \equiv \frac{\gamma(\nu)}{\sqrt{1 + \frac{I}{\frac{\pi\Delta\nu_c}{2\eta}}}} \end{aligned}$$

which is the standard result. And the conventional result,

$$I = I_0 e^{-\gamma(\nu)z} \tag{AIV.12}$$

obtains at low intensities. This says that at low intensities in an inhomogeneously broadened medium monochromatic light is absorbed exponentially as a function of distance and absorption coefficient $\gamma(\nu)$.

This expression for $\gamma(\nu)$ may be reduced to a more familiar form with the following manipulations. First, for simplicity, assume that

$Z_{23}^* = Z_{32}^* = 0$. Then equation (AIV.5) for k_0 becomes

$$k_0 = h\nu \frac{B_{32}}{4} \left[\frac{Z_{30}}{A_3} - \frac{g_3}{g_2} \frac{(Z_{20}A_{32} + Z_{20}A_3)}{A_2 A_3} \right]$$

Substituting for Z_{30} and Z_{20} ,

$$k_0 = h\nu \frac{B_{32}}{4\pi} \frac{2\sqrt{\ln 2}}{\sqrt{\pi} \Delta\nu_D} \left[\frac{\sum_{j \neq 3} n_e n_j S_{j3}}{A_3} - \frac{g_3}{g_2} \frac{A_{32} \sum_{j \neq 3} n_e n_j S_{j3} + A_3 \sum_{j \neq 2} n_e n_j S_{j2}}{A_2 A_3} \right]$$

Noting the usual relationship between A and B coefficients,

$$B_{32} = \frac{A_{32} c}{8\pi h\nu^3}$$

$$k_0 = \frac{c}{4\pi} \frac{A_{32}}{8\pi \nu^2} \quad [\text{as above}] \quad \frac{2\sqrt{\ln 2}}{\Delta\nu_D \sqrt{\pi}}$$

Removing the $c/4\pi$ that was a consequence of redefining B,

$$\gamma(\nu) = \frac{A_{32} \lambda^2}{8\pi c^2} [\text{above}] g_D(\nu)$$

where $g_D(\nu)$ is the normalized Doppler lineshape.

Noting that

$$\frac{\sum_{j \neq 3} n_e n_j S_{j3}}{A_3} \approx n_3$$

and similarly,

$$\frac{A_{32} \sum_{j \neq 3} n_e n_j S_{j3} + A_3 \sum_{j \neq 2} n_e n_j S_{j2}}{A_3} \approx A_2 n_2$$

the usual low intensity monochromatic absorption coefficient is found:

$$\gamma(\nu) = \frac{A_{32}\lambda^2}{8\pi c^2} \left(n_3 - \frac{g_3}{g_2} n_2 \right) g_D(\nu)$$

b) Pure homogeneous broadening

In the limit of homogeneous broadening, $p \rightarrow \infty$, equation (AIV.10)

now becomes

$$\sqrt{1+C_2} \frac{1}{I} \frac{dI}{dz} = k_0 \frac{1}{\sqrt{\pi}} \frac{p}{p^2+q^2} = k_0 \frac{1}{\sqrt{\pi} \ell n^2} \frac{\Delta\nu_D}{\Delta\nu_c + \frac{4(\nu-\nu_0)^2}{\Delta\nu_c}}$$

$$\frac{1}{I} \frac{dI}{dz} = \frac{k_0}{\sqrt{\pi} \ell n^2} \frac{\Delta\nu_D}{\Delta\nu_c (1+C_2) + \frac{4(\nu-\nu_0)^2}{\Delta\nu_c}}$$

which is the usual expression for absorption with pure homogeneous broadening.

c) Intermediate case on line center

The intermediate case of very small homogeneous broadening and large inhomogeneous broadening may be solved exactly, provided the exciting radiation is on line center, $\nu = \nu_0$ (Gordon et al., 1963). Then equation (AIV.10) becomes

$$\begin{aligned} \frac{1}{I} \frac{dI}{dz} &= \frac{k_0}{\pi} \int \frac{ds e^{-(ps)^2}}{1+s^2+C_2} \\ &= \frac{k_0}{(1+C_2)^{1/2}} e^{-(1+C_2)p^2} [1 - \text{erf}[(1+C_2)^{1/2} p]] \end{aligned} \quad (\text{AIV.13})$$

For small $p = \frac{\Delta\nu_C}{\Delta\nu_D} \sqrt{\ln 2}$,

$$\text{erf}[(1 + C_2)^{1/2} p] \approx 2(1 + C_2)^{1/2} p / \sqrt{\pi}$$

In the low intensity limit, $C_2 \approx 0$, and

$$I = I_0 \exp[-k_0 z / (1 + \frac{2p}{\sqrt{\pi}})] \quad (\text{AIV.14})$$

Thus at line center, a small homogeneous linewidth reduces the gain slightly over the pure inhomogeneous case. Examination of Table AIV-1 shows that even off line center, at low intensity, a small homogeneous linewidth does not much change the pure inhomogeneous case.

At high intensity and small homogeneous linewidth, equation (AIV.13) may be integrated. The result is

$$2[1 + G\bar{\nu}_0]^{1/2} - 2(1 + \bar{\nu}_0)^{1/2} + n \left[\frac{(1 + \bar{\nu}_0)^{1/2} + 1}{(1 + \bar{\nu}_0)^{1/2} - 1} \right] \left[\frac{(1 + G\bar{\nu}_0)^{1/2} - 1}{(1 + G\bar{\nu}_0)^{1/2} + 1} \right] + \frac{2p}{\sqrt{\pi}} [G - D\bar{\nu}_0 + \ln G] = k_0 L$$

where $G = \bar{\nu}/\bar{\nu}_0$, and $\bar{\nu} = [2/\pi\Delta\nu_V] = C_2$. This may be used to calculate the saturated absorption on line center. For details, see Gordon et al. (1963).

C. APPLICATION TO THE OPTOGALVANIC EFFECT

1. Introduction

In order to calculate the optogalvanic effect from the previous model, the finite bandwidth of the illuminating laser must be included,

as well as the longitudinal absorption of the laser light. That is, R_{23} in the rate equations must be calculated for a given illumination source, and the results must be spatially integrated. The calculations below are done for sources that have a much greater bandwidth and for those with a much narrower bandwidth than the Doppler width of H_{α} in a discharge (about 6 GHz). This is sufficient to account for both of the lasers available in the laboratory, a Coherent CR-699-21 with a bandwidth of 40 GHz and a Coherent CR-699-21 with a bandwidth of 1 MHz (which was never used in OGE measurements.)

2. Small Signal Theory

The hydrogen discharges used in the experiments typically had a 5 Torr helium buffer. At this pressure, the homogeneous (collisional) linewidth is about 2×10^8 Hz, or about 3% of the inhomogeneous (Doppler) linewidth. As noted in equation (AIV.11) and Table AIV-1, at low intensity the absorption on line center and in the "wings" of the Doppler profile is not much changed by a small collisional linewidth from the case of pure inhomogeneous broadening. Thus, it is reasonable to assume that $\Delta\nu_c = 0$, as the corrections to the gain coefficient are of the order of a few percent. This level of inaccuracy in the absorption is much less than the uncertainty in the measurement of the OGE.

In this limit, equation (AIV.14) reads

$$I(z, \nu) = I_0 e^{-\gamma(\nu)z}$$

where

$$\gamma(\nu) = \frac{Ng_3/g_2\lambda^2 A_{32}}{8\pi n^2} g_D(\nu)$$

and

$$\Delta N = n_2 - \frac{g_2}{g_3} n_3 \approx n_2$$

$\frac{1}{I} \frac{dI}{dz} = \gamma(\nu)$ from equation (AIV.12); however,

$$\frac{1}{I} \frac{dI}{dz} = R_{23} [n_3 - \frac{g_3}{g_2} n_2] h\nu$$

Therefore, the rate of induced transitions per unit power of low intensity narrow band illumination is

$$\frac{R_{23}}{I} = \frac{(g_3/g_2)c^2 A_{32}}{8\pi n^2 h\nu^3} g_D(\nu)$$

This says that the number of transitions induced per second, R_{23} , is directly proportional to the local field intensity I .

In the rate equations in Chapter III, R_{23} is included as an independent variable. From the results of computation in the small signal regime, where there is no saturation the change in local electric field is directly proportional to R_{23} . That is,

$$\Delta E_{\text{local}} \equiv c'R_{23} \equiv c''I_{\text{local}}$$

which is equivalent to saying that $R_{32}n_3$ does not much affect n_2 and n_3 . It should be emphasized that the net result of the rate equations

is to produce the number c' . The optogalvanic voltage measured at the terminals of the discharge is just the sum of the local changes in electric field induced by illumination:

$$\begin{aligned}
 \Delta V(\nu) &= \int_0^L dz \Delta E_{\text{local}}(\nu, z, I) \\
 &= \int_0^L dz c'' I_{\text{local}} \\
 &= c'' \int_0^L dz I_{\nu_0} e^{-\gamma(\nu)z} \\
 &= c'' I_{\nu_0} \frac{1}{\gamma(\nu)} [1 - e^{-\gamma(\nu)L}] \tag{AIV.15}
 \end{aligned}$$

Equation (AIV.15) is the basic result for the OGE resulting from narrowband illumination as a function of frequency in the limit of zero homogeneous linewidth. As noted, this limit is approximately realized in a hydrogen discharge.

It is interesting to note that the dependence of the OGE on the detuning from line center (OGE "lineshape") depends on the bracketed quantity $[1 - e^{-\gamma(\nu)L}]$; near line center where $\gamma(\nu)L \gg 1$ all the incident light is absorbed. Far off line center, $e^{-\gamma(\nu)L}$ approaches one, and the OGE drops off. For the excitation conditions considered, and for $L = 20$ cm, all the light is absorbed ($\gamma(\nu)L \gtrsim 1$) except in the far "wings" of the Doppler profile, and thus the OGE lineshape is expected to be much "flatter" (fall off less rapidly) than the Gaussian Doppler lineshape. Some numerical results and discussion are given in Chapter III.

3. Broadband Small-Signal Theory

The OGE resulting from broadband illumination (illumination bandwidth much greater than the transition Doppler width) may be calculated by integrating equation (AIV.15) over frequency.

The simplest way of accounting for the finite bandwidth of the laser is to say that all the radiation is absorbed in approximately the same distance ℓ in the discharge; in this case,

$$g_D(\nu) \approx \frac{1}{\Delta\nu_D}$$

and

$$\gamma(\nu) = \frac{1}{\ell} = \frac{N(g_3/g_2)A_{32}}{8\pi n^2} \frac{1}{\Delta\nu_D} \quad (\text{AIV.16})$$

For the hydrogen discharge conditions considered, $\ell \approx 1\text{-}3$ mm.

Again letting c'' designate the constant of proportionality between the change in E per centimeter of discharge and the local excitation intensity $I(z)$,

$$E_{\text{local}} = c'' I(z)$$

and the total voltage change in the column is again

$$\Delta V = \int_0^L \Delta E_{\text{local}} dz$$

where L is the length of the discharge, so

$$\begin{aligned} \Delta V &= c''' I_0 \int_0^L e^{-z/\ell} dz \\ &= \ell c''' I_0 [1 - e^{-L/\ell}] \end{aligned}$$

and ℓ , the folding length, is defined in equation (AIV.16). This is the basic result for the "crude" broadband theory. The results of this are compared with the experiment in Chapter III

It is not difficult to extend the above theory to include a more precise evaluation of the effect of the finite bandwidth of the laser. In fact, in the typical discharges discussed in Chapter VII, the visual observation of sidelight fluorescence, the folding length is much longer than a few millimeters. Heuristically, this might be expected, since the absorption coefficient decreases rapidly off line center. Radiation "in the wings" of the Doppler profile propagates much farther than that on line center. Thus, a broadband illumination source will have a hole "burned" in its flat spectral profile as it propagates through a medium that absorbs within a narrow (Doppler) band.

Mathematically, in the limit of homogeneous broadening, the monochromatic intensity at frequency ν , $I(\nu)$ is

$$I(\nu) = I_{\nu_0} e^{-\gamma(\nu)z}$$

where, as before,

$$\gamma(\nu) = \frac{\Delta N g_e g_2 \lambda^2 A}{8\pi n^2} g_D(\nu)$$

But now $g_D(\nu)$ is the precise Doppler expression

$$g_D(\nu) = \frac{c}{v_0} (M/2\pi kT)^{1/2} e^{-(M/2 kT)} (c^2/v_0^2)(\nu-\nu_0)^2$$

Figure AIV-1 shows the calculated change in the spectrum of a white source near 6563\AA as it passes through a hydrogen discharge; the lower state density is $7 \times 10^{12} \text{cm}^{-3}$, and the electron temperature is 5.5 eV (parameters were taken from the atomic discharge model of Chapter III.)

Calculating the OGE in this more precise theory is fairly straightforward. E, the change in electric field, must now be summed over ν as well as z . In the absence of saturation, the sum is straightforward: two monochromatic beams (spectral components of the broadband illumination) at ν and ν' within the Doppler width of the transition contribute independently to the OGE. That is to say, R_{23} is now a sum over spectral components. Calling I'_0 the illumination spectral power density $I_0/\Delta\nu_L \equiv I'_0$ ($\Delta\nu_L$ is the laser bandwidth), the "exact" OGE is now

$$\begin{aligned} \Delta V &= c'' I'_0 \int_{-\infty}^{\infty} d\nu \frac{1}{\gamma(\nu)} [1 - e^{-\gamma(\nu)L}] g(\nu) \\ &= c'' I'_0 \frac{8\pi n^2}{N_2 \lambda^2 A_{32}} \int_{-\infty}^{\infty} d\nu [1 - e^{-\gamma(\nu)L}] \end{aligned} \quad (\text{AIV.17})$$

This integral was evaluated numerically on a HP-34C programmable calculator. The results as a function of N_2 are presented for two values of L (20 cm and 1 cm) in Figure AIV-2.

Fig. AIV-1 Spectrum of a white source in the vicinity of the H_{α} line passes through a hydrogen discharge. The numbers on each line are the distance of propagation in cm. Note that essentially all the radiation at line center is absorbed within a few millimeters.

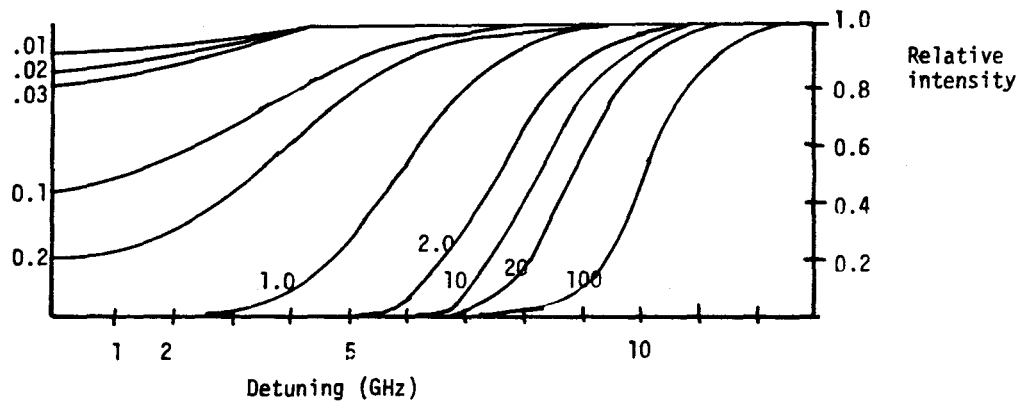
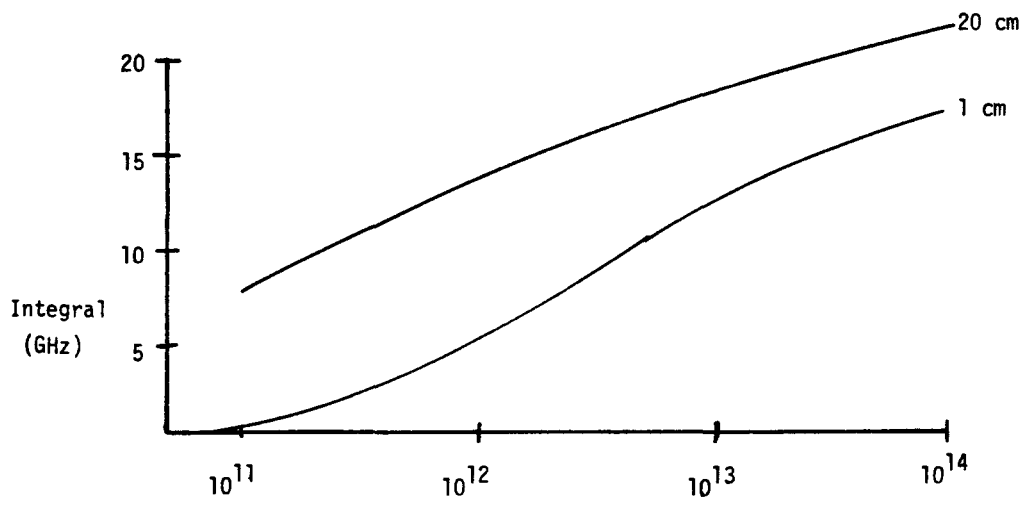


Fig. AIV-2 Absorption integral of equation (AIV.17) as a function of N_2 for two different discharge lengths. There is less absorption at shorter lengths, and more at higher populations.



The question arises as to how much the OGE would change if the illumination were lateral instead of longitudinal. The change in OGE compared to longitudinal illumination can easily be estimated from the preceding theory. In reality, such an experiment would involve the use of a square cross-section discharge tube, since circular walls would refract much of the light away from the plasma. To the extent that the internal conditions in a square discharge of width and depth $2R$ are the same as those in a cylindrical one, reducing the intensity by $\pi R^2/2RL$ and changing L in the absorption integral from the tube length to its width, $2R$, should yield an estimate of the "lateral" OGE per cm. Multiplication by L then yields the total voltage change. From Fig. AIV-2, the absorption integral decreases by a factor of ~ 2 ; $\pi R/2L \approx 0.5\pi/40 \approx 4 \times 10^{-2}$, so the OGE measured at the terminals would be reduced by $\sim 2 \times 10^{-2}L$ for broadband illumination, putting it, in all probability, below the tube noise.

4. Saturation Effects--Mixed Homogeneous and Inhomogeneous Media

Intense narrowband illumination of a Doppler-broadened transition can create a small band of atoms (within $\sim \Delta\nu_c$ of the frequency of the exciting light) with population significantly different from that of the rest of the line. This is generally referred to as "hole burning," and may be derived as follows.

Rewriting equation (AIV.8),

$$\frac{1}{I} \frac{dI}{dz} = \frac{2k_0}{\pi\Delta\nu_C} \int dv' \frac{\exp[-[2(\nu-\nu_0)/\Delta\nu_D]^2 \ln 2]}{1 + (2(\nu-\nu')/\Delta\nu_C)^2 + \eta I(\nu, z) \frac{2}{\pi\Delta\nu_C}}$$

After some rearrangement,

$$\begin{aligned} \frac{1}{I} \frac{dI}{dz} = \frac{2k_0}{\pi\Delta\nu_C} \int dv' \frac{\exp[-[2(\nu-\nu_0)/\Delta\nu_D]^2 \ln 2]}{1 + (2(\nu-\nu')/\Delta\nu_C)^2} \\ \times \frac{1 + (2(\nu-\nu')/\Delta\nu_N)^2}{1 + (2(\nu-\nu')/\Delta\nu_C)^2 + \frac{2\eta I}{\pi\Delta\nu_C}} \end{aligned}$$

This will be recognized as the unsaturated absorption multiplied by the local reduction factor

$$\frac{1 + (2(\nu-\nu')/\Delta\nu_N)^2}{1 + (2(\nu-\nu')/\Delta\nu_C)^2 + \frac{2\eta I}{\pi\Delta\nu_C}}$$

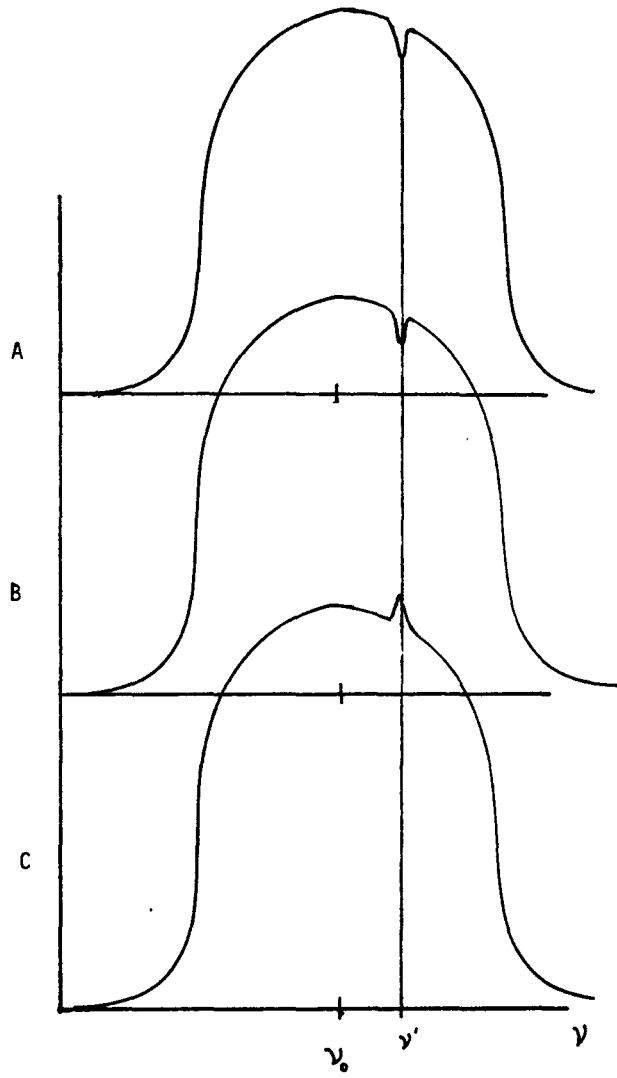
Narrowband saturation effects start to appear at $2\eta I/\pi\Delta\nu_C \approx 0.2$, or $I \approx 1$ watt.

The absorption coefficient $\frac{1}{I} \frac{dI}{dz}$ and the population profiles of the upper and lower states are shown schematically in Fig. AIV-3. It should be noted that the population profiles in Fig. AIV-3 B and C are explicitly non-equilibrium.

a) Narrowband saturated OGE

The optogalvanic voltage may be computed in a fairly straightforward manner when there is narrowband saturation or "hole burning" provided the electron density does not change much. As noted, n_e is

- Fig. AIV-3 Absorption profile of homogeneous and inhomogeneously broadened media demonstrating hole burning. Saturating beam is at ν .
- A) Absorption coefficient
 - B) Lower state population
 - C) Upper state population



determined primarily by the external circuit, so this is a good assumption.

From equation (AIV.15), the unsaturated OGE (narrowband intensity less than ~ 1 watt) is directly proportional to the total amount of light absorbed in the discharge, $I_0(1 - e^{-\gamma(\nu)L})$. This is still true in the steady state when there are saturation effects, provided n_e does not change, but the total absorption must be calculated from equation (AIV.10) and the R_{32} terms in the rate equations are superfluous since downward transitions are already accounted for. That is, using the rate equations (without R_{32}) and power balance equation of Chapter III, the change in local electric field per absorbed photon per unit time is calculated. In the absence of $R_{32}n_3$, this number is a constant except perhaps at very high intensities where n_e is significantly perturbed. Here, the model may break down anyway because T_e may change from the high energy input from the light.

It is relatively easy to see that n_e is only weakly perturbed by the presence of radiation. Equation (III.52) reads

$$n_e = \frac{I}{\pi R^2 \sqrt{.432}} \sqrt{\frac{m_e \nu_e}{\omega_e}}$$

where

$$\begin{aligned} \nu_e = & n_0(S_{12} + S_{13} + S_{1c})(0.432) \\ & + n_2(S_{23} + S_{2c})(0.269) \\ & + n_3(S_{3c})(0.269) \end{aligned}$$

and

$$\begin{aligned}\omega_e &= 0.432n_1(S_{12}\epsilon_{12} + S_{13}\epsilon_{13} + S_{1c}\epsilon_{1c}) \\ &+ 0.269n_2(S_{23}\epsilon_{23} + S_{2c}\epsilon_{2c} - S_{21}\epsilon_{21}) \\ &+ 0.269n_3(S_{3c}\epsilon_{3c} - S_{32}\epsilon_{32} - S_{31}\epsilon_{31})\end{aligned}$$

In the event that the frequency dependence of the pumpin terms S_{ij} in the rate equations is included, the ratio ν_e/ω_e is unchanged, meaning in the absence of radiation, n_e will be independent of frequency even though the pumping terms from which it is calculated have an explicit frequency dependence.

When radiation is present at some frequency ν' , the pumping rates S_{ij} are unaffected, which supports the claim that n_e does not depend strongly on radiation. However, $n_2(\nu)$ and $n_3(\nu)$ will be affected by the radiation, so n_e may be affected. However, as noted previously, the main contributors to ν_e and ω_e are the ground state terms proportional to n_1 . Unless the excitation is so strong that terms proportional to n_2 and n_3 become comparable to those proportional to n_1 , the effect on n_e is negligible. These conclusions are borne out by the previous results for hydrogen where $\Delta n_e/n_e \approx 10^{-5}$ because $n_2/n_1 \approx 10^{-5} \lll 1$ and $n_3/n_1 \approx 10^{-10} \lll 1$.

In the presence of narrowband illumination at any intensity that does not change n_e and T_e , the local change in electric field is proportional to the local absorption.

$$\Delta E_{\text{local}} = d' \frac{(n_3 - n_2 g_3/g_2) A_{32}^2 I(\nu)}{8\pi n^2 h\nu} g_D(\nu) \quad (\text{AIV.18})$$

In the absence of saturation, $n_3 \approx 0$ and n_2 is a constant, so

$$\Delta E = - \frac{d' n_2 g_3 / g_2 A_{32}^2}{8\pi n^2 h\nu} I_\nu g_0(\nu)$$

$$\equiv c'' I_\nu \quad \text{as before.}$$

However, at higher intensities, n_2 and n_3 depend on I . Then, from equation (IV.18)

$$\Delta E_{\text{local}} = \frac{d'}{h\nu} \frac{dI(\nu)}{dz}$$

since

$$\frac{1}{I} \frac{dI}{dz} = \frac{(n_3 - n_2 g_3 / g_2) A_{32} \lambda^2}{8\pi n^2} g_0(\nu)$$

Then, at any intensity,

$$\Delta V = \int \Delta E dz = - \frac{d'}{h\nu} (I(0) - (I(L))). \quad (\text{AIV.20})$$

The quantity d' is derived, like c' in the low intensity case, from the results of the computer program (and includes, as before, the effect of energy balance on E as well as that of the changes in ν_e and ω_e from population changes.)

$$d' = \frac{\Delta E \text{ from code}}{\text{net absorption density/Rc}}$$

$$= \frac{\Delta E \text{ from code}}{R^*}$$

R^* , the net absorption/cm³sec, is a variable in the actual computation; in the unsaturated case, $R^* \equiv R_{23}n_2$, and with saturation $R^* \equiv R_{23}n_2 - R_{32}n_3$.

The saturated result reduces to the unsaturated result if $I(0) - I(L) = I_0(1 - e^{-\gamma(\nu)L})$; to see this,

$$\begin{aligned} \Delta V &= - \frac{\Delta E \text{ from code}}{R_{23} n_2} \frac{1}{h\nu} [I_0(1 - e^{-\gamma(\nu)L})] \\ &= - \frac{\Delta E}{I} \frac{I}{R_{23}} \frac{1}{n_2 h\nu} [I_0(1 - e^{-\gamma(\nu)L})] \\ &= -c'' \frac{1}{\gamma(\nu)} I_0 [1 - e^{-\gamma(\nu)L}] \end{aligned} \quad (\text{AIV.19})$$

since in the absence of saturation,

$$\gamma(\nu) = \frac{-n_2 g_3/g_2 A_{32} \lambda^2 g_0(\nu)}{8\pi n^2}$$

and

$$\frac{I}{R_{23}} = \frac{8\pi n^2 h\nu^3}{c^2 A_{32} g_3/g_2 g_0(\nu)}$$

Equation (AIV.19) is the same as equation (AIV.15).

(b) Application: The "optogalvanic Lamb dip"

The above derivation may be applied to calculating the OGE caused by a weak monochromatic beam scanning across a Doppler line that is strongly saturated at its center frequency by a second beam. The homogeneous linewidth is assumed small compared to the Doppler linewidth. The weak beam will produce the usual unsaturated OGE (given by equation AIV.15) everywhere except within $\Delta\nu_{\text{hole}} \approx \Delta\nu_c \sqrt{1 + I^{\text{strong}}/I_s}$ of the center frequency. In the absence of the saturating beam, the OGE on line center would be

$$\Delta V = c'' I_{\nu_0}^{\text{weak}} \frac{1}{\gamma(\nu_0)} [1 - e^{-\gamma(\nu_0)L}]$$

where

$$\gamma(\nu) = \frac{\Delta N g_3/g_2 \lambda^2 A_{32}}{8\pi n^2} g_D(\nu)$$

where the effect of the homogeneous linewidth is assumed zero at low intensity.

On line center the saturated beam propagates according to equation (AIV.13);

$$\frac{1}{I} \frac{dI}{dz} = \frac{k_0}{(1+I)^{1/2}} e^{(1+I)p^2} [1 - \text{erf}([1+I]^{1/2} p)]$$

At very high intensity, $I \rightarrow \infty$,

$$\text{erf}([1+I]^{1/2} p) \rightarrow 1 - \frac{e^{-(1+I)p^2}}{(1+I)^{1/2} p \pi^{1/2}}$$

Thus at high intensity

$$\frac{1}{I} \frac{dI}{dz} = \frac{k_0}{(1+I)p\pi^{1/2}} \approx \frac{k_0}{p\pi^{1/2}} \frac{1}{I}$$

Thus, $(I - I_0) = \frac{k_0}{p\pi^{1/2}} (z - z_0)$, which is the usual result that at high intensities linear absorption holds (note $k_0 < 0$ for absorption).

$$I(z) = I_0 - \frac{|k_0|}{p\pi^{1/2}} z$$

The OGE due to the saturating beam is, from equation (AIV.20)

$$\Delta V(\nu) = - \frac{d'}{h\nu} (I_{\nu}^{\text{sat}}(0) - I_{\nu}^{\text{sat}}(L)) = \frac{d'}{h\nu} I_{\text{sat}} \frac{k_0 L}{p\sqrt{\pi}}$$

The OGE resulting from the probe beam is also given by equation (AIV.20)

$$\Delta V^{\text{probe}} = - \frac{d'}{h\nu^{\text{probe}}} (I_{\nu}^{\text{probe}}(0) - I_{\nu}^{\text{probe}}(L))$$

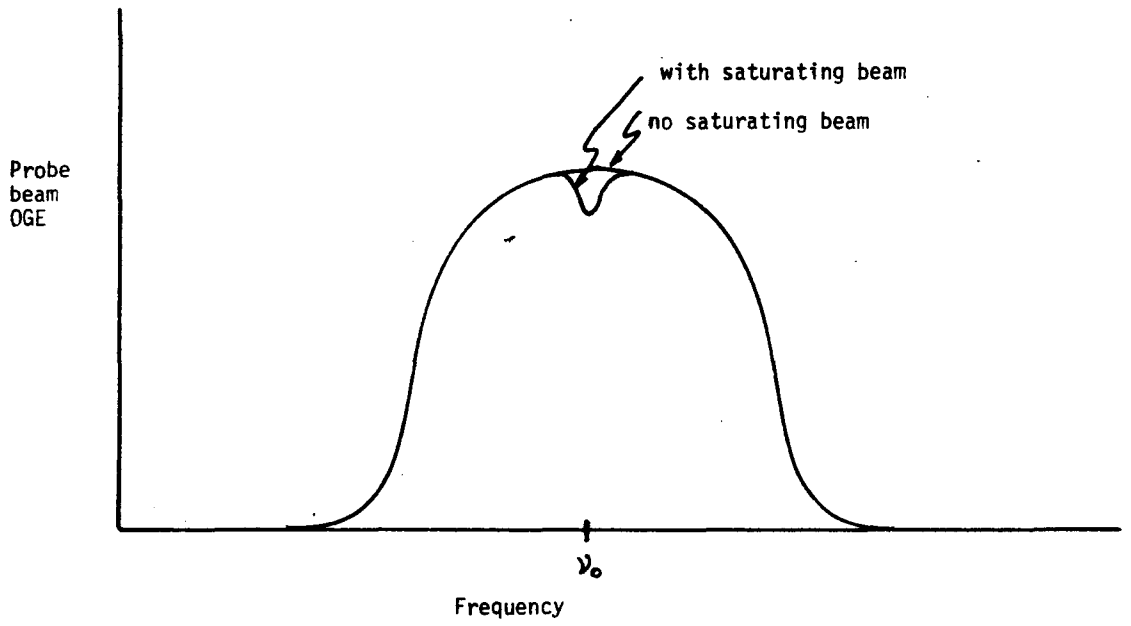
In a narrowband OGE experiment where only the effects of the probe beam are measured (for example, synchronous detection of a chopped probe beam with a steady-state saturating beam) the OGE is shown schematically in Fig. AIV-4. The peaks (line center) without the saturating beam are given by equation (AIV.15) ; the OGE on line center with saturation is given by equation (AIV.20) . The depth of the "hole" is given by

$$\begin{aligned} \nu_{\text{probe}}^{\text{unsat}} - \nu_{\text{probe}}^{\text{sat}} &= c'' I_{\nu_0}^{\text{probe}} \frac{1}{\gamma(\nu_0)} [1 - e^{-\gamma(\nu_0)L}] \\ &\quad - \frac{d'}{h\nu} I_{\text{sat}} \frac{k_0 L}{p\sqrt{\pi}} \end{aligned}$$

and the hole width is approximately $\Delta\nu_H \approx \Delta\nu_c \sqrt{1 + \frac{I_{\text{probe}}}{I_{\text{sat}}}}$. From the above equations, it is easy to see that

$$\frac{\Delta\nu_{\text{probe}}^{\text{sat}}}{\Delta\nu_{\text{probe}}^{\text{unsat}}} < 1$$

Fig. AIV-4 OGE of probe beam with and without saturating beam



REFERENCES - Appendix IV

- Gordon, E., A. White, and J. Rigden, Proc. Symp. Optical Masers (Polytechnic Inst. of Brooklyn, 1963), pp. 309-319.
- Zemansky, M. W., Phys. Rev. 36, 219 (1930); also, Mitchell, A. and M. W. Zemansky, Resonance Radiation and Excited Atoms (Cambridge University Press, 1971).

--But let's not talk about love.

Cole Porter